Surface Modification of Magnesium Alloy AZ31 for Improved Biocompatibility

By

Xiaoxi Yang

A thesis submitted in partial fulfillment

of the requirements for the degree of

Master of Science (MSc) in Chemical Sciences

The School of Graduate Studies

Laurentian University

Sudbury, Ontario, Canada

THESIS DEFENCE COMMITTEE/COMITÉ DE SOUTENANCE DE THÈSE

Laurentian Université/Université Laurentienne
School of Graduate Studies/École des études supérieures

Title of Thesis Titre de la thèse	SURFACE MODIFICATION OF MAGNESIUM ALLOY AZ31 FOR IMPROVED BIOCOMPATIBILITY
Name of Candidate Nom du candidat	Yang, Xiaoxi
Degree Diplôme	Master of Science

Department/Program Département/Programme	Chemical Sciences	Date of Defence Date de la soutenance	July 10, 2014

APPROVED/APPROUVÉ

Thesis Examiners/Examinateurs de thèse:

Dr. Joy Gray-Munro
(Co-supervisor/Co-directrice de thèse)

Dr. Éric Gauthier
(Co-supervisor/Co-directeur de thèse)

Dr. Louis Mercier
(Committee member/Membre du comité)

Approved for the School of Graduate Studies
Approuvé pour l'École des études supérieures

Dr. Robert Lafrenie
(Committee member/Membre du comité)

Dr. David Lesbarrères
M. David Lesbarrères

Dr. Mark Staiger
(External Examiner/Examinateur externe)

Director, School of Graduate Studies
Directeur, École des études supérieures

ACCESSIBILITY CLAUSE AND PERMISSION TO USE

Abstract

In order to apply magnesium alloys as an ideal innovative degradable biomaterial for implantation, the development of biocompatible surface modification strategies that can increase the corrosion resistance of magnesium-based implant materials is essential.

The surface modification strategy in this study involves deposition of a mixed organosilane pre-layer on Mg AZ31 followed by covalent bonding of RGD peptides to the organosilane layer through a linker molecule. Our results indicate that with optimized coating deposition conditions (pH, pre-hydrolysis time, temperature and deposition time) uniform organosilane coatings can be successfully deposited on Mg AZ31 substrates. Furthermore, by changing the ratio of the two different organosilanes in the mixed organosilane coating bath, the surface density of functional groups on the surface was varied, thus allowing control over the surface density of RGD peptides. Futhermore, an increase in corrosion resistance, cell adhesion and cell proliferation were observed on the coated Mg AZ31 samples in comparison to uncoated samples.

Table of Contents

List of Abbreviations

AFM   Atomic Force Microscope

APTS   (3-Aminopropyl)triethoxysilane

ATR-FTIR   Attenuated Total Reflection Fourier Transformer Infrared Spectroscopy

AuNP   Gold nanoparticles

DMF   N,N-Dimethylformamide

ECM   Extracellular Matrix

EDS   Energy Dispersive Spectroscopy

FAAS   Flame Atomic Absorption Spectroscopy

FBS   Fetal Bovine Serum

MPTS   3-Mercaptopropyltrimethoxysilane

PBS   Phosphate Buffered Saline (1x)

RGD   Arginylglycylaspartic acid

SEM   Scanning Electron Microscopy

SMP   3-(Maleimido)propionic acid N-hydroxysuccinimide ester

TEOS   Tetraethyl orthosilicate

XPS   X-ray Photoelectron Spectroscopy

List of Tables

List of Figures

Chapter 1 : Introduction

1.1 Biomaterials and Biocompatibility

By the end of the 20th century, many materials had been attempted for use as surgical implants and the term "biomaterial" was introduced to define the materials used as implants in the medical field. A biomaterial is a nonviable material used in a medical device, intended to interact with biological systems [1]. Current biomaterials normally consist of non-living materials which can be basically divided into several groups: synthetic and natural polymers, ceramics, metals and composites which combine different characteristics from two or several categories [2]. Different classes of biomaterials are used for specific applications depending on their unique physical and chemical properties. Generally, these medical applications fall into two broad categories: "hard-tissue replacement" and "soft-tissue replacement" [1]. Research in the field of "hard-tissue replacement" mainly focuses on ceramic and metallic materials which are typically used as orthopedic or dental implants. Experts working on "soft-tissue replacement" typically study polymers which have properties consistent with the needs of cardiovascular and general plastic-surgery materials [1, 2]. While the current definition of biomaterials uses the term "nonviable" this does not mean that biomaterials are inert in the human body. In fact, they are expected to produce positive interactions with biological systems and to perform the function they were intended for.

In order to better define the goal of biomaterials, another significant term, "biocompatibility", was introduced by biomaterial scientists. Biocompatibility is the ability of a material to perform with an appropriate host response in a specific application [1]. Unfortunately, after medical devices are implanted into the human body, most of them induce a sequence of adverse rejection reactions [3] called the foreign body effect. The blood or body fluid contacting interfaces adsorb non-specific proteins from the physiological environment which may induce a variety of

iatrogenic reactions such as interface thrombosis formation, non-self rejection and infection. At the same time, there are also some adverse reactions that occur at the implant/tissue interface, including local inflammation, phagocyte attack, and the formation of thick collagenous capsules around the implant [3-7]. These adverse reactions may enhance the corrosion rate of implants, affect the integrity of the medical implants, drive the poor integration between implants and local tissue and even worse make implants lose their desired functions. From these non-self rejection responses of the human body, it is believed that improving the biocompatibility of biomaterials is essential to control the unplanned biological responses occurring at the medical device/host interfaces. Appropriate solutions, such as surface modification, not only reduce patient suffering but also decrease the body's immunogenic attack on implants, allowing improved long-term performance. Due to the interdisciplinary nature of this field, scientists from different backgrounds, such as chemistry, biology, physics, materials science, genetics, and applied medicine, have worked together to build the field of Biomaterials Science. Their efforts have resulted in the development of many new biomaterials which function much better than those originally used.

1.2   Orthopedic Biomaterials

As an interdisciplinary subject, Biomaterials Science is applied in multiple fields including medical implants, biosensors and biochips for diagnostics, tissue engineering, bioelectronics, artificial photosynthesis and biomimetic materials [8]. The continued development of biomaterials is being driven by the need for improved performance of these materials. The need for better biomaterials has attracted increased investments, funding and grants supported by governments and worldwide organizations, thereby promoting the growth of the biomaterials market. Moreover, as a result of an aging worldwide population, active modern lifestyle and a desire for a higher quality of life, orthopedic implants have become a very important part of the biomaterials industry [9].

1.3.1 Classification of Orthopedic Implants

1.3.1.1 Bone and Bone Fractures

Bone plays a pivotal role in our daily lives, it acts as a support skeleton maintaining our body shape, and it combines with muscles and tendons to govern our movements. Moreover, some parts of the bones cover important organs, such as the lungs, to provide protection from outside impacts. Therefore, every single tiny bone in the human body has an indispensable role in our daily lives. An aging population, coupled with continued medical materials advances, has become the driving force for the increased utilization of medical implants and the demand for new medical devices in the years ahead. Furthermore, the human life span is constantly lengthening, and thus there is a need to extend the population's productive lifespan.

At times, due to carelessness in sports and exercise activities, accidents, and the natural aging process, cracks or fractures may occur in bone tissue. Generally, there are three different levels of bone damage. The first level of bone fracture can undergo self-recovery, requiring either no treatment or in certain cases only medical supplements to heal small cracks in the bone. At the second level of damage, the bone tissue can undergo self-recovery but needs some sort of external support to prevent the bone from moving during healing. Normally this type of damage takes several months to heal. At the third, most serious level, the bone is permanently damaged and it cannot heal by itself. This is typically the result of necrosis due to disease or bone aging. This type of bone damage needs whole tissue replacement; some common examples include hip, knee and dental replacements.

1.3.1.2 Current Treatments and Orthopedic Implant Materials

The type of medical intervention required depends on the type of fracture and its location. For the third level of bone damage, the implant is exposed to constant wear and high compressive

loads, so the biomaterial must possess outstanding mechanical properties and corrosion resistance. Furthermore, a permanent implant is required, because the surgical procedure will remove a part of the bone tissue to make room for implant fixation. This has a serious impact on the strength of the bone tissue limiting the number of times this surgery can be performed in a person's lifetime. For example in a total hip replacement, the damaged femoral head is removed and replaced with a metal stem which is either cemented or press fit into the femur bone leaving only a small amount of the original tissue and necessitating the use of a long-term implant. The commonly used biomaterials for permanent implants, cobalt-chrome and titanium alloys, have been widely applied in knee and hip replacements for several decades. Ceramic materials have also been applied as a bearing surface in hip replacements due to their high hardness, lubricity, scratch resistance and biocompatibility [9, 10].

In contrast, the implants for the second level of bone damage are relegated to temporary devices which need to be removed by a second surgery after the fracture has completely healed. The most commonly used material for this purpose is surgical stainless steel. This material is widely used as medical fracture plates and bone screws because of its good biocompatibility, mechanical properties, and reasonable cost of fabrication [11]. However, the required second surgery increases the risk of re-damaging the healed bone, leads to additional discomfort for the patient and is an economic burden on the health care system. As a result, although the patient does not need the supporting implant after healing has occurred, doctors often opt to leave the implant in the patients' body unless adverse effects such as chronic inflammation and stress shielding occurs.

Stress shielding is another challenge faced by scientists in the application of metallic biomaterials as orthopedic implant. After the orthopedic implant devices are introduced into damaged bone tissue, the loads originally carried by local bone tissue are redistributed and carried by both the prosthesis and natural bone tissues. When the elastic moduli of implant devices are much higher than that of natural bone tissue, the loads or stresses on bone tissues are

diminished and the stress shielding effect occurs on bone tissues [1, 12-15]. The bone growth and resorption processes are driven by the load or stress from the environment. The areas undergoing the high load or stress are stimulated to increase in bone mass, and in contrast, the areas experiencing low load or stress will lead to a decrease in bone mass [12]. Therefore, the bone responses to stress shielding effect can hinder the bone recovery at the surgery site. Moreover, as a long term concern, stress shielding can cause bone resorption around the implant devices which leads to loosening of implant devices, and further increases the risk of bone fracture and implant failure [12, 14].

The metallic biomaterials currently in use normally have high elastic moduli which are not a match with that of natural bone, such as stainless steel, Co-Cr alloys and Ti alloys [1, 14, 16]. Thus, in order to solve the stress shielding effect of implant devices, a metallic biomaterial with lower elastic modulus is desired to effectively inhibit bone atrophy, while at the same time inducing better bone remodeling around the implant.

Magnesium and its alloys are the ideal candidates due to their outstanding mechanical properties, biocompatibility and biodegradability.

1.3 Metallic Biodegradable Implant Materials

A metallic biodegradable implant that provides the necessary stability during healing but gradually degrades when no longer needed would eliminate both the need for a second surgery and the problems associated with the stress shielding effect. Current biodegradable materials are commonly made of polymers [1]. Their main disadvantage is that they have poor mechanical strength and therefore do not provide adequate support to the damaged bone tissue during the healing process [1]. Traditional metallic biomaterials such as titanium and stainless steel offer improved mechanical strength but as discussed earlier do not biodegrade. However, in recent years the possibility of developing biodegradable metallic implants from chemically reactive

metals such as iron and magnesium has been proposed by a number of biomaterials scientists [15-18].

1.3.1 Magnesium Mechanical Properties

Table 1.1 Comparison summary of the physical and mechanical properties of implant materials and natural bone [16].

Properties	Natural bone	Magnesium	Ti alloy	Stainless steel	Synthesis hydroxyapatite
Density (g/cm^3)	1.8-2.1	1.74-2.0	4.4-4.5	7.9-8.1	3.1
Elastic modulus (Gpa)	3-20	41-45	110-117	189-205	73-117
Compressive yield strength (Mpa)	130-180	65-110	758-1117	170-310	600
Fracture toughness (MPam$^{1/2}$)	3-6	15-40	55-115	50-200	0.7

Magnesium and its alloys are lightweight metals with a density of 1.74-2.0 g/cm^3 which is much closer to that of natural bone (1.8-2.1g/cm^3) compared with other metallic implant materials and synthetic hydroxyapatite. The elastic modulus of magnesium is around 41-45 GPa which is a 4-fold increase in comparison to currently used degradable polymeric implant materials. In addition, the elastic modulus of Mg and its alloys are very close to that of natural bone compared with other currently used metallic implant biomaterials. This appropriate elastic modulus is one important property that makes magnesium and its alloys a good choice for use as rigid internal fixation devices which can also reduce the stress shielding effect on surrounding bone tissues. Moreover, the compressive yield strength of magnesium is both similar to that of natural bone tissue and 2-fold higher than degradable polymeric implant materials. Furthermore, the fracture toughness of magnesium is increased significantly in comparison to ceramic materials such as synthetic hydroxyapatite. All of these mechanical properties contribute to making magnesium

materials ideal bone fixation devices that provide good mechanical stability in the early stages of healing without inducing the stress shielding effect [16-18].

1.3.2 The Essential Role of Magnesium in the Human Body

The chemical properties of magnesium are also an important factor in determining its suitability as an orthopedic implant material. Magnesium is a macro-mineral which is needed in large amounts by the human body. The magnesium ion (Mg^{2+}) is the fourth most abundant cation in the human body and approximately 50% of the Mg^{2+} in the body is stored in bone tissues. Mg^{2+} is also essential to living cells and human metabolism, where it functions as a common co-factor involved in more than 300 enzyme-driven biochemical reactions and is crucial for the formation of the MgATP complex which is essential for muscle contraction [19]. Moreover, magnesium ions can help to stabilize the structure of nucleic acid and participate in the process of DNA repair enabling healthy protein synthesis and cell reproduction. Furthermore, magnesium assists in maintaining the homeostasis of the primary minerals including sodium, calcium and potassium which govern the neural currents and heart rhythm. Additionally, any excess magnesium is excreted harmlessly in the urine in order to keep the electrolyte balance in the human body. In short, magnesium is not only non-toxic to the human body but is actually an essential element for proper cell function [19-22].

1.3.3 The Performance of Magnesium Implants *In Vitro* and *In Vivo*

Several recent publications examining the *in vitro* and *in vivo* performance of these materials indicate that magnesium based implants exhibit good biocompatibility, osteoconductivity and osseointegrative properties, as well as being non-toxic [23-29]. Research by Pietak et al. has shown that magnesium-based substrates can assist stromal cells to adhere to the implant surface and further support their differentiation to an osteoblast-like phenotype, producing a bone like

matrix on the surface, and also demonstrating significant alkaline phosphatase activity *in vitro* [23]. Moreover, Li et al. reported that the release of magnesium ions from the magnesium substrate during biodegradation improved cell viability as well as enhanced cell adhesion, spreading and growth on the substrate [29]. In addition, *in vivo* studies of biocompatibility have demonstrated that the level of newly formed bone in the area around the magnesium-based implants was higher than that observed for both titanium and biodegradable polymer implants [28, 29]. For example, in another in vivo study, the formation of new bone was found around the titanium implants, but the newly formed bone tissue was mostly isolated by connective tissues indicating the osteoconductivity of the unmodified titanium implant was not ideal [30]. On the other hand, several authors have postulated that the reason for the good connection between magnesium metal substrates and newly formed bone tissue is that the biodegradation products lead to enhanced bioactivity of the material through fast deposition of magnesium-containing calcium phosphate at the implant/tissue interface [26, 27].

1.3.4 Challenges in Using Magnesium as an Orthopedic Implant

The major drawback to the use of magnesium materials as orthopedic implants is their poor corrosion resistance leading to fast degradation. Magnesium and its alloys are easily corroded in chloride containing environments such as human body fluid. In one recent study, the authors reported that a 400 mm^3 untreated polished pure magnesium sample almost completely dissolved in Hank's balanced salt solution after an immersion period of only 9 days [25].

The anodic dissolution of magnesium metal in aqueous solutions is coupled with the reduction of water thus producing hydroxide ions and hydrogen gas. Therefore, when magnesium is exposed to water, a low water-solubility film of magnesium hydroxide is formed on the magnesium surface which acts as a barrier layer between the magnesium substrate and the corroding solution, slowing down the rate of corrosion. However, the physiological environment is complex and the presence of ions such as chloride plays an important role in the accelerated corrosion of

magnesium in body fluids. This accelerated corrosion is triggered when chloride ions react with the magnesium hydroxide layer to form highly soluble magnesium chloride. This disrupts the magnesium hydroxide layer resulting in re-exposure of the underlying substrate and continued corrosion of the metal. This process has a negative impact on the mechanical integrity of the implant, leading to loss of implant stability before the impaired bone tissue has time to heal as well as production of large volumes of hydrogen gas that cannot be readily dealt with by the body. This fast degradation can also lead to poor osteointegration of the magnesium implant [24, 25, 28]. The relevant chemical reactions are shown below:

(1) $Mg(s) + 2H_2O(l) \rightarrow Mg(OH)_2(s) + H_2(g) \uparrow$

(2) $Mg(OH)_2 (s) + 2Cl^-(aq) \rightarrow MgCl_2 (aq) + 2OH^-(aq)$
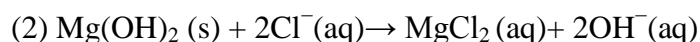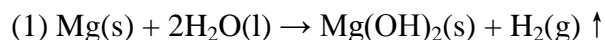
While biodegradation is essential in the case of a temporary implant, the implant should be able to maintain its mechanical integrity over 12-18 weeks in order to immobilize the damaged bone tissue until it is sufficiently healed to bear the required mechanical load on its own [28].

1.4   Corrosion Resistance Improvement

In order to control the corrosion rate and extend the functional lifetime of magnesium implants in the human body, giving the body sufficient time to deal with the degradation products and to regenerate new bone tissue around the magnesium implant, there are two appropriate methods: alloying and surface coating [31].

1.4.1 Alloying

Alloying is a very efficient way to improve the mechanical properties and corrosion resistance of magnesium [16, 28, 29]. An appropriate choice of alloying elements which lead to good mechanical properties and corrosion resistance but are also non-toxic is essential to guarantee the

biosafety of implants. There are two primary groups of magnesium-based alloys, magnesium-aluminum alloys and magnesium-rare earth alloys [16]. The first group can significantly improve the corrosion resistance of magnesium, and both groups have been shown to enhance magnesium's mechanical properties [32]. In an effort to produce more biocompatible implants, recent studies have evaluated the *in vitro* and *in vivo* behavior of Mg-Ca and Mg-Zn alloys. These studies demonstrated that both calcium and zinc had a positive impact on the mechanical properties, and also enhanced the biocorrosion behaviour of magnesium by increasing the deposition of hydroxyapatite at the interface and inducing the formation of new bone tissue *in vivo* [29, 31].

1.4.2 Coatings

Although alloying is a viable option for controlling the degradation rate of magnesium, it is still a challenge to develop innovative alloys with optimum performance due to the low solubility of many elements in magnesium [31]. Therefore, coatings have become an attractive approach to improve the corrosion resistance of magnesium-based materials. In the case of temporary orthopedic implants, protective coatings should not only act as a barrier slowing substrate corrosion, but they should also enhance biocompatibility and osteointegration [16, 31]. These coatings generally fall into two categories: conversion coatings and deposited coatings. In a conversion coating process, dissolved ions from the metallic substrate itself are incorporated into the coating to form conversion layers such as oxides, phosphates, fluorides or chromates. The simplest example of a conversion coating on magnesium and its alloys is the magnesium hydroxide layer that forms when these materials are exposed to the atmosphere. However, the protection of this passivation layer is limited in harsh physiological environments; therefore more advanced coating methods are being investigated such as chemical treatment, anodization and ion implantation [31]. Despite this, chemical conversion coatings still play an important role as a pre-treatment strategy in many coating technologies as they have been shown to significantly enhance the adhesion of subsequently deposited coatings [34].

Coating materials can be metallic, inorganic or organic. Of these, organic-based coatings are the most widely used for biomedical applications because of their good biocompatibility, biodegradability and the availability of functional groups that can be used for further surface modification [31]. However, an appropriate coating on magnesium needs to have excellent adhesion properties as well as the ability to enhance the biocompatibility and slow the corrosion rate [35]. Organosilane-based coatings that can covalently bind to the magnesium alloy substrate are of significant interest for this purpose.

1.4.2.1 Organosilane Coating

Organofunctional silanes are of interest for a broad range of applications due to their outstanding performance as coupling agents between organic and inorganic materials [35-38]. Moreover, recent studies have reported that organosilane coatings can also increase corrosion resistance, improve scratch resistance, and enhance wear resistance of a number of different metals including aluminum, iron and zinc [39-44]. Furthermore, due to their low toxicity and relative environmental-friendliness, organosilane treatments have become an important alternative to chromate coating which is toxic to both human health and the environment [39, 40]. These successful applications on metals, combined with the outstanding biocompatibility, have inspired researchers to utilize organosilane coating onto Mg alloy substrates to achieve the ideal controlled biodegradable implant material.

1.4.2.2 General Structure of Organosilanes

The general structure of an organosilane is $R_nSi(OR')_{(4-n)}$. The R' group is typically an alkyl group such as $-CH_3$ or $-CH_2CH_3$. Trialkoxysilanes have been commonly used as coupling agents to produce covalent bonds between organic and inorganic materials [38-40,45]. R is an organofunctional substituent which usually contains a propylene bridge ($-CH_2CH_2CH_2-$) linked to the central silicon atom through an Si-C bond and terminated with a specific functional group

[36]. A variety of terminal functional groups can be exploited depending on the desired surface chemistry, some of these including thiol, amine, alcohol, methacrylate or carboxylic acid [36, 38, 39, 45].

1.4.2.3 Organosilane Chemistry

In order to covalently bond to the substrate surface, trialkoxysilanes must undergo both hydrolysis and condensation reactions. During hydrolysis, the alkoxy groups of the silane molecules react with water giving silanol (Si-OH) groups. The silanol groups can then undergo condensation reactions with other hydrolyzed organosilane molecules in solution leading to the formation of solution phase oligomers, or with hydroxyl groups on the substrate surface. In general, at low pH, the organosilane solutions exhibit a very slow condensation rate compared with the hydrolysis rate, therefore, it is assumed that the condensation occurs after hydrolysis is completed. In addition, various conditions are known to affect the hydrolysis/condensation reactions; these will be discussed in the following sections.

An ideal simplified reaction scheme is shown below:

$R\text{-}Si(\text{-}OR')_3 + 3H_2O \rightarrow R\text{-}Si(OH)_3 + 3R'\text{-}OH$ — Hydrolysis

$R\text{–}Si(OH)_3 + R\text{–}Si(OH)_3 \rightarrow R\text{–}Si(OH)_2\text{–}O\text{–}Si\text{–}R(OH)_2 + H_2O$ — Condensation between the organosilane molecules

$R\text{-}Si(OH)_3 + MOH \rightarrow R\text{-}Si(OH)_2\text{–}O\text{–}M + H_2O$— Condensation between organosilane molecules and metallic surfaces through surface metal hydroxides
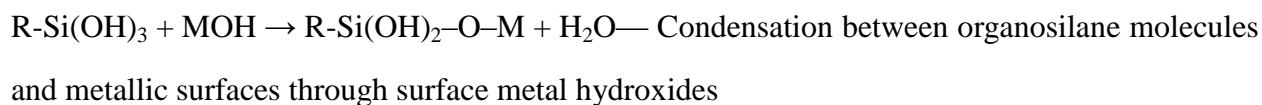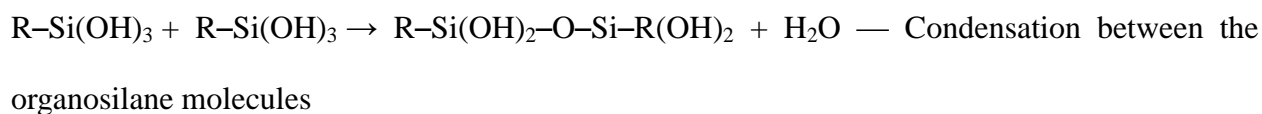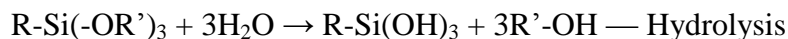
After the hydrolysis is complete, silanols condense between the molecules themselves to form

organosilane polymers with a siloxane network of Si-O-Si covalent bonds. Once the organosilane is capable of reaching the substrates at the interface, further condensation takes place between the silanol groups and hydroxyl groups at the metal surface resulting in covalent bonding and a metal-siloxane interface. After the curing and drying process, the water molecules are completely released from the deposited film and the interface, eventually leading to a stable multilayer of cross-linked polysiloxane on the metallic substrate. A schematic diagram of this process is shown in Figure 1.1. The siloxane network is very hydrophobic if one of the substituents on the Si atom is a carbon atom. So, it can efficiently hinder the ability of water molecules to penetrate the film network and reach the substrate underneath, thereby providing corrosion protection for the substrate [36-39, 46].
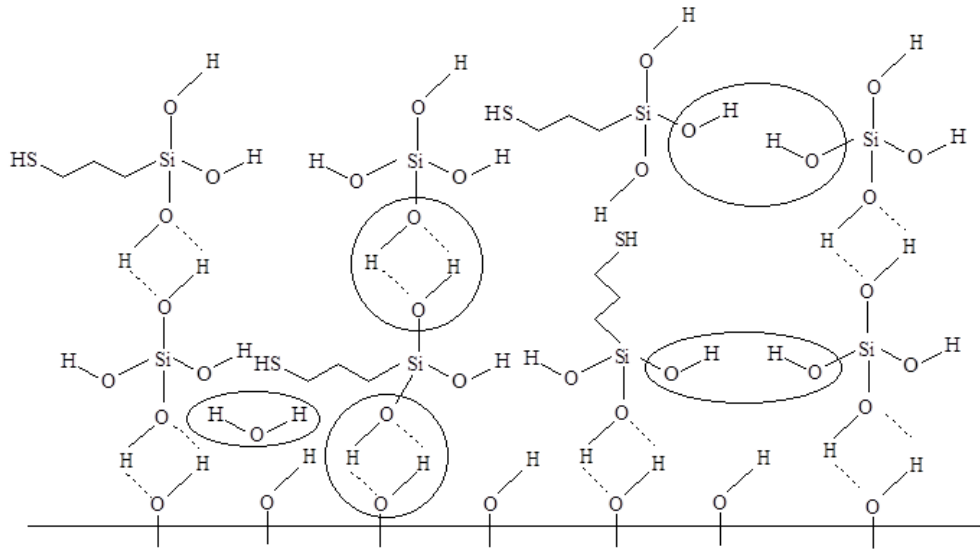
Mg AZ31 Alloy Substrate
(a) After coating deposition
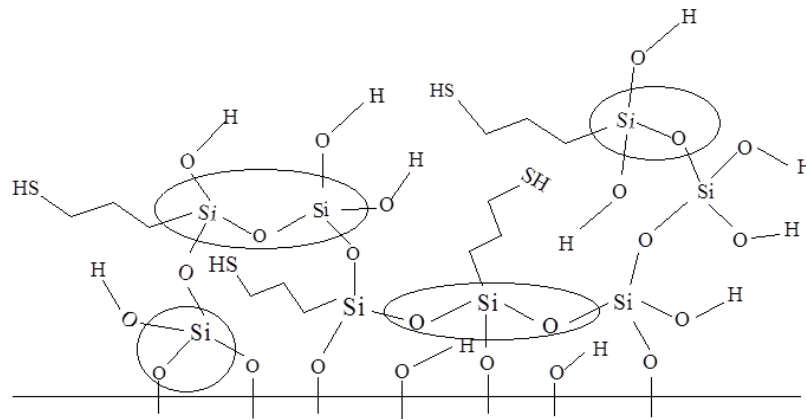
Mg AZ31 Alloy Substrate
(b) After curing process

Figure 1.1 General schematic of organosilane coating condensation mechanism on Mg AZ31 before (a) and after (b) curing process. Adapted from [46].

1.4.2.4 Factors Influencing Organosilane Chemistry

The extent and rate of reaction are affected by various factors including the chemical properties of the organosilane, the solvent, pH of solution, organosilane pre-hydrolysis time, temperature, and the substrate to be coated. These factors can also influence the performance and quality of the deposited coating [39, 40, 46, 47]. Organosilane hydrolysis and condensation reactions are often carried out in alcohol solutions because most organosilanes have poor solubility in water [48]. In order to enhance the graft density of the organosilane to the substrate surface, it is important to promote hydrolysis leading to a large number of reactive silanol (Si-OH) groups in the solution. However, the condensation reaction must be controlled to minimize the condensation reaction between hydrolyzed organosilane molecules in solution. Water is essential for hydrolysis [39] and can come from several sources including addition, absorption from the atmosphere, or adsorption to the substrate surface. Typically, the water is added during pre-hydrolysis. In clinical dental applications, 0.5-1.0% silanes are pre-hydrolysed in 90-95% alcohol; the remaining balance is deionized water [36].

The solution pH is another essential factor that must be controlled to achieve the desired balance of hydrolysis and condensation reactions. In general, low pH conditions favour hydrolysis whereas high pH conditions favour condensation. For example, at pH 4, the rate of hydrolysis has been shown to be 1000 times greater than the rate observed at pH 7 while the rate of condensation reaches a minimum at pH 4 [38, 40]. Moreover, the pH of the solution further impacts the quality and properties of the organosilane coating deposited on a metal substrate. Scott, et al. reported that a uniform film was developed from MPTS deposited on a magnesium alloy substrate at pH 4 while non-uniform films were observed at pH of 7 or 10 [38]. In addition, Najari, et al. demonstrated that under acidic conditions (pH 4), the aged r-MPS primarily condensed with the zinc substrate through reactive Si-OH groups instead of S-H functional groups which occur at the neutral pH 7, resulting in an increase in the availability of free S-H functional groups at the surface for further modification [40].

15
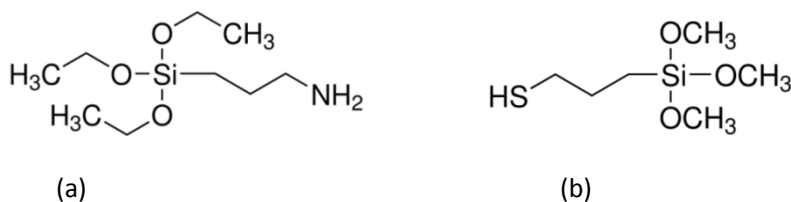
Figure 1.2 Chemical Structures of APTS (a) and MPTS (b).

Silane coupling agents are commonly used to promote adhesion between an inorganic substrate and an organic molecule. The selection of silane coupling agents depends on the desired surface chemistry or the functional group needed to covalently bond a specific molecule to the surface. The organosilane, (3-Aminopropyl)triethoxysilane (APTS), is often chosen as an adhesion promoter between metal substrates and the final organic layer. APTS, as shown in Figure 1.2, contains three ethoxy-chains as well as an amine functionalized chain bonded to a central silicon atom. In a number of studies, it has been shown that the amino group can be a very reactive site for linking organic molecules, such as peptides [49, 50], enzymes [51] and DNA probes [52], onto different type of substrates. However our preliminary studies revealed that although uniform APTS coatings were deposited on the magnesium substrates, the films were not stable in aqueous solution which means that APTS coatings did not enhance the corrosion resistance of the substrate and also were not useful for further surface modification. Therefore, based on our previous, a thiol terminated organosilane, (3-Mercaptopropyl)trimethoxysilane (MPTS) was chosen as the organosilane of interest for this thesis. The structure of the MPTS molecule is shown in Figure 1.2. This organosilane has three methoxy groups and a thiol terminated short alkyl chain attached to a central silicon atom. The presence of a thiol terminated alkyl group makes MPTS a hydrophobic organosilane which means it can act as a water barrier coating to improve substrate corrosion resistance [53]. Furthermore, the corrosion resistance of organosilane coatings is dependent on the surface packing density of the molecules on the substrate. MPTS contains a highly nucleophilic thiol group on the linear alkyl chain which can promote cross-linking between the MPTS molecules, aiding in the development of a densely packed organosilane coating on the substrate. This reduces the number of surface oxygen

16

adsorption sites resulting in improved corrosion resistance for these coatings [54]. For example, Cabral et al. evaluated the corrosion resistance of different silane coatings on an aluminum alloy substrate. The results of this study showed that the MPTS coating was a thin layer that exhibited good adhesion to the substrate surfaces, and it also enhanced the corrosion resistance and fatigue life compared to untreated aluminum alloy substrates [55]. Moreover, the electrochemical impedance spectroscopy studies performed by Underhill and Duquesnay demonstrated that the MPTS coatings deposited on alloys commonly used in the aerospace industry, had a better performance than the more often used 3-glycidoxypropytrimethoxysilane coating in terms of corrosion resistance and the adhesive bond's resistance to moisture. The improvement in corrosion resistance was found to be strongly dependent on the MPTS concentration in the coating bath [54].

As well as providing improved corrosion resistance, the thiol functional group of MPTS provides reactive sites for the covalent immobilization of functional biomolecules. For example, in a recent study, Bhatia et al. used a succinimide heterobiofunctional crosslinker to covalently immobilize functional antibodies at a high surface density on thiol-terminated organosilane modified silica surfaces. They demonstrated that the surface modification procedure was both simple and reproducible [56].

1.5 Influence of Surface Modification on Biocompatibility

In order to choose surface modification strategies with optimum biocompatibility, it is necessary to understand the biological interactions that occur on substrate surfaces after the implant is applied to the fracture site, as well as the general cell adhesion process and the factors which influence the latter.

1.5.1 Host Response to Biomaterials

When a non-self material is implanted into the body, a complex cascade of reactions called the "foreign body response" is induced [57]. In brief, inorganic ions and water molecules are immediately adsorbed at the interface between the biomaterial and the contacted tissue or blood [58]. Subsequently, proteins reach the substrate surface and are non-specifically adsorbed at the interface through different binding mechanisms based on the surface properties of the implants and the chemical and physical properties of the protein. After attachment to the surface, the adsorbed proteins undergo conformational changes that can ultimately lead to denaturation [58]. This layer of nonspecific adsorbed protein is believed to be the trigger that leads to the foreign body response [57, 59, 60]. As a result, a number of different cells, which play key roles in normal wound healing, such as monocytes, leukocytes, and platelets, adhere to implanted surfaces and are involved in reactions that lead to the foreign body responses, including pro-inflammatory processes, chronic inflammation or even formation of collagenous fibrous tissue around the implant device to insulate it from the biological environment [57]. Hence, the surface properties and the adsorbed proteins at the interface are very important for controlling the cellular responses to the implanted device which will further determine the overall implant performance including the device lifetime and tissue integration capability.

1.5.2 Osteoblast Adhesion to Implant Surfaces

For orthopedic implants, biocompatibility is determined by the behaviors of osteoblasts and their adhesion to the implant surface. It is essential to establish a surface that is osteoconductive and osteoinductive and does not lead to fibrous tissue formation. Osteoconduction refers to the ability of surfaces to permit bone growth. After the bone implant is introduced into a damaged bone region, an osteoinductive surface can efficiently recruit and stimulate surrounding immature cells to differentiate into bone-forming cells, and further promote bone healing [61]. Therefore, a complete understanding of osteoblast adhesion and the main molecules involved is very

important in order to optimize the contact interface between the osteoblasts and the orthopedic implant. For most types of adherent cells, cell adhesion generally depends on the interaction between ligands in the extracellular matrix (ECM) and the corresponding integrin receptors on the cell surface; this cell adhesion is essential for cell survival of non-malignant cells [60, 62]. The ECM of bone tissue is composed of 90% collagenic proteins with the balance primarily made up of non-collagenic proteins, such as osteocalcin, osteonectin, fibronectin and growth factors. Most of these proteins are involved in osteoblast adhesion [58]. The osteoblasts interact with specific ligands on the proteins in the surrounding ECM through integrins which are present on cell membranes.

1.5.2.1 Integrins

The integrin family is one of the major classes of adhesion molecules. Integrins specifically recognize ligands in the ECM to facilitate adhesion between the cell and its environment [58, 62-66]. Integrins are transmembrane heterodimeric proteins containing two non-covalently bonded subunits, α and β. Signals from the ECM can be efficiently transduced into cells and sequentially control cell behaviors by specific signaling pathways which involve cytoplasmic molecules. There are 16 different α subunits that can associate with 9 β subunits to create approximately 22 different heterodimers. The structural diversity of the integrins provides a number of possibilities for specific ligand binding [58, 62-65, 67]. In human bone tissue, the α_2, α_4, α_5, α_v, β_1, β_3 and β_5 subunits are expressed on the osteoblasts. Gronthos et. al. have reported that the β_1 subfamily is the most predominant receptor group involved in osteoblast-like cell adhesion to collagen, laminin and fibronectin [63]. Furthermore, the interactions between the integrins and the corresponding ligands can also influence several cellular processes including adhesion, survival, proliferation, differentiation, motility and apoptosis [64, 65]. Another study demonstrated that the β_1 integrin subfamily is also utilized by stromal precursor cells to adhere and proliferate, and that β1 integrin interactions may further affect osteoblast development and bone formation [62].

19

1.5.2.2 Biomimetic Surface Modification to Enhance Osteoblast Adhesion

The discovery of the essential role of integrin-mediated mechanisms of cell adhesion has led scientists from the fields of materials science, biochemistry, surface engineering and medicine to develop methods to functionalize biomaterial surfaces with ECM proteins, like vitronectin, fibronectin, collagen, or laminin, in order to elicit specific cell-surface interactions [68]. Schneider and Burridge demonstrated that in comparison with uncoated substrates, osteoblasts exhibited better formation of focal adhesions on both glass coverslips and titanium disks which were precoated with either fibronectin or vitronectin [69]. In addition, Kilpadi et al. illustrated that the excellent osseointegration of hydroxylapatite substrates could be explained by their higher capacity to adsorb fibronectin and vitronectin from serum than commercially pure titanium or 316L stainless steel [70]. Moreover, nutrient depletion experiments showed that the surface adhesion and spreading abilities of bone-derived cells on several biomaterial surfaces were reduced by 73-83% when cells were seeded in vitronectin-depleted media, however, no significant decrease was observed in fibronectin-depleted media. The results in this study indicated that the attachment and spreading of human bone-derived cells on biomaterials surfaces during the first 90 min are related to the adsorption of vitronectin onto surfaces [71]. Although the immobilization of adhesion-related proteins to implant surfaces has been reported to enhance cell adhesion and spreading on substrate surfaces, there are still some limitations in terms of medical applications. First, the proteins may give rise to undesirable immune responses and infection is a risk since the proteins must be isolated from other organisms [72]. In addition, the conformation and the orientation of the proteins are easily influenced by the surrounding environment and immobilization process [66, 68]. For example, the hydrophobicity of the substrate surface can affect the structure of the adsorbed proteins. On hydrophobic surfaces, proteins tend to unfold to maximize their interaction with the substrate surface. This structural rearrangement can denature the proteins, decreasing the availability of specific binding domains for ligand/integrin interations [59, 73].

In order to overcome these problems, it is necessary to identify the structure of specific adhesion-recognition motifs in ECM proteins which can then be grafted to the surface, eliminating the need for immobilization of whole protein molecules. As a potential substitute, the arginylglycylaspartic acid (RGD) amino acid sequence has been found in a number of extracellular molecules, and this specific peptide of only a few hundred daltons may mainly mediate cell attachment [68].

1.5.2.3 The RGD Binding Motif

In order to confirm the integrin recognition motif on ECM proteins, the ability of various RGD-containing and RGD-free peptides to inhibit the binding of fibronectin receptors to solid-phase anchored fibronectin was evaluated by ELISA. The results showed that addition of the GRGDSP peptide decreased the ligand affinity of fibronectin receptors to fibronectin pre-coated microtiter wells, and that control peptides, GRADSP and GRGESP, were significantly less potent than GRGDSP group by at least several hundred times [74]. Moreover, many other studies have demonstrated that most ECM proteins, such as collagen type I, and fibronectin, contain the unique tri-peptide RGD sequence (arginine-glycine-aspartate) and that several known integrins can recognize and specifically bind to ECM proteins through this sequence, resulting in cell adhesion [72]. For osteoblast-like cells, Puleo et al. and Garcia et al. demonstrated that cell culture medium containing the RGD peptides, GRGDSP and GRGDS, partially inhibited cell adhesion to bioactive glass substrates and microtiter plates which were pre-coated with fibronectin [75, 76]. Garcia et al. further demonstrated that both antibodies against fibronectin and against the specific RGD region of fibronectin were able to significantly decrease osteoblast-like cell adhesion to fibronectin pre-coated bioactive glass by more than 80% [76]. These studies have illustrated the pivotal role of the RGD sequence in osteoblast-like cell adhesion, thus an appropriate surface modification that immobilizes RGD containing peptides to a substrate should improve cell-surface adhesion onto biomaterials. In fact, over the past decade, a number of studies have showed that RGD-sequence containing peptides can be successfully

immobilized onto different biomaterials surfaces including titanium [77-80, 81, 82], polymers [83-87], glass [88], hydroxylapatite [89] and silicon [90] substrates. In a recent study, the adhesion of human osteoblasts to pretreated titanium and to polymers modified with synthetic RGD sequence-containing peptides was studied. In order to evaluate human osteoblast adhesion capacity on RGD treated and untreated substrates, Bagno et al. trypsinized the cells 15 and 60 minutes after seeding. The data showed that human osteoblasts had higher adhesion capacities on RGD-modified substrates compared with unmodified ones, even after a short (15 minute) adhesion period [89, 91]. In another study, a cell/surface interaction test was carried out with human fetal osteoblasts. Compared with untreated titanium alloys, the RGD-modified substrate efficiently promoted more osteoblast adhesion, and the osteoblasts exhibited better spreading and proliferation on RGD-modified substrates as observed by fluorescence microscopy [92]. Furthermore, Hu et al. also studied the differentiation of osteogenic precursor cells on polymer scaffolds, by measuring the alkaline phosphatase activity and calcium levels of cells adhered to RGD-modified polymer scaffolds which were higher than cells adhered to both unmodified and other positively charged functional group modified samples, such as $-NH_2$ or poly(L-lysine). This study demonstrated that the presence of the RGD sequence can enhance the differentiation of osteogenic cells [84].

Although immobilizing the RGD-containing sequence to a substrate surface can efficiently biomimic the natural ECM environment and significantly enhance cell adhesion to substrate surfaces, as an artificial surface, there are still some differences in comparison to the natural ECM. For example, the RGD surface density, orientation and distribution have been shown to have an effect on cell adhesion and spreading. Cell adhesion is an RGD dose-dependent interaction. Generally, the amount of cells adhered on a substrate surface is influenced by the number of RGD molecules present on the substrate surfaces which can further affect cell spreading, migration and proliferation [85-87, 90].

Chapter 2 : Objectives

Metallic implants such as titanium and stainless steel are commonly used in fracture fixation to provide stability to the damaged bone tissue. However, in many cases these implants are unnecessary after healing has occurred. Therefore biodegradable metallic materials such as magnesium and its alloys have become of interest to Biomaterials scientists due to their outstanding mechanical strength and relatively non-toxic degradation products. Unfortunately, the poor physiological corrosion resistance of magnesium has limited its clinical application as an orthopedic implant material. Therefore, the overall objective of this thesis was to develop a biocompatible protective coating that can slow the biodegradation rate in the early stages of healing while enhancing cell/surface interactions.

The short term objectives of this thesis were:

1. To develop a method for depositing a uniform, corrosion resistant mixed organosilane coating composed of MPTS and TEOS on Mg AZ31. These mixed layers provide the opportunity to vary the surface density of the thiol functional group which should have an influence on the surface density of subsequently immobilized biomolecules.

2. To characterize the effects of total organosilane concentration, MPTS/TEOS ratio and deposition time on the surface chemistry, surface thiol density and corrosion resistance of the coated Mg AZ31.

3. To develop a surface modification strategy for covalent bonding of peptides containing the RGD motif to the organosilane coated Mg AZ31 surface.

4. To characterize the surface chemistry of the organosilane coatings prepared with different MPTS/TEOS ratios after covalent immobilization of the RGD peptide. Varying the amount of thiol at the surface is expected to yield different surface densities of the RGD peptide.

5. To determine the influence of the proposed surface modification on the *in vitro* biocompatibility of Mg AZ31 with human derived bone cells.

Chapter 3 : Materials and Methods

3.1 Project Overview
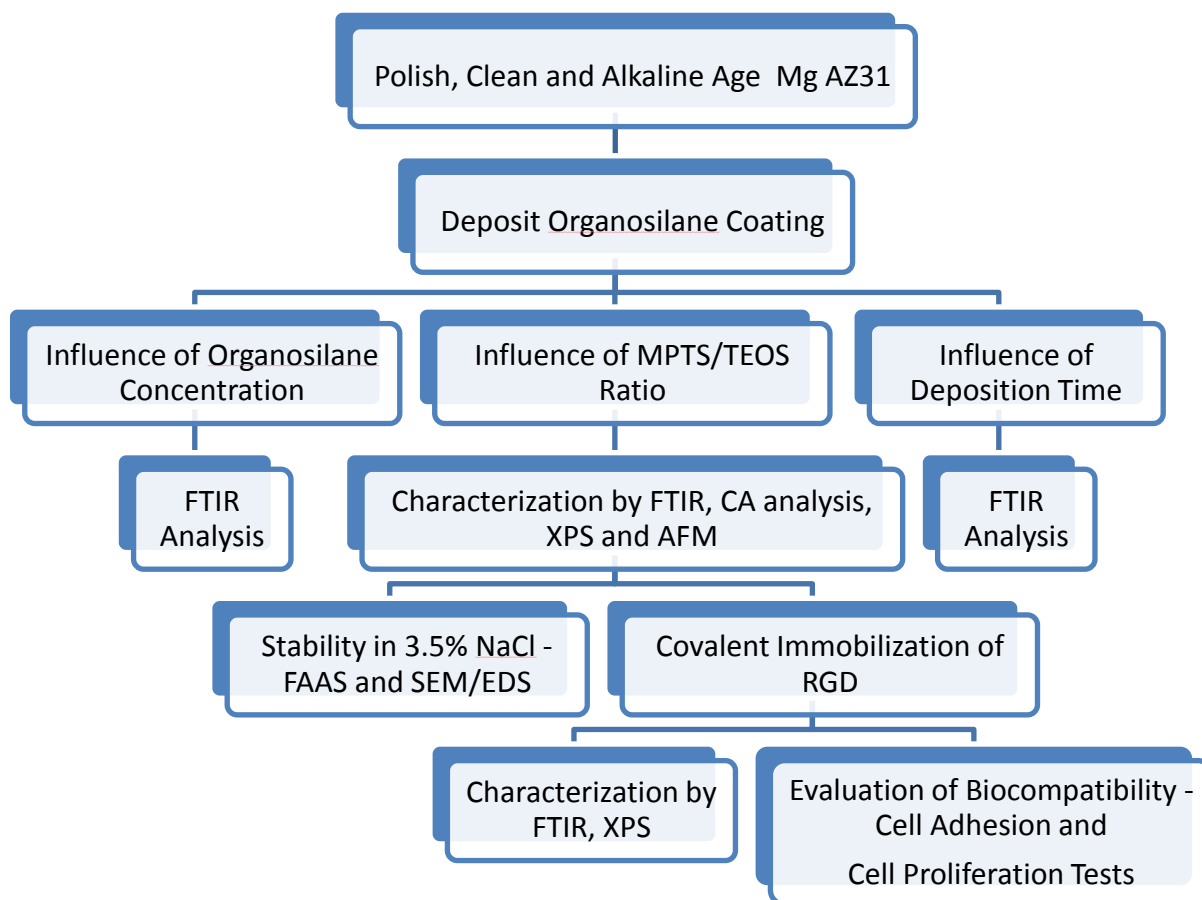
Figure 3.1 Flowchart of the overall experimental procedure.

Figure 3.1 is a general flowchart showing the overall experiments performed in this thesis. In general, polished and cleaned samples were immersed in a methanolic mixed (MPTS and TEOS) organosilane solution. The influence of total silane concentration and deposition time on the deposited coatings was analyzed by Fourier Transformer Infrared Spectroscopy (FTIR). The MPTS/TEOS ratio in the coating bath was varied to produce coatings with different surface densities of the thiol functional group and the resulting coating chemistry and morphology were

examined by FTIR, Contact Angle (CA) Analysis, X-ray Photoelectron Spectroscopy (XPS) and Atomic Force Microscopy (AFM). The stability of the organosilane coatings was evaluated by quantifying the amount of magnesium released into a 3.5% NaCl solution compared to an uncoated substrate using Flame Atomic Absorbance Spectroscopy (FAAS). The corrosion products and stability of the coatings were further characterized using Scanning Electron Microscopy- Energy Dispersion Spectroscopy (SEM/EDS). Finally a procedure was developed for covalent immobilization of RGD peptide to the organosilane coated Mg AZ31 surfaces. The RGD peptide was covalently bonded to the organosilane coated Mg AZ31 substrates through the cross-linking molecule, N-Succinimidyl 3-maleimidopropionate (SMP). The overall chemical reaction is based on established chemistry [56, 77] and is shown in Figure 4.1. The surface density of RGD peptide was controlled by varying the MPTS/TEOS concentration in the organosilane coating bath thus controlling the concentration of the reactive thiol functional group at the surface. The surface properties of the modified coatings were characterized by FTIR, CA and XPS while the *in vitro* biocompatibility was evaluated through cell adhesion and cell proliferation tests. Detailed descriptions of the methodologies employed are given below.

3.2 Materials

Mg AZ31 sheets (1 mm thickness) and SMP were purchased from Alfa Aesar (US). All polishing supplies were purchased from Buehler. 3-Mercaptopropyltrimethoxysilane (MPTS), Tetraethyl orthosilicate (TEOS), N,N-Dimethylformamide (DMF), Sodium Hydroxide and Arginylglycylaspartic acid (RGD) were purchased from Sigma-Aldrich (Canada). Sulfuric acid and Trypan Blue were purchased from Fisher Scientific (Canada). Phosphate Buffered Saline (PBS) (1x), McCoy's 5a, Trypsin EDTA (1X) and Fetal Bovine Serum (FBS) were purchased from Corning (Canada). Penicillin-Streptomycin Solution was purchased from HyClone (Canada). CyQUANT Cell Proliferation Assay was purchased from Life technologies (Canada). Acetone (reagent grade) was purchased from Caledon Laboratory Chemicals. Ethyl alcohol (95%) and methanol were purchased from Commercial Alcohols. All chemicals were used as received

without further purification.

The Saos-2 cell line was purchased from American Type Culture Collection and cultured for further experiments.

3.3 Preparation of Organosilane Solutions

Organosilane solutions were prepared with 3 different volume ratios of MPTS to TEOS including 1:1, 3:1 and pure MPTS while keeping the total volume of organosilane constant. In order to determine the conditions that yielded optimum coatings, the influence of total silane concentration in solution (2%, 4% and 8% (v/v)) at 3 hours and 20 hours deposition time were investigated. Table 3.1 gives the composition of the coating baths for different MPTS/TEOS ratios with 8% (v/v) total organosilane concentration. All other solutions were prepared similarly with a constant 12% (v/v) deionized water and sufficient methanol added to make up the balance. The pH of all silane solutions was adjusted to 4.20 by dropwise addition of 0.1M H_2SO_4 immediately after mixing of the organosilane/water/methanol mixture. All solutions were aged with stirring for 7 hours to ensure complete hydrolysis and optimum conditions for condensation of the silanol groups with hydroxyl groups on the substrate surface.

Table 3.1 The volume percentage of MPTS, TEOS, deionized water and methanol in three different organosilane coating bath solutions.

	MPTS (v/v)	TEOS (v/v)	H_2O (v/v)	CH_3OH(v/v)
1:1	4%	4%	12%	80%
3:1	6%	2%	12%	80%
Pure MPTS	8%	0%	12%	80%

3.4 Preparation of the Magnesium AZ31 Substrate

Mg AZ31 sheets (1 mm thickness) were cut into circular samples with a diameter of 1 cm. The samples were first polished with Buehler-Met II 320 abrasive discs in order to remove the oxide layer and other contaminants on the surface; deionized water was used as the lubricant. After rinsing with acetone, the samples were sequentially polished to a mirror finish with TexMet C polishing pads using MetaDi 9 μm, 3 μm and 1 μm diamond polishing suspension; AutoMet lapping oil was used as the lubricant. The mirror polished AZ31 coupons were sonicated for 15 minutes in acetone and then rinsed well with deionized water for 5 minutes. The polished, degreased coupons were immediately air dried to prevent tarnishing.

The coupons were then immersed in 0.05 M NaOH solution at 50°C for 1 hour, followed by rinsing with copious amounts of deionized water and immediately air dried. The purpose of this step was to produce a surface rich in metal-hydroxyl groups to promote condensation with the SiOH groups in hydrolyzed organosilane solutions, as shown in Figure 1.1.

3.5 Coating Deposition

Each coupon prepared as described in section 3.4 was immersed in 25ml of organosilane solution (section 3.3) polished side up during silanization. Silanization was carried out at 50°C in a water bath without stirring for a designated time. The optimal deposition time was determined in a preliminary test to be 20 hours. The coated coupons were removed from solution, immediately air dried and then cured in an oven at 100°C for 1 hour to promote crosslinking between the organosilane coating and substrate surface as well as the organosilane molecules themselves. This was shown to enhance the stability and strength of multi-layered organosilane coatings in previous studies [39]. The surface chemistry was evaluated by a combination of FTIR and XPS analysis. Contact angle analysis was used to determine the surface wettability as a function of MPTS/TEOS ratio. The topography of the coatings was evaluated by AFM.

3.6 Study of Distribution of Thiol Functional Groups

In order to evaluate the distribution of thiol functional groups on the three different organosilane coatings, a 10 nm gold nanoparticles (AuNP) solution (citrate buffer) was reacted with the organosilane-modified samples. It is well documented that AuNP can specifically bond to thiol functional groups [93, 94], therefore the distribution of AuNP's on organosilane-modified sample substrates is expected to reflect the corresponding distribution of thiol groups on organosilane-modified sample substrates. Four hundred microliters of a 10 nm AuNP solution was allowed to react with each organosilane-modified sample. After 1 hour, samples were removed from the AuNP solution, rinsed with deionized water three times and immediately air dried. Different organosilane-modified samples treated with sodium citrate buffer were applied as a control group, and the preparation of the control group followed the same procedure mentioned above. The surface topographies of samples before and after either AuNP solution or sodium citrate buffer treatment were detected by AFM. The experiment was repeated 3 times.

3.7 Evaluation of Coating Stability – Immersion Test in 3.5% NaCl

The stability of three different silane-coated samples and bare Mg AZ31 were evaluated at room temperature by immersion in 3.5% NaCl solution. The sodium chloride solution was prepared by dissolving 35.0784g of NaCl in 1L of deionized water. Five samples of each type were prepared. Polished, untreated Mg AZ31 coupons were used as a control. The edges and backs of all coupons were sealed with epoxy to ensure that only the coated surface was exposed to the corrosion medium thus ensuring a constant surface area from sample to sample. Each coupon was immersed in 50ml of 3.5% NaCl solution. After 1, 3, 5, 7 and 14 days immersion times, the solutions were mixed well, and then a 25 μl aliquot of this corrosion medium was removed from each tube with a micropipette, and diluted to 10ml in a 2% nitric acid solution. The concentration

of magnesium in the diluted solutions was determined using FAAS. One sample of each type was removed from the NaCl solution after a 1, 3 and 7 day immersion period, washed with deionized water, air dried and further characterized by SEM/EDS.

3.5 Immobilization of RGD Peptide by Cross-linker SMP

After characterization of the organosilane coatings, RGD peptides were covalently bonded through the surface thiol functional groups on the coated Mg AZ31 substrates by using the heterobifunctional cross-linker SMP as previously described in the literature [56, 77]. The SMP solution was prepared at a concentration of 5 mg/ml in dimethylformamide (DMF) and then diluted with pure ethanol to a final concentration of 1.7 mg/ml. Each silanized Mg AZ31 substrate was placed, polished side up, in a separate glass vial; 500 μl of freshly prepared SMP solution was added to each glass vial and allowed to react at room temperature for 1 hour. After reaction with the crosslinker, SMP, the samples were rinsed three times with pure ethanol and once with deionized water to remove non-bonded SMP molecules. The samples were immediately air dried and then immersed in RGD solution. The RGD solution was prepared by dissolving the peptide in warm PBS (1X) to a concentration of 5 mg/ml. Each SMP modified sample was incubated in 400 μl of the RGD solution for 1 hour at room temperature. The RGD modified samples were rinsed with warm PBS solution 3 times to remove the unbonded RGD molecules from the surface, followed by immediate air drying. FTIR spectroscopy, contact angle analysis and XPS were used to evaluate changes in the surface chemistry at each stage of the modification process.

3.6 Surface Characterization

3.6.1 Infrared Spectroscopy

Infrared spectroscopy was performed with a Bruker Optics Hyperion infrared microscope equipped with either a grazing angle objective (GA-FTIR) or an attenuated total reflectance

objective (ATR-FTIR) with a germanium crystal. A liquid nitrogen cooled mercury cadmium telluride (MCT) detector was employed for all studies. The resolution of the spectrometer was 4 cm^{-1} and each spectrum was the result of 100 co-added scans. FTIR spectra were collected from three samples of each type at three different spots per sample (9 measurements/sample type). All presented spectra were baseline corrected and corrected for atmospheric CO_2 and H_2O with the OPUS software. The areas under the peak of the Si-O-Si bands were measured using the OPUS software Mode B.

3.6.2 X-ray Photoelectron Spectroscopy

XPS spectra were recorded on a Kratos Ultra spectrometer at the Alberta Centre for Surface Engineering and Science (ACSES), University of Alberta. The vacuum in the analytical chamber was less than 3×10^{-8} Pa. A monochromatic Al Kα source operated at 168 W was used and the analyzer resolution was 0.80 eV for Au 4f peaks. Two survey scans were recorded from 0-1100 eV at three different spots on each sample surface with a spot size of 300 x 700 μm. The relative concentrations of chemical elements were calculated using the CASAXPS software and a standard quantification routine that included Schofield sensitivity factors and a Shirley background.

3.6.3 Contact Angle Analysis

The geometric water static contact angle was applied in order to analyze the hydrophilicity of organosilane-modified magnesium substrates. Three random spots were analyzed for each sample, and two samples were characterized for each type of organosilane-modified magnesium.

Four microliters of purified 18m Ω water was introduced to the surfaces, and the contact angles were evaluated using a PG-2 Pocket Goniometer with static angles.

3.6.4 Atomic Force Microscopy

Atomic force microscopy images were collected with a Bruker multimode III D AFM. The instrument was run in tapping mode using Bruker AFM TESPA probes. The cantilever probes had a resonant frequency of approximately 320 kHz. Images (10 x 10 μm) were collected at 512 samples/line and a scan rate of 0.5 Hz. The presented images are representative of the whole surface; each image was flattened using the software provided with the instrument.

3.6.5 SEM/EDS analysis

The SEM images were collected with a JEOL 6400 field emission scanning electron microscope operated at an accelerating voltage of 20kV and a beam current of 1nA. The microscope was also equipped with an Oxford EDS detector. The vacuum in the chamber was maintained at approximately 10^{-6} torr and all samples were carbon-coated prior to analysis.

3.7 Cell Culture

Human osteosarcoma Saos-2 cells, purchased from American Type Culture Collection, were stored at -80℃ in a liquid nitrogen dewar for preservation. Cells were recovered and cultured for at least a week prior to performing cell assays. Cells were quickly thawed and pipetted from the storage vial to a 15 ml centrifugation tube and diluted with 5 ml McCoy's 5a cell culture medium containing 15% fetal bovine serum and 1% penicillin (all from Fisher Scientific). The cells were recovered by centrifugation at 2,000 rpm for 5 minutes. The supernatant was discarded gently, and the cell pellet was re-suspended with 5 ml fresh complete McCoy'5a cell culture medium. Saos-2 cells were seeded on a 25 cm^2 Corning cell culture flask and cultured in McCoy's 5a completed medium at 37℃ in a 5% CO_2 atmosphere. The cell culture medium was refreshed every two days. The growth of Saos-2 cells was monitored every morning using an inverted microscope. After a one week incubation period, Saos-2 cells normally grew to

confluence over the bottom of the cell culture flask. Thus, cells were split into two flasks to continue cell growth. To achieve this, the cells were first rinsed with warm PBS solution, and then detached from the flask with 1 ml 0.05% Trypsin/0.53 mM EDTA solution (Fisher Scientific) for 3 minutes at 37℃ in a 5% CO_2 atmosphere. Complete McCoy's 5a cell culture medium was then applied to neutralize the trypsin/EDTA solution. The cell suspension was pipetted to a centrifugation tube and centrifuged at 2,000 rpm for 5 minutes. The cell pellet was re-suspended with complete cell culture medium, split into two flasks, and culture was resumed as described above.

3.8 Cell Adhesion Assay

3.8.1 Preliminary experiments in the absence of Mg AZ31 samples

Prior to performing the adhesion assay with RGD-modified samples, the optimal cell number for the adhesion assay was determined using a CyQUANT kit (Life Technologies). The CyQUANT kit was used according to the instructions provide by Life Technologies. This assay is designed for cell proliferation studies and also can be utilized to detect the adherence of cells to surfaces. By using the completed CyQUANT kit, the cells are first lysed and nucleic acids are dyed in the same solution, the cell number can be obtained by detecting the fluorescence intensity of solution. Saos-2 cells were trypsinized following the procedure described in section 3.7; cell counts were determined in a Neubauer hemacytometer using trypan blue. Serial dilutions were prepared in a 24-well cell culture plate with cell numbers ranging from 150,000 to 9,375 in 600 μl of cell suspension; wells containing 600 μl of cell culture medium were set as the control group. All cell numbers were plated in triplicate. Saos-2 cells were allowed to adhere to the plate for 16 hours in cell culture medium at 37℃ in a 5% CO_2 atmosphere. After the incubation period, the cell culture medium was discarded, and the wells were gently washed with warm PBS solution three times to remove dead and loosely attached cells, and to eliminate residual cell culture medium

containing Phenol red (which could interfere with the fluorescence of the CyQUANT Kit dye). The cell culture plates were placed upside down on paper towels to remove residual liquid from the wells and then 400 μl of freshly prepared CyQUANT solution was added to each well. The plate was wrapped in aluminum foil to avoid light and then incubated for 5 minutes at room temperature. At the end of the incubation period, 100 μl of the CyQUANT solution was pipetted out from each well to black EIA/RIA 96-Well plate (Costar) and the fluorescence intensities of each solution was measured with Fluostar OPTIMA fluorescence microplate reader. The detected signal intensities versus of known cell numbers were plotted and the linear range was determined.

The optimal time point for the Saos-2 cell adhesion assay was also investigated. The optimal cell number obtained from preliminary experiments was seeded on 24-wells cell culture plates and 1, 2, 4, 6 and 8 hours were selected as potential time points for the cell adhesion assay. Triplicate wells were prepared for each time point. At the desired time, the wells were washed and dried, and then cell numbers were measured with the CyQUANT assay as described above.

3.8.2 Cell adhesion on Mg AZ31 samples

Prior to the adhesion experiment, all investigated samples were sterilized in 70% ethanol for 1 hour followed by rinsing with warm, sterile PBS and allowed to dry in a laminar flow hood. In order to evaluate the capacity of RGD-modified Mg AZ31 to promote Saos-2 cell adhesion, 40,000 cells were allowed to adhere on the substrates for 3 hours at 37℃ in a 5% CO_2 atmosphere. The cell number and adhesion time were determined in section 3.8.1. Unmodified Mg AZ31 and organosilane-coated RGD-free samples were used as negative controls. After the incubation period, the samples were gently rinsed with warm PBS three times in order to remove non-adherent cells. Four hundred microliters of CyQUANT solution was added to each sample and incubated for 5 minutes. One hundred microliters of the cell lysate was pipetted into a black microplate and the fluorescence level was determined as described above.

3.9 Cell Proliferation Assay

To investigate the appropriate cell number for the cell proliferation assay, two groups containing 5,000 and 15,000 cells were evaluated in terms of cell proliferation for up to 10 days. Cells plated on 24-well cell culture plates were measured with the CyQUANT kit at 3, 6, 7, 9 and 10 days after seeding. The cell culture medium was refreshed every two days. Each time point was performed in triplicate. Cell number as a function of incubation period was plotted to evaluate Saos-2 cell proliferation.

RGD-modified and unmodified Mg AZ31 samples were sterilized as described in section 3.8.2. The appropriate cell number, 5,000 cells, determined at the experiment mentioned above were seeded on investigated substrates and incubated at 37℃ in a 5% CO_2 atmosphere for 3 and 10 days. The cell culture medium was refreshed every two days. After the required incubation period, cell numbers on the substrates were measured using the CyQUANT kit as described in section 3.8.

Chapter 4 : Results and Discussion

The main objective of this thesis was to develop a surface modification strategy for Mg AZ31 that gives controlled degradation rates and improved cell/surface interactions. The first stage of the project was to deposit stable covalently bonded mixed organosilane coatings on the magnesium substrate surface to improve its corrosion resistance. These mixed organosilane layers were further surface modified to improve their biocompatibility through covalent immobilization of the RGD cell adhesion peptide. The proposed surface modification procedure is illustrated in Figure 4.1.

The organosilane coated Mg AZ31 substrates were produced by immersion coating in a mixed organosilane coating bath containing MPTS and TEOS in various ratios. The hydrolysis and condensation reactions are shown in steps 1 and 2 of Figure 4.1. These mixed organosilane layers contain the thiol functional groups with different surface densities. These surface thiols then react with the maleimidyl group of the heterobifunctional cross-linker SMP (step 3) followed by immobilization of RGD peptide through amide bond formation between the free ends of the succinimidyl group and the primary amines of RGD peptide (step 4). The final proposed surface modified product is illustrated in step 5 of Figure 4.1.

Step 1:

CH₃O—Si(—OCH₃)(—OCH₃)—(CH₂)₃—SH   +   CH₃CH₂O—Si(—OCH₂CH₃)(—OCH₂CH₃)—OCH₂CH₃

Hydrolysis

Step 2:

Mg AZ31 (—OH, —OH, —OH)   +   HO—Si(—OH)(—OH)—(CH₂)₃—SH   +   HO—Si(—OH)(—OH)—OH

Condensation

Step 3:

O—Si(—OH)—(CH₂)₃—SH ; O—Si—OH   +   (succinimidyl group) N—(CH₂)₂—C(=O)—O—N (succinimidyl)

Step 4:

O—Si(—OH)—(CH₂)₃—S—(maleimide ring) N—(CH₂)₂—C(=O)—O—N (succinimidyl)   +   NH₂ — RGD

Step 5:

O—Si(—OH)—(CH₂)₃—S—(maleimide ring) N—(CH₂)₂—C(=O)—NH — RGD
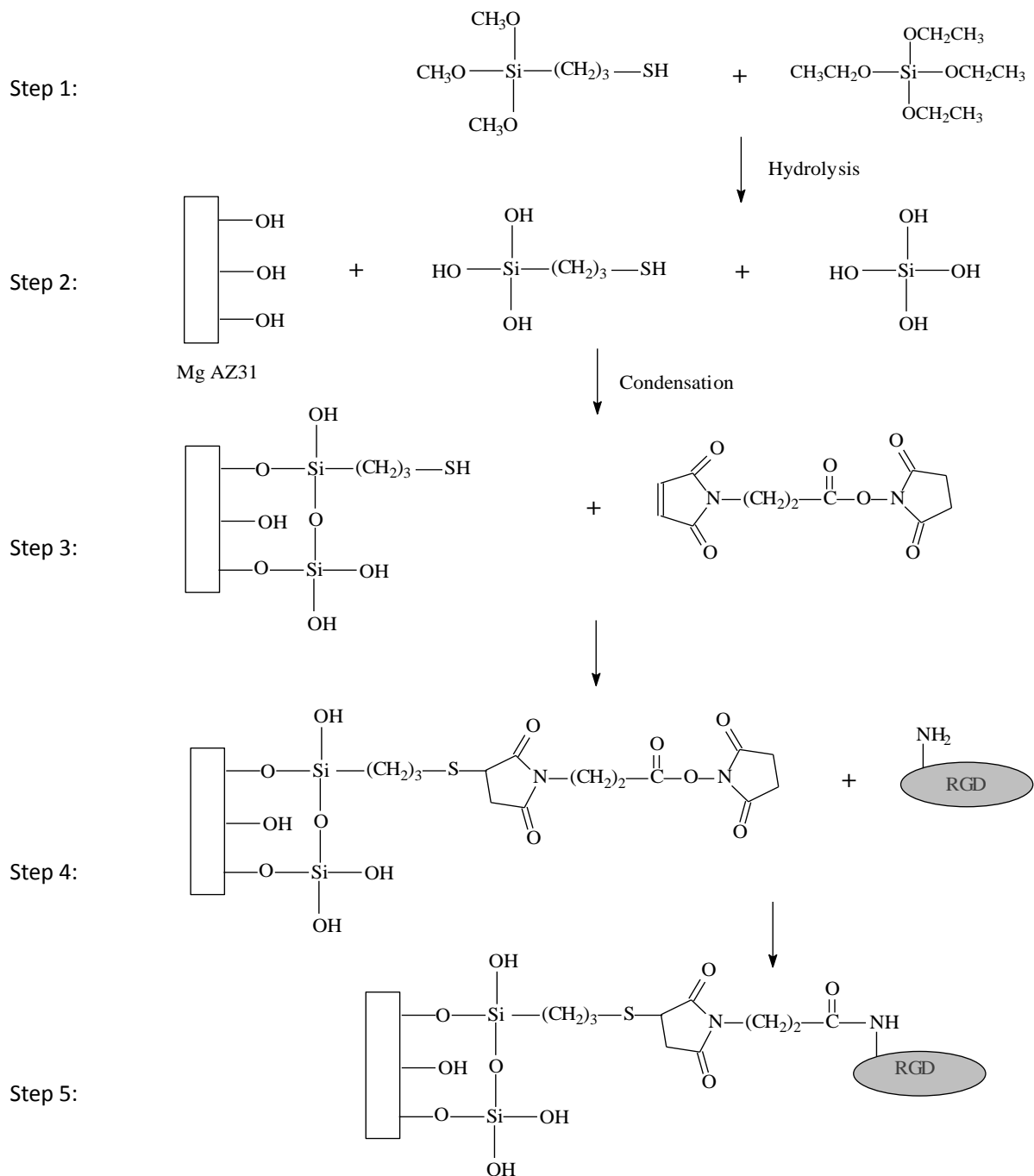
Figure 4.1 Schematic representation of the proposed surface modification strategy. Steps 1 and 2 illustrate the formation of the organosilane coating on the surface. Step 3 and 4 show the reaction of the crosslinker SMP with surface thiols and peptide amine groups. Step 5 is a schematic diagram of the final modified surface.

4.1 Characterization of the Mixed Organosilane Coating

In this section of the thesis, the influence of total organosilane concentration in the coating bath, deposition time and MPTS/TEOS ratio on the surface chemistry, wettability and thiol surface density and distribution in the film were investigated with a combination of FTIR spectroscopy, XPS, CA analysis and AFM.

4.1.1. Optimization of Coating Conditions

There are various factors that affect the extent and rate of organosilane hydrolysis and condensation reactions including pH, the amount of water present, pre-hydrolysis time and temperature. These factors have been shown to further affect the performance and quality of the deposited coating [39, 40, 46, 47]. For example, previous studies in our laboratory have demonstrated that, compared with pH 7 and pH 10, the hydrolysis reaction of MPTS at pH 4 was favored and that complete hydrolysis occurred within 6 hours. Moreover, a uniform MPTS coating with high corrosion resistance was deposited on a magnesium substrate as a result of an increase in Si-OH groups available for surface bonding, coupled with minimal condensation oligomers present in solution at pH 4. TEOS has also been observed to have a higher hydrolysis rate in acidic aqueous media compared to neutral pH [95]. Therefore, pH 4 with a pre-hydrolysis time of 7 hours were chosen as optimum conditions for the coating solution used to deposit the mixed MPTS/TEOS coatings on Mg AZ31 in the experiments described below.

In addition, Zucchi et al demonstrated that higher local pH of the substrate surface led to improved organosilane deposition which may be due to the ability of the higher pH to promote the condensation reaction at the substrate/coating bath interface [96]. Therefore, metal hydroxyl groups were produced by alkaline aging Mg alloy AZ31 in 0.05M sodium hydroxide solution to induce a strongly bonded metal-siloxane film on the substrate.

The influence of two other experimental factors, total organosilane concentration and deposition time, were experimentally determined in this thesis and the results are discussed in section 4.1.1.1 below.

4.1.1.1 Influence of Organosilane Concentration and Deposition Time

After alkaline aging, the Mg AZ31 samples were immersed into organosilane solutions (pH 4, pre-hydrolyzed for 7 h) with an MPTS/TEOS ratios of 1:1 at total silane concentrations of 2% (v/v), 4% (v/v) and 8% (v/v) for either 3 h or 20 h. The coatings were analyzed by grazing angle infrared spectroscopy. Infrared spectroscopy has been widely used as a reliable tool to study the types of chemical bonds in organic films, and can further identify a molecule's structure. In this study, a grazing angle objective coupled with infrared microscopy was used to analyze the thin surface coating due to its improved surface sensitivity.

First, the optimum concentration of mixed organosilane solution that gave uniform coatings was determined at short deposition time. The alkaline aged Mg alloy AZ31 samples were placed into 1:1 MPTS/TEOS mixed organosilane solution containing different total concentrations of organosilanes for 3 hours. Representative infrared spectra of the deposited organosilane coatings collected by GA-FTIR are shown in Figure 4.2.

There are three important peaks observed in the spectra collected on the coated magnesium samples; Si-O-Si, S-H and -CH$_2$/-CH$_3$ stretching vibrations at approximately 1050 cm^{-1}, 2550 cm^{-1} and 2900 cm^{-1}, respectively. The strong peak around 1050 cm^{-1} are from the Si-O stretching vibration which indicates siloxane film formation on the magnesium substrates [36]. The S-H and -CH$_2$/-CH$_3$ stretching vibrations can be attributed to the thiol functionalized aliphatic propyl chain of MPTS.
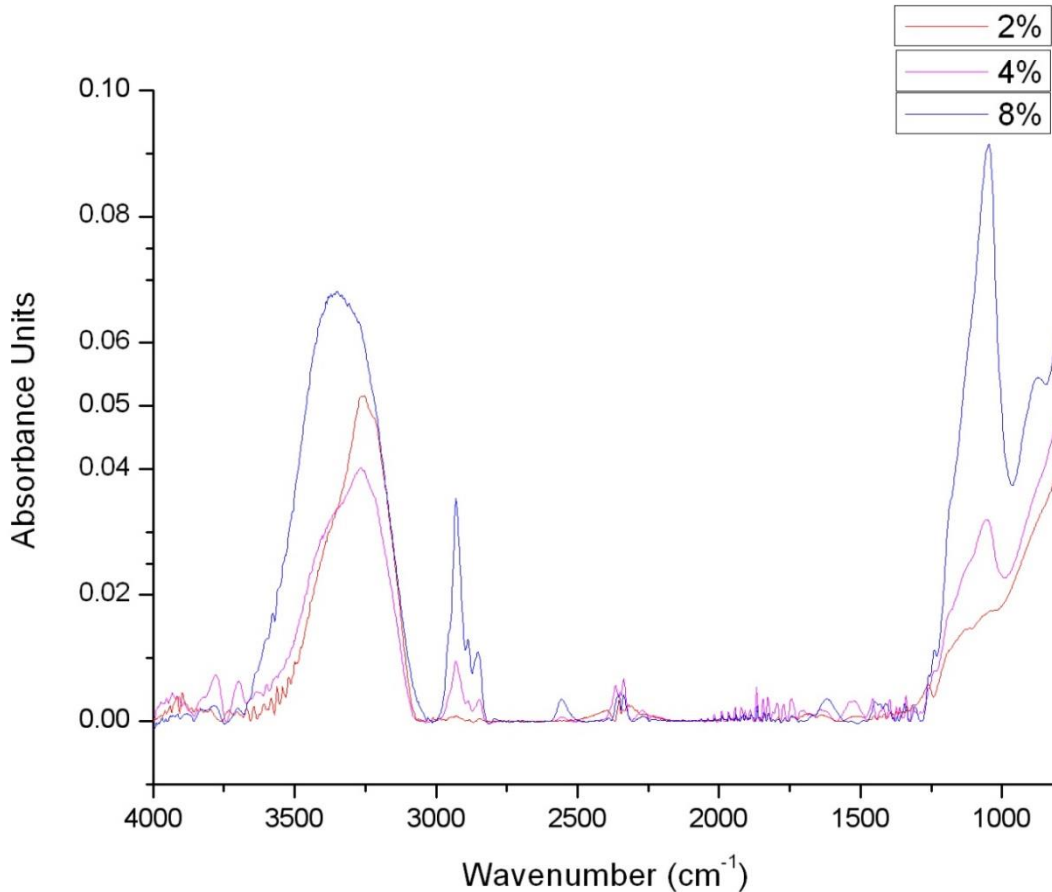
Figure 4.2 The GA-FTIR spectra of Mg AZ31 substrates coated in coating baths containing 3 different total concentrations (──── 2% (v/v), ──── 4% (v/v) and ──── 8%(v/v)) of a 1:1 MPTS/TEOS mixed organosilane solution for 3 hours.

As shown in Figure 4.2, the spectra collected for coatings prepared from the 2% organosilane solution did not contain the peaks typically associated with organosilane coatings, in fact only the O-H stretch peak at 3230 cm^{-1} was observed. However, by raising the organosilane concentration in solution, peaks due to the Si-O stretching vibration at 1050 cm^{-1} appeared for the coatings deposited from 4% (v/v) and 8% (v/v) solutions. The intensity of this peak and those of peaks due to stretching vibration from –SH and -CH$_2$/-CH$_3$ all increased as a function of increasing concentration of organosilane in solution. This result demonstrates that as the

concentration of organosilane in the coating bath increases, the organosilane molecules efficiently condense with each other and also with magnesium hydroxyl groups on the substrate surface. Furthermore, the thickest organosilane coatings were deposited on the Mg AZ31 substrate from the 8%(v/v) mixed organosilane solution.
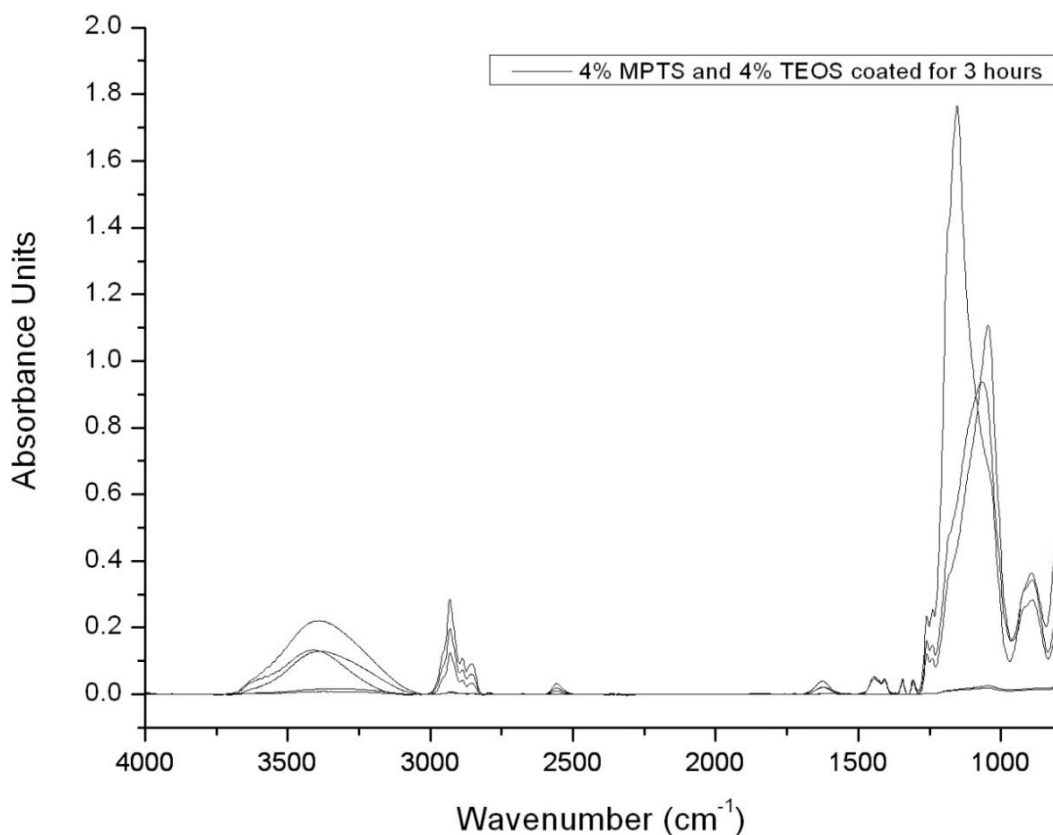
Figure 4.3 The GA-FTIR spectra of Mg AZ31 substrates coated from an 8% (v/v) mixed organosilane coating (1:1 MPTS/TEOS) bath for 3 hours. The presented spectra were collected from 5 different spots on the same sample.

However, the organosilane coating deposited from the 8% (v/v) mixed organosilane solution was non-uniform. This is illustrated in Figure 4.3 which presents the spectra obtained on 5 different areas of a sample coated from an 8% (v/v) solution. The intensity of the Si-O peak was observed to vary significantly from spot to spot. In two spots on the sample no peaks were detected

indicating little to no organosilane deposition in these areas. On the other hand, there was one random spot with an extremely intense Si-O-Si peak around 1050cm^{-1} representing a specific spot where more organosilane molecules had condensed onto the magnesium surface forming a relatively thick film. This non-uniform distribution of the organosilane coating could cause localized corrosion which would affect the corrosion resistance of the coating and further decrease its stability in aqueous media. This non-uniformity of coating may be caused by the formation of oligomers in solution or low surface condensation at short deposition time. In this thesis, a final biocompatible coating will be applied on top of the organosilane coating; a stable pretreatment is essential for subsequent immobilization of biomolecules. Thus the influence of increasing the deposition time was studied as a means to develop a better protective coating with higher uniformity and increased thickness.

The deposition time for 2% (v/v) and 8% (v/v) mixed (1:1 MPTS/TEOS) organosilane solutions was increased to 20 h. A total of 9 GA-FTIR spectra were collected for each deposition time (3 samples, 3 different spots on each) in order to compare the sample thickness and uniformity as a function of deposition time at the two different concentrations. The average area under the Si-O-Si band at 1050 cm^{-1} is representative of the difference in coating thickness while the error bars are indicative of film uniformity. The results are shown graphically in Figure 4.4.
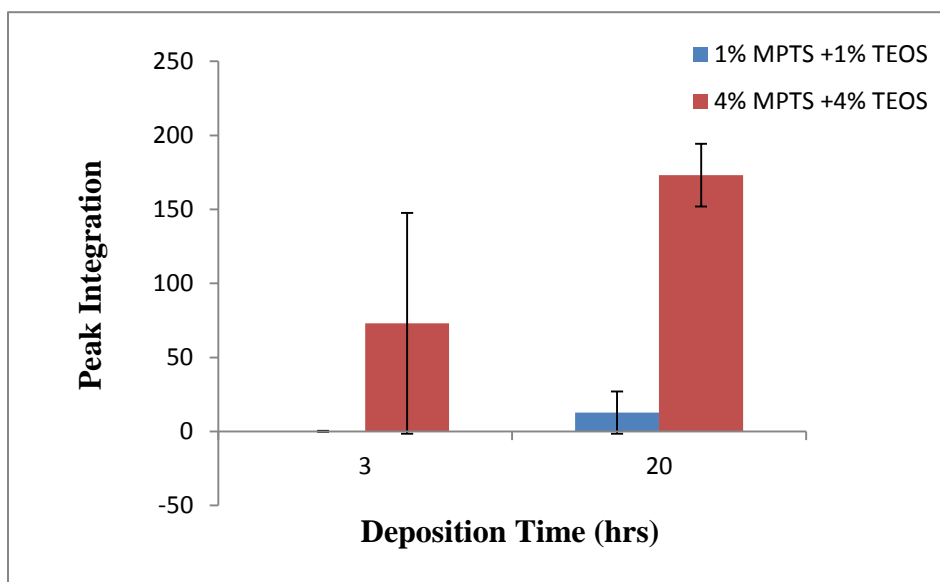
Figure 4.4 The calculated peak areas for the Si-O-Si peak at 1050 cm^{-1} of the coatings deposited from 2% (blue) and 8% (red) 1:1 (MPTS/TEOS) coating baths for 3h and 20h on Mg AZ31 substrates. Data are the average ±standard deviation of 9 measurements.

It is clear from Figure 4.4 that extending the deposition time leads to a significant increase in the thickness of the coatings deposited from either 2% (v/v) or 8% (v/v) coating baths. However, the coating deposited from 2% (v/v) solution for 20h had a relatively low film thickness with a large standard deviation indicating spot to spot and sample to sample variations in film thickness at this concentration. When the organosilane concentration was increased to 8% (v/v) but deposition was for a short deposition time, the film thickness did increase in comparison to coatings prepared from a 2% (v/v) coating bath. However, the error bars remained large due to film non-uniformity. In comparison, when the deposition time was increased to 20 h the average area under the Si-O-Si peak increased two-fold and the spot to spot/sample to sample standard deviation decreased significantly indicating good film uniformity. In summary, these results indicate that the optimum conditions for depositing a uniform functionalized coating with an appropriate thickness are 8% (v/v) total organosilane concentration coupled with a coating deposition time of 20 h.

4.1.2 Surface Thiol Density and Distribution as a Function of MPTS/TEOS Ratio.

In this thesis, mixed organosilane solutions were used to control the surface density and distribution of a thiol functional group which will be subsequently used to covalently bond the RGD peptide to the Mg AZ31 surface through the heterobifunctional crosslinker, SMP.

The mixed organosilane solutions used in this thesis contained two different organosilanes, MTPS and TEOS. The MPTS molecule contains three methoxy-chains and a thiol functionalized short alkyl chain attached to a central silicon atom while the TEOS molecule has four ethoxy groups attached to a central silicon atom (Figure 4.1). The surface density of the thiol groups in the organosilane coating was expected to be controlled by varying the volume ratio of the two organosilanes in mixed coating bath solutions. The total concentration of organosilane in solution was kept constant for all ratios (8% (v/v)). The compositions of the mixed organosilane coating solutions are given in Table 3.1. The influence of the MPTS/TEOS ratio in the coating bath on surface wettability was examined by CA analysis. The thiol surface density was evaluated with a combination of ATR-FTIR spectroscopy and X-ray photoelectron spectroscopy (XPS). The topography of the deposited coatings and the distribution of the thiol groups were analyzed by AFM.

4.1.2.1 Water Contact Angle Results

The influence of the MPTS/TEOS ratio in the coating bath on the wettability of the deposited coatings was examined by contact angle analysis. Due to the hydrophobic nature of the thiol functionalized alkyl chain of the MPTS molecule, it was expected that an increase in the amount of MPTS in the final coating should result in increased hydrophobicity of the coating surface. Three spots were analyzed on each sample, and 2 samples were chosen randomly for each type of organosilane-modified magnesium substrates. Figure 4.5 shows the water contact angle, θ

(H$_2$O), of three different organosilane-modified magnesium substrates as a function of the mole % of MPTS in the coating bath. The contact angle of unmodified magnesium substrates was 74.4 ° (±1.0 °), indicating that the polished and cleaned Mg AZ31 surfaces were slightly hydrophobic. The contact angle for organosilane coatings deposited from a pure MPTS coating solution was 71.1 ° (±4.9 °), for coatings deposited from the 3:1 and 1:1 mixed coatings solutions the contact angles decreased to 63.5 °(±1.9 °) and 56.9 °(±1.0 °). This demonstrates that the wettability of the coatings increased as the amount of MPTS in the coating bath decreased. In addition, as shown in Figure 4.5, θ (H$_2$O) linearly correlates with the mole fraction of MPTS in the coating solution. This linear relationship demonstrates that the MPTS/TEOS ratio in the coating bath translates to a controlled variation of the MPTS/TEOS ratio at the Mg AZ31 surface. Furthermore, the small low standard deviations observed (approximately ±4.9 °) confirm that all three organosilane coatings were evenly distributed across the surface of the Mg AZ31 substrates and that the coatings were reproducible.
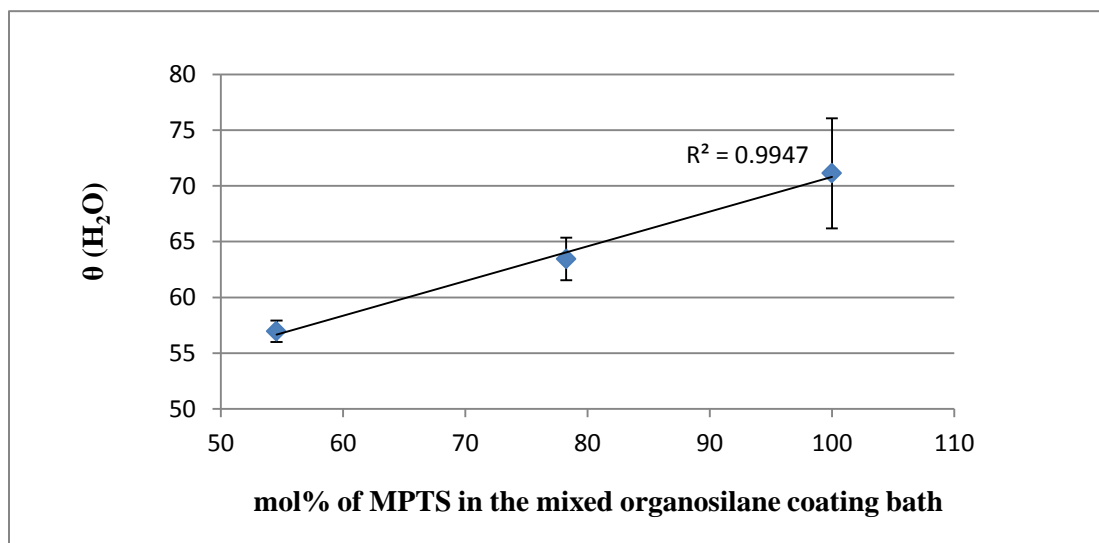
Figure 4.5 The water contact angles, θ (H$_2$O), of three different organosilane-modified magnesium substrates as a function of the mole fraction of MPTS in the coating bath. Data are the average ± standard deviation of 6 measurements.

4.1.2.1 ATR-FTIR Results

A total of 9 ATR-FTIR (3 samples, 3 spots on each) spectra were collected for each coating deposited from solutions with 1:1 and 3:1 MPTS/TEOS ratios as well as pure MPTS solutions. In each case, the films were uniform across the surface of the Mg AZ31 substrates and the spectra were reproducible from sample to sample (results not shown).
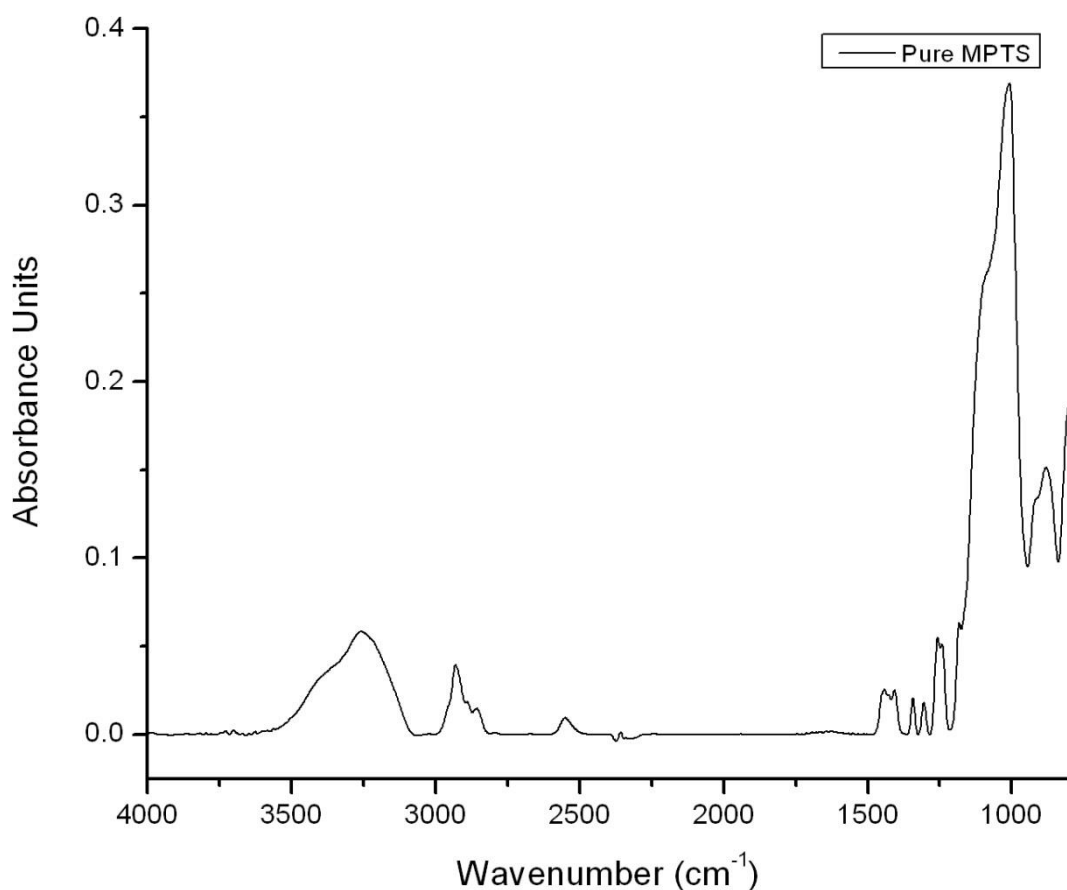
Figure 4.6 The ATR-FTIR spectrum of Mg AZ31 coated from an 8% (v/v) pure MPTS organosilane coating bath for 20h.

Figure 4.6 shows the ATR-FTIR spectrum of Mg AZ31 coated from a solution containing only 8%

(v/v) MPTS. The broad peak at 3261 cm^{-1} with a shoulder at 3414 cm^{-1} can be attributed to O-H stretching vibrations associated with intermolecular hydrogen bonding between adjacent Si-OH groups within the coating. The presence of this broad peak confirms that the MPTS coating is a "polymeric" network structure rather than an organosilane monolayer [97] confirming that the deposited coating is multilayered. The absence of a sharp O-H stretch peak at 3650 cm^{-1} from Mg-OH confirms that the coating thickness exceeds the sampling depth of the instrument (approximately 1 μm). The peaks at 2930 cm^{-1} and 2856 cm^{-1} are due to the asymmetric stretching (v_{as} CH$_2$, CH$_3$) and symmetric stretching (v_s CH$_2$, CH$_3$) respectively from the alkyl chain of MPTS and any unhydrolyzed alkoxy side chains.

The S-H stretching vibration from the thiol group at the end of the alkyl chain of MPTS was observed at 2552 cm^{-1}. The S-H stretching band is weak and is difficult to detect when the surface density of thiol group is low [97]. However, in Figure 4.6 the thiol peak at 2552 cm^{-1} was readily observed (Intensity = 0.01 a.u) which means that the surface density of thiol groups is high. The peaks detected at 1448, 1411, 1345 and 1305 cm^{-1} were attributed to the bending vibrations of CH$_2$ in the alkyl chain while the peaks exhibited at 1257 and 1242 cm^{-1} are a combination of Si-C, C-C and C-S stretching vibrations. The peaks due to S-H (2552 cm^{-1} and Si-C (1257 cm^{-1}) are particularly useful for identifying the presence of MPTS in the mixed organosilane layers described in the sections to follow, as these functional groups are not present in TEOS. The highest intensity peak centered around 1050 cm^{-1} is due to the Si-O-Si stretching vibration. The small peak at 1088 cm^{-1} is a C-O stretching band; the presence of this peak may be due to incomplete hydrolysis of all of the alkoxy groups on the organosilane molecules.
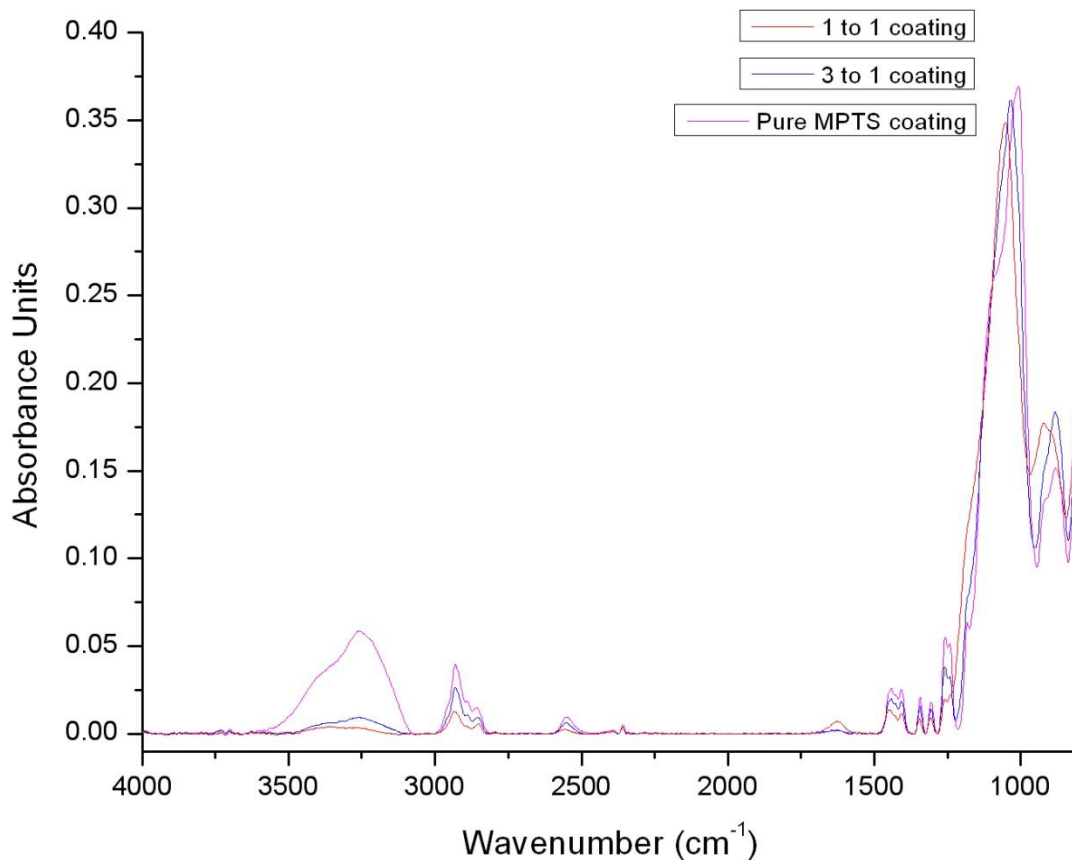
Figure 4.7 The ATR-FTIR spectra of Mg AZ31 substrates coated from mixed organosilane coating baths (⎯⎯ 1:1 coating, ⎯⎯ 3:1 coating and ⎯⎯ Pure MPTS coating) under the optimized conditions.

Figure 4.7 compares representative ATR-FTIR spectra of organosilane coatings on Mg AZ31 deposited from solutions with 1:1 and 3:1 MPTS/TEOS ratios as well as pure MPTS. The specific infrared peaks mentioned above were clearly seen for all three spectra indicating the presence of MPTS in all three coatings. The Si-O-Si peak were at similar peak intensity on all three coating types, indicating that the organosilane surface density was constant for all three different coatings. However, an increase in the Si-C peak intensity at 1250 cm^{-1} was observed as the molar percentage of MPTS in the coating bath was increased. Moreover, all of the specific

peaks of MPTS were decreased as the ratio of MPTS to TEOS decreased. These result indicated that TEOS and MPTS were both successfully deposited on magnesium substrates to give mixed (3:1 and 1:1 MPTS/TEOS) coatings.
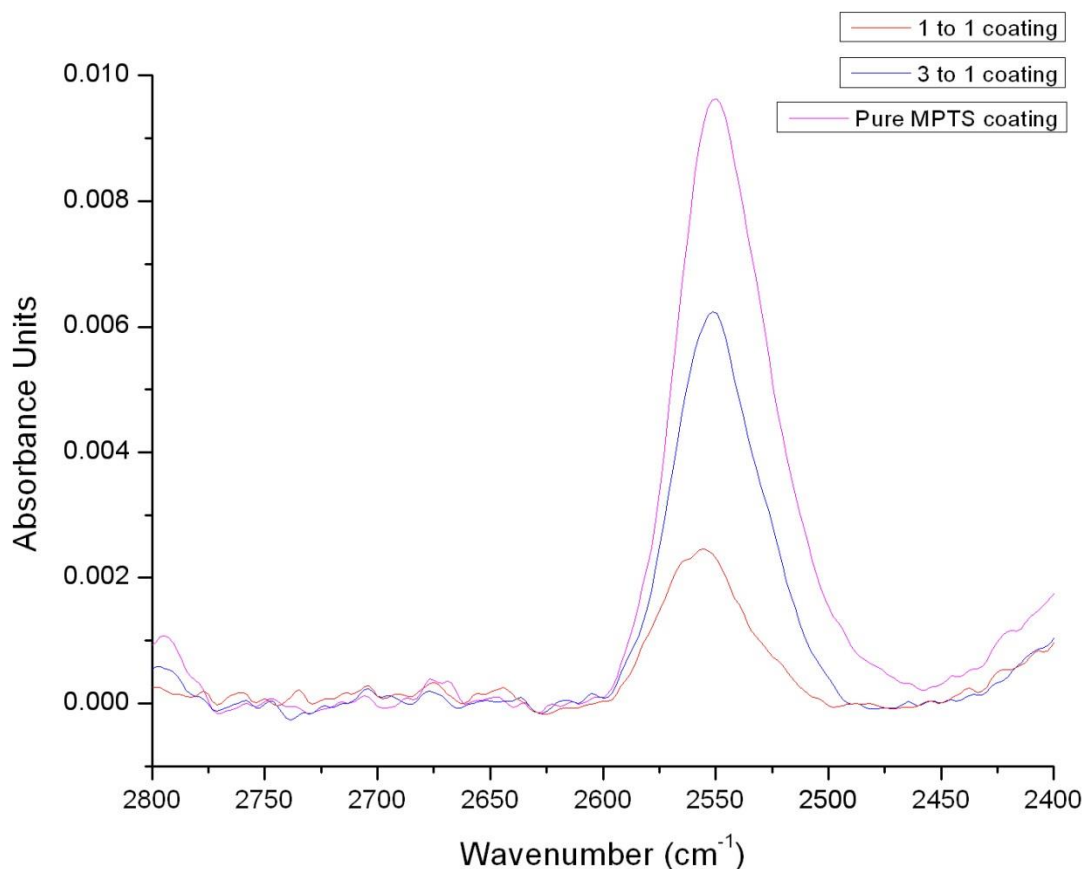
Figure 4.8 The ATR-FTIR spectra of Mg AZ31 substrates coated from mixed organosilane coating baths (—— 1:1 coating, —— 3:1 coating and —— Pure MPTS coating) under the optimized conditions in the range of 2400 to 2800 cm^{-1}.

Figure 4.8 shows the same spectra but is enlarged in the region where the thiol functional group is typically observed (2400 to 2800 cm^{-1}). In this region, it is apparent that the intensity of the peak due to the S-H stretch of the thiol group at 2550 cm^{-1} gradually decreased as the

MPTS/TEOS in the coating bath ratio decreased. These results confirm that mixed organosilane coatings were successfully deposited on the Mg AZ31 substrate surface. Furthermore, variations in the MPTS/TEOS ratio in the coating bath solution were observed to affect the surface density of the thiol group in the protective coating.

4.1.2.3 X-Ray Photoelectron Spectroscopy Results

The ATR-FTIR technique has limited surface sensitivity as the probing depth is on the order of a micrometer. Therefore, a more surface sensitive technique (5-10 nm probing depth), XPS, was used to further evaluate the thiol surface density of the coatings. Three different random spots were detected on three different organosilane-modified magnesium substrates. The atomic percentages obtained by XPS from each type of silanized sample are given in Table 4.1.

Table 4.1. XPS atomic concentrations of oxygen, nitrogen, carbon, sulfur and silicon for three different organosilane coatings on Mg AZ31 substrates. The reported values are an average of three measurements on three different areas of each sample.

Peak	Type of Coating		
	1:1 MPTS/TEOS	3:1 MPTS/TEOS	Pure MPTS
O 1s	38.55±0.14	32.64±0.35	28.53±0.77
N 1s	0.68±0.15	0±0	0.83±0.04
C 1s	39.35±0.10	44.70±0.11	50.45±0.87
S 2s	6.19±0.23	8.22±0.44	8.95±0.33
Si 2p	15.24±0.31	14.44±0.15	11.25±0.16

The absence of the Mg 1s peak in all recorded spectra confirms that the coating uniformly covers the surface of the Mg AZ31 substrate with a thickness greater than 5-10 nm. For all three organosilane coatings, four main peaks, O 1s, C 1s, S 2s and Si 2p, were observed in the XPS spectra at 530, 283, 225 and 101 eV, respectively. These signals can be attributed to the organosilane coatings. Moreover, N 1s peaks appeared at 400 eV in the spectra of both the 1:1 and pure MPTS silanized substrates. This is likely due to a small amount of contamination from the atmosphere or other sources. The atomic % of oxygen decreased as the ratio of MPTS to TEOS in the coating increased, while that of both of carbon and sulfur were generally higher. These observed trends can be explained by differences in the MPTS/TEOS ratios in the coatings. As the overall concentration of MPTS in the coating bath increased, the carbon and sulfur levels also increased as expected. In comparison to the 3:1 and pure MPTS coatings, the surface of the 1:1 coating showed the highest atomic concentration of oxygen. This was expected as the amount of TEOS in the coating increased because hydrolyzed TEOS molecules contain only silicon and oxygen atoms, resulting in the presence of silanol groups at the coating surface. In general, as the amount of MPTS was increased in the coating bath, there was a gradual increase in the number of MPTS molecules in the surface coatings and a concomitant decrease in the number of TEOS molecules. This is reflected by a decrease in surface hydroxyl groups coupled with an increase in surface thiol as the MPTS/TEOS ratio in the coating increases. The variation in the surface MPTS/TEOS ratio of the coating is further reflected in the observed increase in C/Si ratio from 2.6 (1:1 MPTS/TEOS) to 3.1 (3:1 MPTS/TEOS) and finally 4.5 (Pure MPTS) coatings. As the amount of MPTS in the coating increases, the relative amount of surface carbon also increases due to the alkyl chain of the MPTS molecule.

In order to confirm that increasing the concentration of MPTS in the coating bath results in an increase in the surface density of thiol groups, the S/Si ratio for each coating was calculated and plotted as a function of mol% of MPTS in the organosilane coating bath (Figure 4.9). A linear relationship was observed indicating that an increase in the ratio of MPTS to TEOS in the coating bath translates to an increase in the surface density of thiol groups on the silanized

substrates. In addition, the small error bars indicate that the thiol surface density is similar over the whole surface of the silanized substrate.
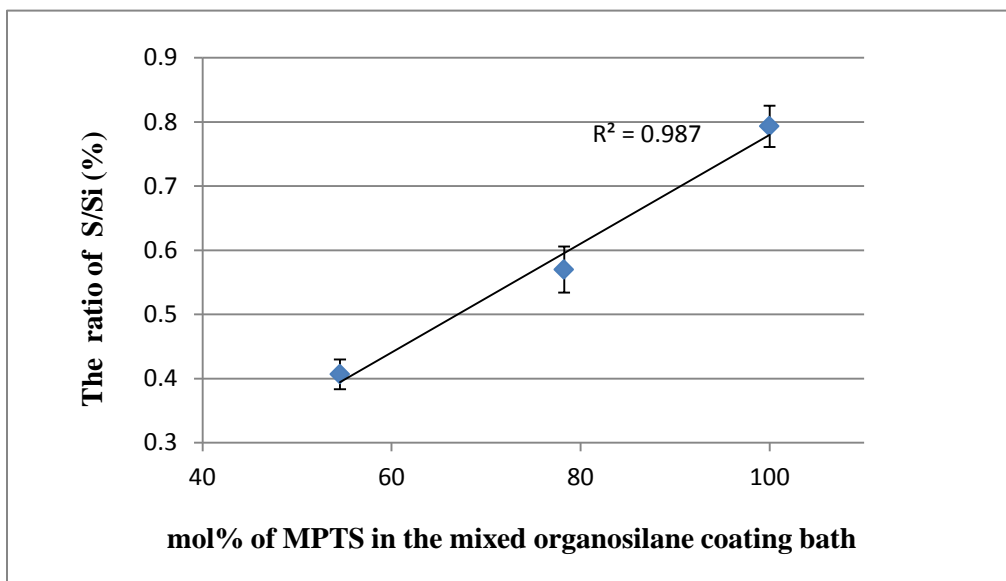
Figure 4.9 XPS analysis of mixed organosilane coatings. S/Si atomic % ratio as a function of mol% of MPTS in the coating bath. Data are the average ± standard deviation of 3 measurements.

These XPS results, coupled with the previously discussed CA analysis and ATR-FTIR results confirm that organosilane coatings deposited from a mixed organosilane coating bath result in the deposition of both types of organosilane molecules on the Mg AZ31 substrate. Furthermore, the combined results indicate that a variation in MPTS/TEOS ratio in the coating bath translates to a controlled variation in the number of thiol groups available for subsequent reaction on the silanized surface.

4.1.2.4 Atomic Force Microscopy Results

The topography of the deposited organosilane films and the overall distribution of the thiol groups at the coating surface were investigated by atomic force microscopy. Figure 4.10 (a-c) shows the topography of the as-deposited organosilane coatings with different MPTS/TEOS ratios. All of the images presented are 10 x 10 μm. No island-like structure were observed on 3:1 and pure MPTS organosilane coating surfaces, (Figure 4.10 (b-c)) and the height scale of these two images were both lower than 7 nm. On the 1:1 coating surface, a few islands of individual spherical clusters were observed. These are likely due to the deposition of a few small organosilane particles originally formed through self-condensation of hydrolyzed organosilane molecules in solution. It can be clearly seen that the majority of the 1:1 surface is a uniform layer with a height scale of approximately 7 nm. Therefore, all three organosilane coatings were smooth and uniform at the 10 x 10 μm scale.

(a)

(b)

(c)

(d)

(e)

(f)

(g)

Figure 4.10 10 x 10 μm scale AFM images of 1:1 (MPTS/TEOS) organosilane coated (a), 3:1 (MPTS/TEOS) organosilane coated (b) and pure MPTS organosilane coated (c) Mg AZ31 before 10 nm AuNP treatment, and AFM images of 1:1 (MPTS/TEOS) organosilane coated (d), 3:1 (MPTS/TEOS) or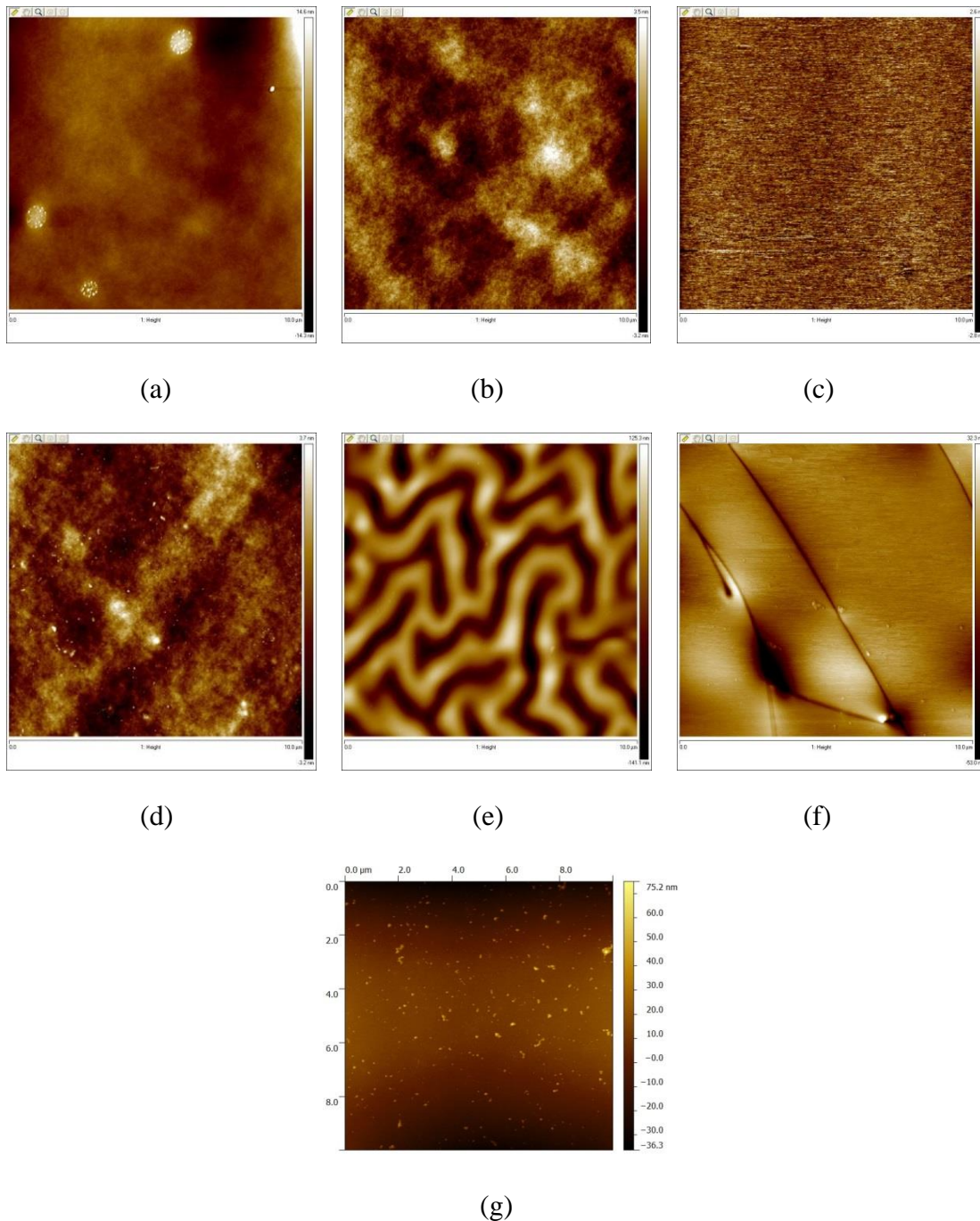ganosilane coated (e) and pure MPTS organosilane coated (f) Mg AZ31 after 10 nm AuNP treatment, and AFM image of 3:1 (MPTS/TEOS) organosilane coated Mg AZ31 control group with sodium citrate buffer treatment (g).

The surface distribution of the thiol groups was examined by immersing the organosilane coated samples in a solution of 10 nm gold nanoparticles (AuNP) for 1 hour followed by vigorous rinsing to remove non-bonded AuNP's. It is well documented that gold interacts strongly with thiol groups to form Au-S covalent bonds [93, 94]. It was our hypothesis that gold nanoparticles should therefore bond to the surface through the thiol groups from MPTS on the silanized substrate. An increase in the number of surface thiol groups was expected to yield an increase in gold nanoparticle coverage. Furthermore, the distribution of the thiol groups (homogeneous distribution of MPTS and TEOS throughout the coating or not) was anticipated to be reflected in the distribution of the gold nanoparticles on the coating surface. AFM images of the organosilane coated Mg AZ31 surfaces after gold nanoparticle treatment are presented in Figure 4.10 (d-e).

The coating prepared from a solution with an MPTS/TEOS ratio of 1:1 showed no significant difference after treatment with gold nanoparticles (Figure 4.10 d). This may indicate that the MPTS and TEOS molecules are uniformly distributed across the surface since individual thiol molecules or regions with low thiol surface density may not provide sufficient binding sites to effectively tether gold nanoparticles to the surface. In comparison, the AFM image for the pure MPTS coating exposed to the AuNP's shows a completely new morphology consisting of a thick (at least 30 nm), smooth and uniform top-layer with a few cracks. In addition, some individual gold nanoparticles can be observed within the layer. This indicates that a uniform distribution of thiol groups leads to extensive interaction of the gold nanoparticles with the sample surface. However, the most interesting result was obtained for the coating prepared from a solution with an MPTS/TEOS ratio of 3:1. A distinct pattern showing an interconnected network not observed on the 3:1 sample prior to exposure to AuNP's was seen (Figure 4.10 e). The observed surface structure is similar to that typically reported for the tapping mode phase images of phase segregated block co-polymers suggesting that when the MPTS/TEOS ratio is high, phase separation of the two organosilanes occurs at the surface [98]. This may be due to the relative hydrophobicity of the hydrolyzed and condensed MPTS compared to that of TEOS.

In addition, the height difference observed between the light and dark regions is approximately 125 nm. This height difference seems large for adsorption of 10 nm diameter gold nanoparticles suggesting that if the high regions are in fact due to AuNP's bonding to these regions, multiple layers of AuNP's must adsorb. In order to confirm that the observed interconnected structure was due to AuNP adsorption and not simply dissolution of one phase of the organosilane coating over another, a control experiment was performed. The 3:1 coating was treated with the citrate buffer solution (same concentration, time, rinsing etc.) that the nanoparticles were suspended in. The corresponding AFM image is shown in Figure 4.10 g. This phase separated structure was not seen in the control experiment confirming that the observed pattern is most likely due to adsorption of AuNP's to MPTS rich regions of the coating and that the thiols are not randomly distributed across the surface of the coating but are localized in the MPTS rich domains of the organosilane film.

4.2 Corrosion Studies

In order to evaluate the influence of the mixed organosilane coatings on the corrosion of the Mg AZ31 substrate and the stability of the coating itself, a simple immersion test was carried out in 3.5wt% NaCl solution. The coated samples and uncoated control samples were immersed in the solution for up to 14 days. The sample loss as a function of time was determined by quantifying the amount of Mg dissolved into solution at each time point using FAAS. The stability of the coating and the nature of the corrosion products were further evaluated by SEM/EDS.

4.2.1 Flame Atomic Adsorption Spectroscopy Results

In order to evaluate the influence of various coatings on the corrosion rate of Mg AZ31, the amount of magnesium dissolved in solution as a function of time was detected by FAAS. The reported values are an average of the magnesium levels detected in aliquots taken from the corrosion solution at various time points. The results are shown in Figure 4.11.
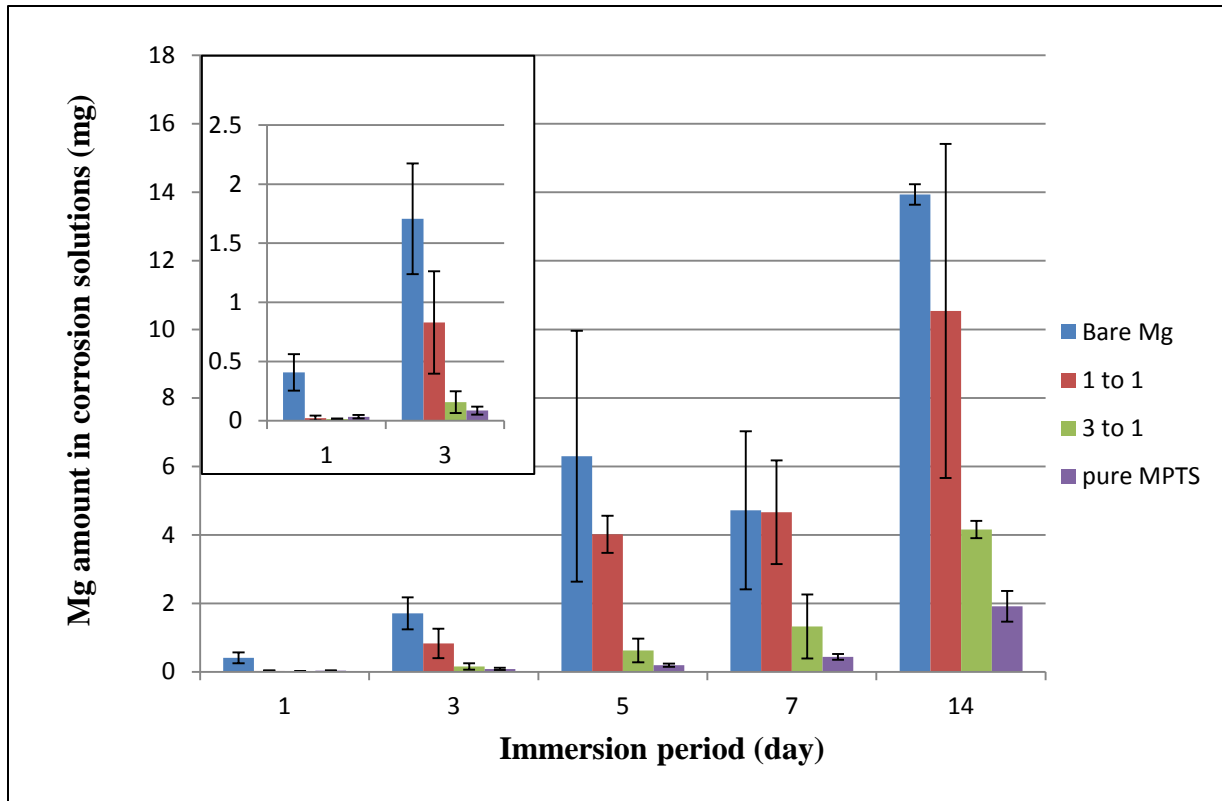
Figure 4.11 Magnesium amount in corrosion solutions of uncoated and coated Mg AZ31 substrates for different immersion periods in 3.5wt% NaCl solution. Bare Mg AZ31 substrates (blue), 1:1 (MPTS:TEOS) mixed organosilane coated substrates (red), 3:1 (MPTS:TEOS) mixed organosilane coated substrates (green) and pure MPTS mixed orgaosilane coated substrates (purple). Data are the average ± standard deviation of at least 3 samples (5 measurements for each), except the data of 14 day which are the average ± standard deviation of 2 samples (5 measurements for each).

An uncoated (polished and cleaned) Mg AZ31 samples was applied as a negative control. After immersion into 3.5 wt% NaCl solutions, the control samples immediately started to corrode as evidenced by the observation of hydrogen bubbles released from the surface within 10 minutes. After one day immersion, the average amount of magnesium in five corrosion solutions of uncoated bare magnesium reached 0.408 mg, while that of the coated magnesium substrates were in the range from 0.012 mg to 0.033 mg. This indicates that the corrosion resistance of all three coated Mg AZ31 were almost the same at the beginning of immersion test. However, differences

in corrosion resistance were observed after 3 days of immersion. The average amount of magnesium in the corrosion solutions of uncoated and coated samples dramatically increased as the immersion time lengthened with the exception of pure MPTS modified substrates which increased to only 0.195 mg by the end of day 5. The average amount of magnesium in the corrosion solutions of 1:1 samples increased dramatically in the first 5 days from 0.022 mg to 4.018 mg which was much higher than that of 3:1 samples at the corresponding immersion time.

Extending the corrosion time to 7 days, the average amount of magnesium in the corrosion solutions of pure MPTS-modified substrates slightly increased from 0.195 mg to 0.440 mg, while that of 3:1 modified substrates increased from 0.624 mg to 1.323 mg; while this was 3 times the amount released for the of pure MPTS samples, it was still distinctly lower than that of the uncoated bare magnesium samples and the 1:1 modified samples. By the end of day 7 immersion, the average amount of magnesium in the corrosion solutions of uncoated samples was almost the same as by the end of day 5; the large error bars indicate big fluctuations from sample to sample. This non-significant difference between day 5 and day 7 may be caused by the newly formed gray oxide film of magnesium hydroxide on bare magnesium substrates. At the same time, this film acted as a protective layer on the uncoated samples thus slowing down the corrosion process. The formation of this magnesium hydroxide layer can also explain the slight enhancement of the average amount of magnesium in the corrosion solutions for 1:1 modified magnesium samples during day 5 to day 7. The average amount of magnesium in the corrosion solutions of both uncoated and 1:1 modified samples went back up after 14 days immersion; this dramatic increase of amount of magnesium in the corrosion solutions can be explained by the dissolution of the magnesium hydroxide film. The abundance of chloride ions in 3.5 wt% NaCl solution reacted with magnesium hydroxide to form highly soluble magnesium chloride which led to the breakdown of the magnesium hydroxide film and continued release of magnesium ions into solution. As the accompanying magnesium hydroxide film dissolution, water molecules were able to reach the magnesium substrates promoting the corrosion reactions leading to corrosion rates rising again. However, after 14 days of immersion, the average amount of magnesium in

the corrosion solutions of both 3:1 and pure MPTS modified samples, which were 4.154 mg and 1.913 mg respectively, were still at lower levels compared with that of the uncoated and 1:1 coated samples, indicating that the 3:1 and pure MPTS coating still had a good protection effect toward magnesium substrates. From the results of Flame Atomic Absorption Spectroscopy, it can be seen that the organosilane coatings enhanced the corrosion resistance of magnesium substrates efficiently compared to the uncoated bare magnesium substrates. For the coated magnesium substrates, pure MPTS coating showed the best corrosion resistance.

4.2.2 SEM/EDS Results

The low magnification SEM images (100x) of uncoated (polished and cleaned) as well as the organosilane coated Mg AZ31 samples before the immersion test are shown in Figure 4.12. Figure 4.12 (a) shows that the polished, uncoated Mg AZ31 surface was smooth and flat with no visible pits or polishing grooves.

The EDS spectrum of the uncoated Mg AZ31 sample is presented in Figure 4.13 (a). The majority element present is magnesium, with slight amounts of aluminum and zinc. A small peak due to oxygen was also detected indicating that the Mg AZ31 substrate surface was readily oxidized by the atmosphere resulting in a thin layer of magnesium hydroxide at the surface.
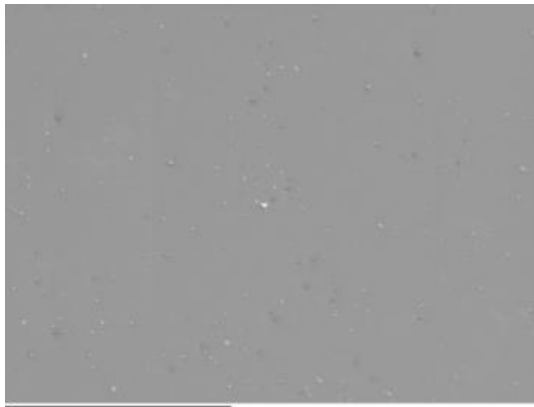
<center>(a)</center>
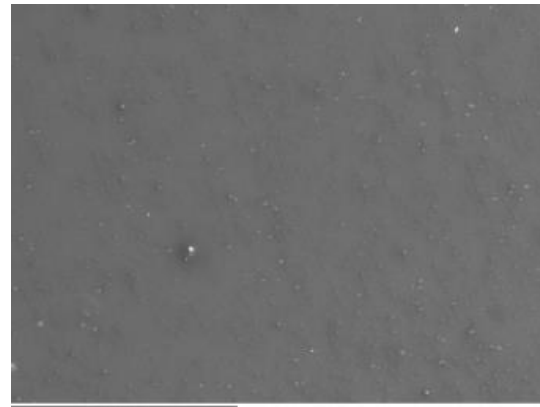
<center>(b)</center>
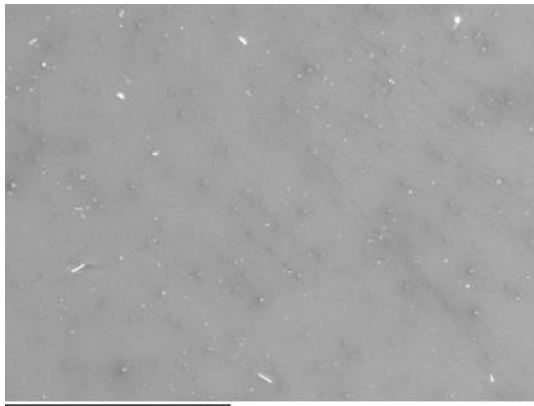
<center>(c)</center>

<center>(d)</center>

Figure 4.12 SEM images (100x) of surfaces of (a) polished bare Mg AZ31, (b) 1:1 organosilane coated, (c) 3:1 organosilane coated and (d) pure MPTS organosilane coated Mg AZ31 before immersion in 3.5% NaCl.
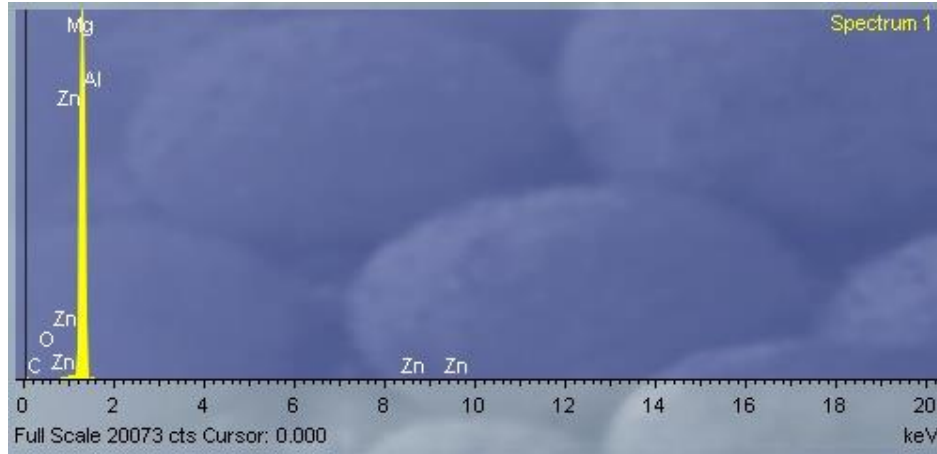
(a)
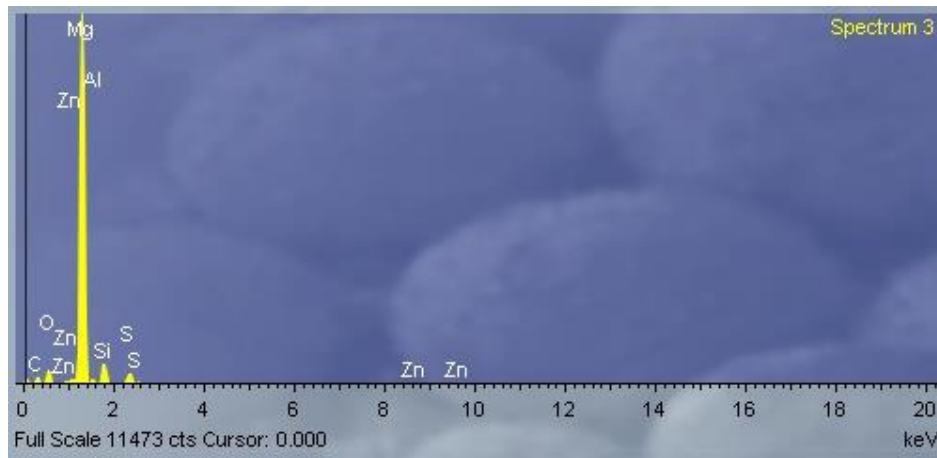
(b)

Figure 4.13 EDS spectra collected on (a) polished bare Mg AZ31 substrate and (b) 3:1 coated Mg AZ31 substrate.

Figure 4.12 (b)-(d) shows the coated samples prepared from 1:1, 3:1 and pure MPTS coating baths, respectively. All of the three different organosilane coatings showed relatively smooth, uniform and crack-free surfaces with a few small white spots. Figure 4.13 (b) shows the EDS spectrum of the 3:1 mixed organosilane coated surface. In addition to the main peak due to the Mg AZ31 substrate, the peaks of carbon, oxygen, silicon and sulfur were also clearly observed in the spectrum. The appearance of these new peaks confirmed that the organosilane were

60

successfully coated onto the magnesium substrate surfaces.

These same peaks appeared on the EDS spectra for both 1:1 and pure MPTS coated substrates but with different intensities (spectra not shown). According to the element atomic percentage data collected by EDS, the atomic percentage of sulfur showed a distinct increase with an increasing amount of MPTS in the mixed organosilane coating bath. Furthermore, the EDS results showed that the white spots (Figure 4.12 b-d) are rich in Si, S and O, but contain less Mg than other areas, indicating that relatively large organosilane oligomers are present on these spots. These oligomers are formed in the coating bath solution due to self-condensation of the organosilane molecules and likely deposit on the surface by sedimentation.

Figure 4.14 (a-d) shows low magnification (100x) SEM images of the surface of uncoated and coated magnesium AZ31 samples after immersion in 3.5% NaCl for 1 day. By the naked eye it was obvious that pitting corrosion on uncoated bare magnesium substrates started within a half hour of immersion into the 3.5% NaCl solution. After one hour, visible black corrosion pits were readily apparent. As seen in Figure 4.14 (a), the uncoated Mg AZ31 surface had a very rough appearance due the dissolution of the substrate and the deposition of corrosion products. From the EDS analysis results shown in Figure 4.15, the corrosion products on the uncoated magnesium substrate surfaces were rich in magnesium and oxygen which indicates that the main component of the corrosion film was magnesium hydroxide. In addition, a small chlorine peak was observed at 2.8 keV which can be attributed to the presence of a small amount of magnesium chloride in the corrosion product.
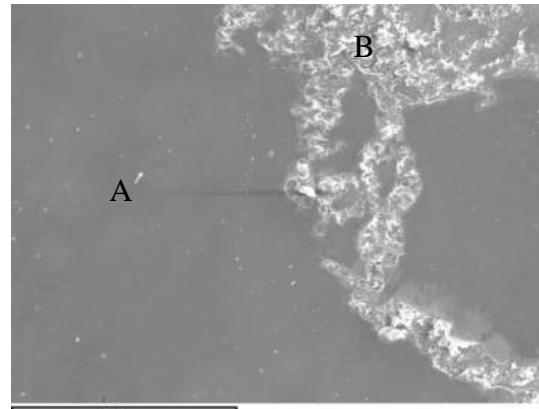
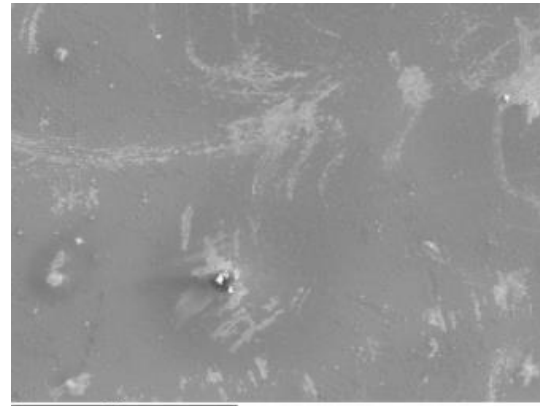(a)   (b)
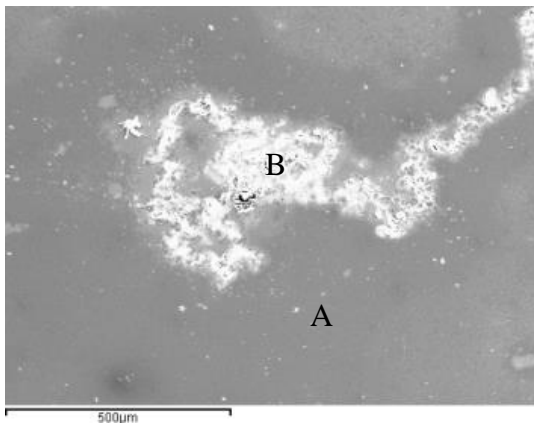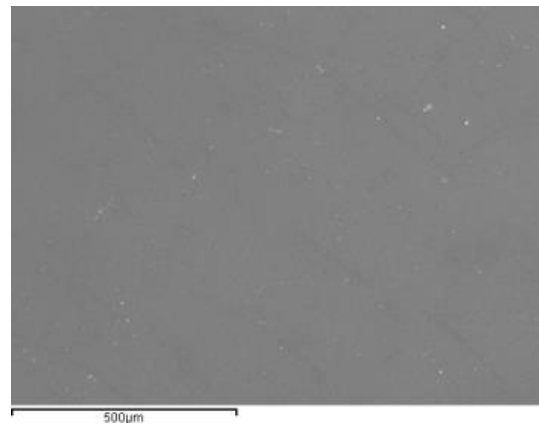
(c)   (d)

Figure 4.14 SEM images (100x) of surfaces of (a) polished bare Mg AZ31, (b) 1:1 organosilane coated, (c) 3:1 organosilane coated and (d) pure MPTS organosilane coated Mg AZ31 after one day immersion test.
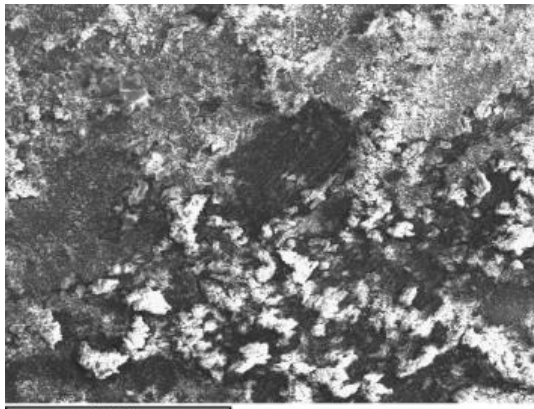
In the case of the 1:1 and 3:1 coated magnesium substrates, after a 1 day immersion period, a few pits due to corrosion could be observed near the edges of the samples but overall the substrates surfaces appeared to be protected from corrosion by the organosilane coatings.
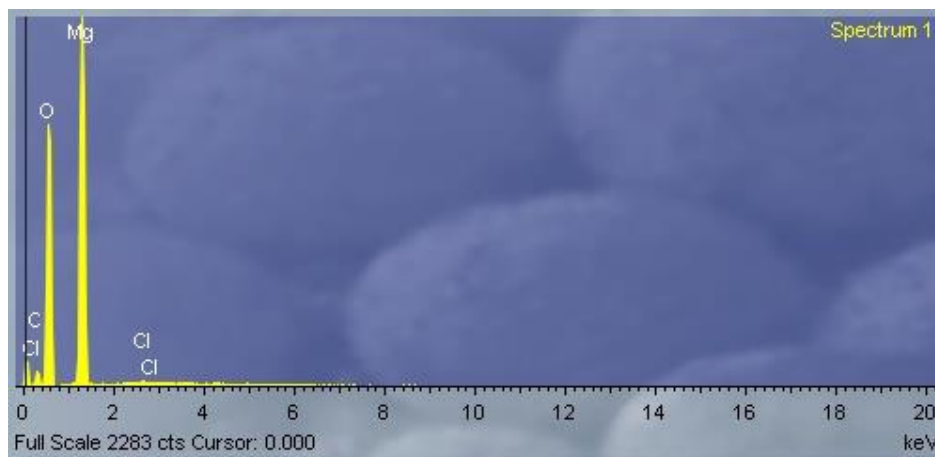
Figure 4.15 EDS spectrum collected on bare Mg AZ31 substrate after immersion in 3.5% NaCl solution for one day.

The SEM images shown in Figure 4.14 (b-c) show the 1:1 and 3:1 organosilane-coated Mg AZ31 after immersion in 3.5% NaCl for 1 day. The EDS analysis results indicate that the flat, smooth areas labelled A have the same spectra as the 1:1 and 3:1 coated Mg AZ31 substrates prior to the immersion test. While the spectra for the rough areas labelled B had higher peak intensities for oxygen and lower peak intensities for silicon in comparison with the intact coating (area A). For the samples coated with pure MPTS, no corrosion pits or corrosion products were observed on the substrates by eye or in the low magnification SEM image (Figure 4.14 (d)). In summary, the pure MPTS coating showed the best corrosion resistance and no significant difference was observed between the 1:1 and 3:1 coatings after a 1 day immersion period. All three coatings were shown to significantly enhance the corrosion resistance of Mg AZ31.
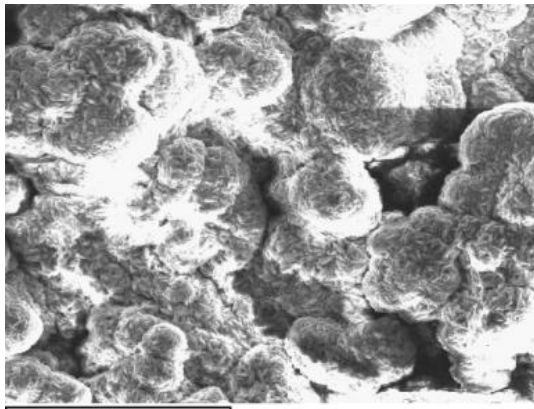
<p style="text-align:center">(a)</p>
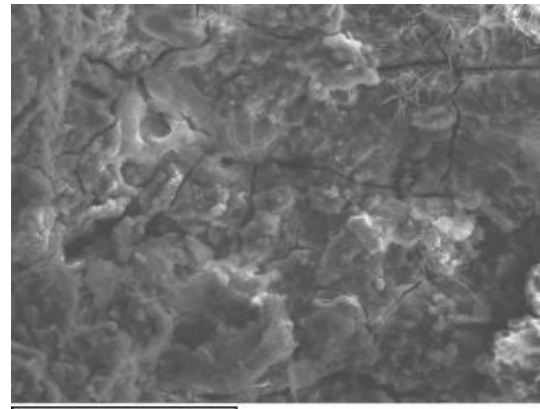
<p style="text-align:center">(b)</p>
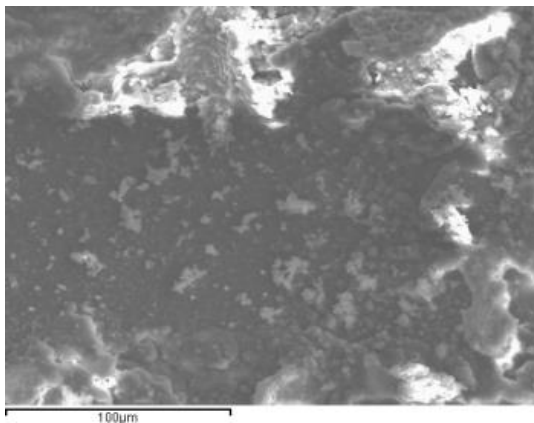
<p style="text-align:center">(c)</p>
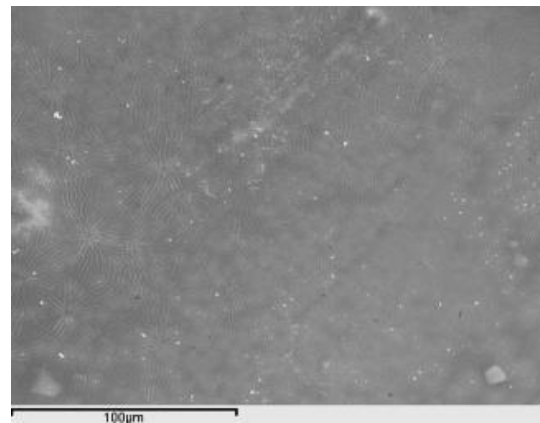
<p style="text-align:center">(d)</p>

Figure 4.16 SEM images of surfaces of (a) polished bare Mg AZ31, (b) 1:1 organosilane coated, (c) 3:1 organosilane coated and (d) pure MPTS organosilane coated Mg AZ31 after seven days immersion test.

Representative SEM images of the surface of the uncoated and coated magnesium AZ31 after immersion in 3.5% NaCl for 7 days are displayed in Figure 4.16 (a-d). Examination of the corroded sample by the naked eye showed that the entire surface of the uncoated Mg AZ31 samples were covered by a thick layer of white precipitate. The SEM image for this sample (Figure 4.16a) shows a thick corrosion product composed of spherical agglomerates of plate-like crystals, a typical morphology for magnesium hydroxide [99, 100]. This assertion was confirmed in the EDS analysis. The O and Mg surface element atomic percentages of this corroded

uncoated sample were 67.75 ± 2.88 and 34.12 ± 2.86, respectively. Therefore, the ratio of O/Mg was close to 2 as would be expected for $Mg(OH)_2$. This indicates that the initially deposited layer of corrosion product on uncoated magnesium AZ31 samples was unstable in 3.5% NaCl solution and that corrosion continued for the entire immersion test. This was an expected result since it is well known that the magnesium hydroxide passive layer is unstable in chloride containing solutions [99, 100].

In the case of the 1:1 coated Mg AZ31 sample, although the coating exhibited good corrosion resistance after a one day immersion period, after 3 days corrosion pits began to appear over the whole surface, and after 7 days the coating was completely removed from the surface and the sample was fully covered with a layer of white corrosion products (Figure 4.16b).

A representative SEM image of the 3:1 coated Mg AZ31 substrate after immersion in 3.5% NaCl solution for 7 days is presented in Figure 4.16c. The corrosion products are not uniformly deposited over the entire surface but are present from spot to spot across the surface. EDS analysis confirmed that the smooth flat areas on the image remained covered with silicon and sulfur indicating that the organosilane coating was still intact in these regions. Finally, Figure 4.16d shows that the surface of pure MPTS-coated Mg AZ31 is unaltered after immersion in 3.5% NaCl solution for 7 days. These SEM images (Figure 4.16 a-d) show that increasing amount of MPTS in the coating results in improved corrosion resistance. Furthermore, the Si/Mg ratios for all types of coated substrates before and after the immersion test for 1 day and 7 days were calculated from the EDS results. This data is shown graphically in Figure 4.17. The ratio of silicon to magnesium can be correlated with the thickness of the coating. The sampling depth for EDS is approximately 3-4 μm, therefore as the coating thickness increases we should expect to see an increase in the Si/Mg as the Mg AZ31 substrate is covered up. The blue bars represent the coated samples before the immersion test. In comparison with the 1:1 and 3:1 coatings, the coating deposited from the pure MPTS organosilane coating bath were on average the thickest but also had the most spot to spot variation in thickness. After a one day immersion period (red

bars), the Si/Mg ratio of all three organosilane coatings slightly decreased indicating some coating loss. The Si/Mg ratio for the 1:1 and 3:1 coatings were not significantly different before immersion in NaCl solution or after a one day immersion period. However, after immersion in the NaCl solution for 7 days, the Si/Mg ratio for the 1:1 coating decreased to zero while a small amount of silicon was still observed on the 3:1 coated sample. On the other hand, the Si/Mg ratio for the MPTS coatings remained constant within error for the entire 7 day immersion test. These EDS results confirm that the corrosion resistance of Mg AZ31 is significantly improved as the amount of MPTS in the coating bath is increased.
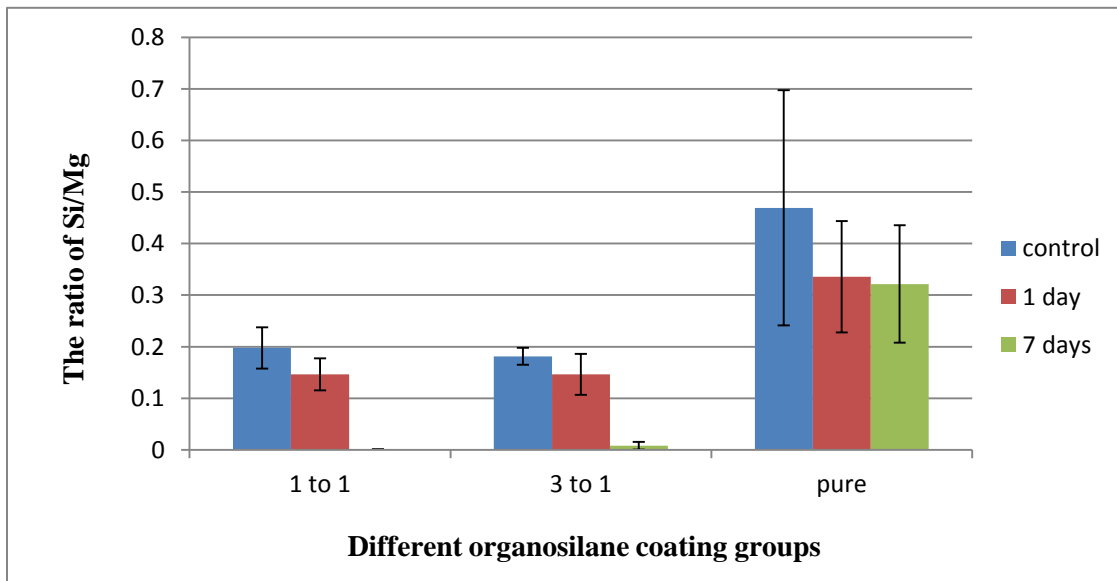
Figure 4.17 EDS analysis of mixed organosilane coatings. Surface Si/Mg atomic % ratios for coated Mg AZ31 substrates before (blue) and after the immersion test for 1 day (red) and 7 days (green). Data are the average ± standard deviation of 15 measurements.

4.3 Improving the Biocompatibility of Organosilane Coated Mg AZ31 through Covalent Immobilization of the RGD Peptide

One of the key objectives of this study was to improve the biocompatibility of Mg AZ31

substrate through immobilization of the RGD peptide. The RGD peptide is a well-known unique amino acid sequence that can be specifically recognized by integrins on the cell membrane aiding in cell adhesion and proliferation at biomaterials surfaces [72, 75, 88, 91]. The role of RGD surface density and distribution has been shown to be important for optimum cell/surface interactions [85-87, 90].

The previous sections in this thesis confirmed that stable organosilane coatings with variable surface thiol densities and distributions were successfully deposited onto Mg AZ31 surfaces. In order to improve the biocompatibility of the organosilane coated substrate, further surface modification with the cross-linker SMP followed by immobilization of the RGD peptide was attempted as shown in Figure 4.1.

4.3.1 Surface Modification with the Cross-linker SMP
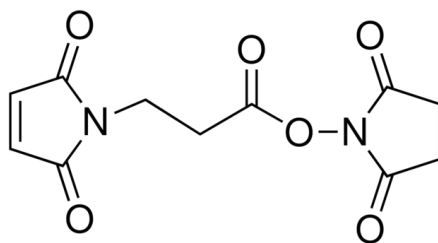
Figure 4.18 Chemical Structure of SMP.

SMP is a heterobifunctional cross-linker which has been widely used in the conjugation and crosslinking between biomolecules and other substrates. The cross-linker serves two main purposes: 1) it provides a functional group that specifically reacts with the thiol of organosilane modified surfaces at one end and a specific functional group for reaction with a primary amine group of RGD at the other, thus providing a route for covalent bonding of the RGD peptide to Mg AZ31 substrates; 2) it is a physical spacer that allows the attached biomolecule some freedom of orientation.

The chemical structure of SMP is shown in Figure 4.18. It contains two reactive groups, the maleimidyl and succinimidyl ester group. By using the reaction between the maleimidyl group and the thiol group the SMP crosslinker was first immobilized on silanized Mg AZ31 substrate surfaces. Then, in a second step, the free end of the succinimidyl group should further react to give an amide bond with the primary amines of the RGD peptide. The general reaction scheme is shown in Figure 4.1.

In this section, ATR-FTIR was applied to detect the chemical changes on the organosilane coating surfaces after covalent bonding of the cross-linker SMP and RGD peptides.

Figure 4.19 compares ATR-FTIR spectra of 1:1 coated Mg AZ31 substrates before and after SMP modification. It was observed that there were no significant changes that appeared in the overall spectrum after the SMP treatment, indicating that the 1:1 coating was stable during SMP treatment.
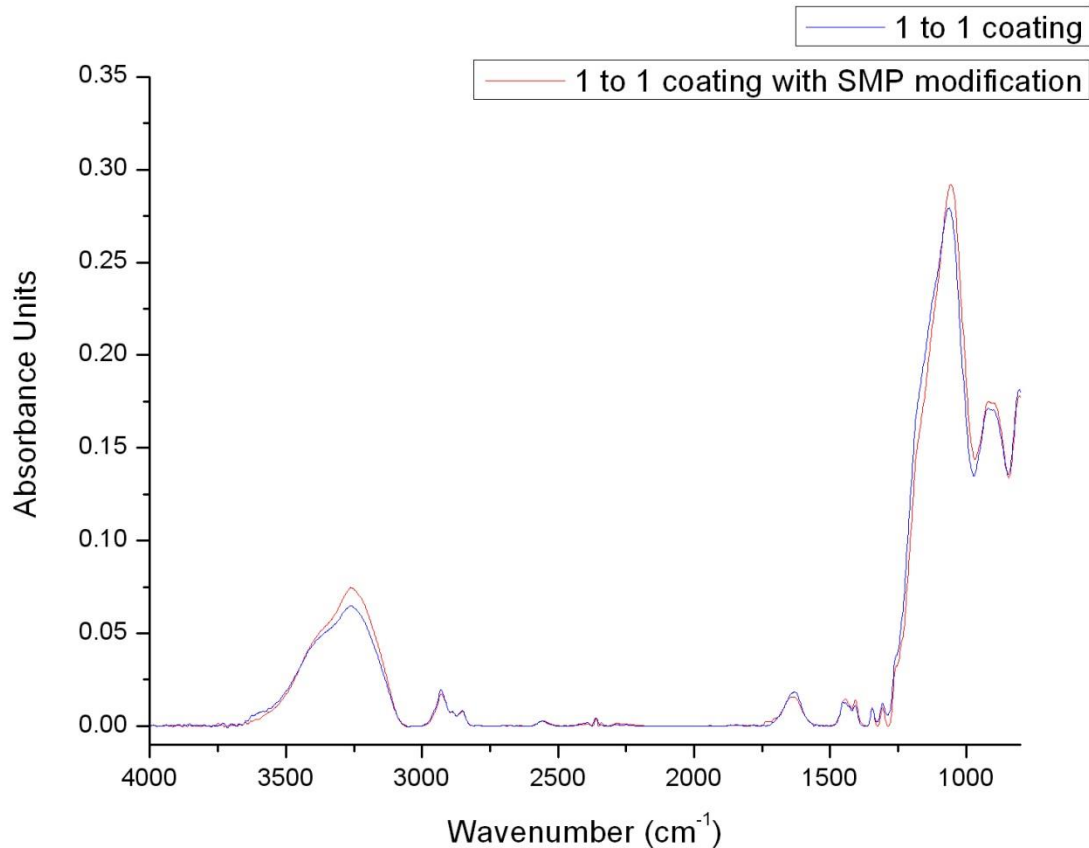
Figure 4.19 ATR-FTIR spectra of 1 :1 (MPTS:TEOS)mixed organosilane modified Mg AZ31 substrates before (blue) and after (red) SMP modification

Figure 4.20 shows the infrared spectra in the fingerprint region (1500 to 1900 cm^{-1}) for an SMP standard, a 1:1 organosilane coating before reaction with SMP and a 1:1 organosilane coating after reaction with SMP. In the SMP standard spectrum (Figure 4.20c), there are four specific peaks located at 1700, 1740, 1780 and 1816 cm^{-1} derived from the symmetric and antisymmetric stretching of cyclic imide carbonyl groups contained in SMP [77].

Figure 4.20 Comparison ATR-FTIR spectra of 1 :1 (MPTS:TEOS)mixed organosilane modified Mg AZ31 substrates before and after SMP modification with standard SMP spectrum. (a) 1 :1 (MPTS:TEOS)mixed organosilane modified Mg AZ31 substrates; (b) 1 :1 (MPTS:TEOS)mixed organosilane modified Mg AZ31 substrates with SMP modification; (c) standard SMP.

On the 1:1 coated Mg AZ31 substrate (Figure 4.20a), a broad peak was observed at $1638cm^{-1}$ which was caused by the bending vibration of hydroxyl groups in the organosilane coating or surface adsorbed/atmospheric water molecules. After SMP treatment, three new weak peaks appeared at 1700, 1740 and 1780 cm^{-1} indicating the presence of SMP at the surface (Figure 4.20b). These peaks are weak due to the low surface density of thiol groups on the 1:1 organosilane coating (section 4.1.2).
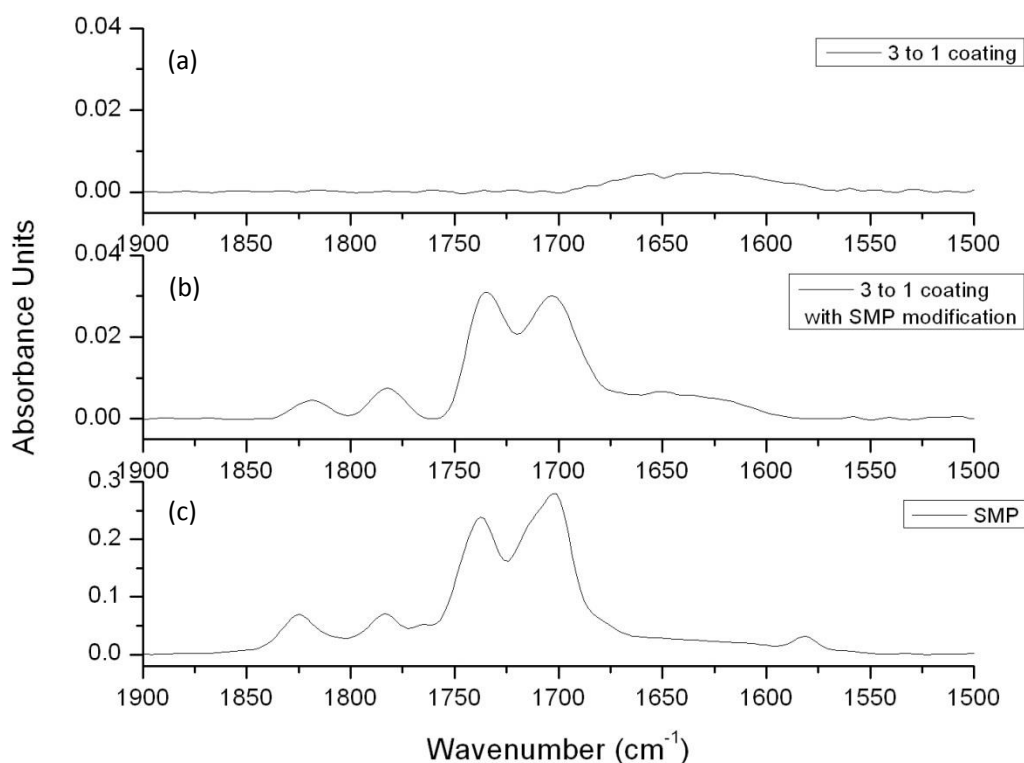
Figure 4.21 Comparison ATR-FTIR spectra of 3 :1 (MPTS:TEOS)mixed organosilane modified Mg AZ31 substrates before and after SMP modification with standard SMP spectrum. (a) 3 :1 (MPTS:TEOS)mixed organosilane modified Mg AZ31 substrates; (b) 3 :1 (MPTS:TEOS)mixed organosilane modified Mg AZ31 substrates with SMP modification; (c) standard SMP.

Figure 4.21 shows ATR-FTIR spectra for the 3:1 organosilane coated surface before and after reaction with SMP. In this case, the organosilane coatings prior to SMP reaction are essentially flat in the 1500-1900 cm^{-1} region of the infrared spectrum (panel a). This is due to fewer –OH groups on the 3:1 coated substrate due to a lower overall concentration of TEOS in the coating. After SMP treatment, four new peaks appeared at 1700, 1740, 1780 and 1816 cm^{-1} confirming the presence of SMP at the surface (panel b). The intensities of these bands is significantly higher than was observed on the 1:1 organosilane coated sample, indicating that more SMP molecules attached to the 3:1 MPTS/TEOS silanized surfaces compared with the 1:1 MPTS/TEOS silanized surfaces. This can be explained by the observed increase in surface thiol density for these

samples (Section 4.1.2). In addition, the spectra collected from random spots on SMP-modified 3:1 substrates gave variable spot to spot intensity of the four SMP peaks (results not shown). This result is in accord with the previously described AFM study (Section 4.1.2.4) on surface thiol distribution which indicated that the MPTS and TEOS are phase segregated at the surface into thiol rich and thiol deficient regions. The SMP should react in the thiol rich regions but cannot covalently bond to the thiol deficient regions.

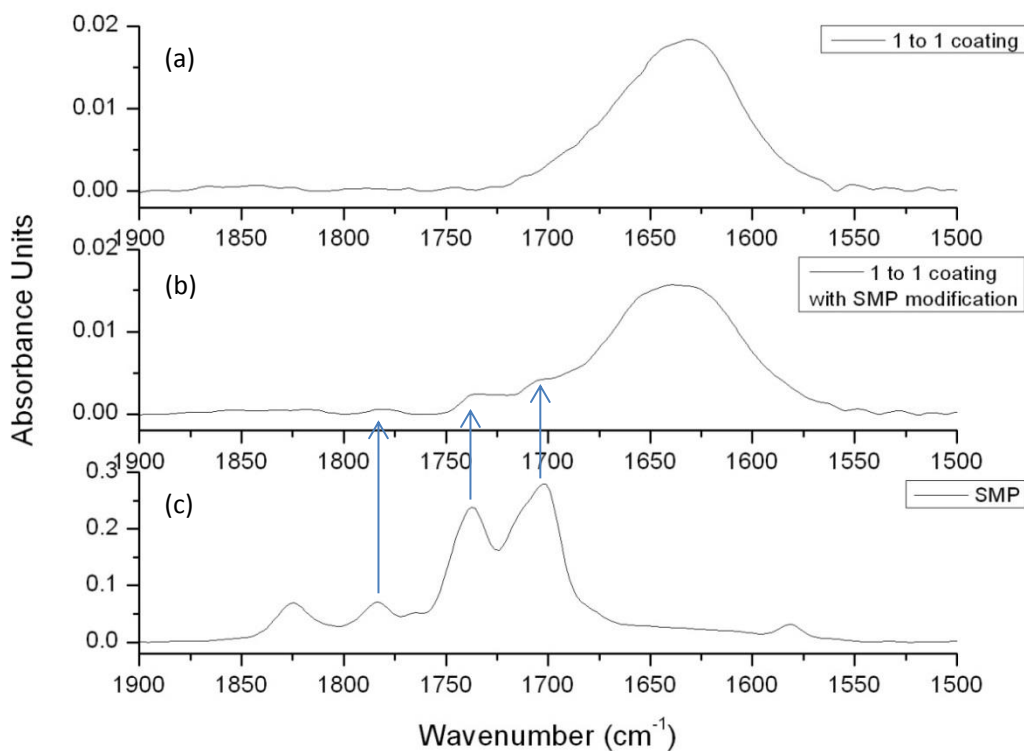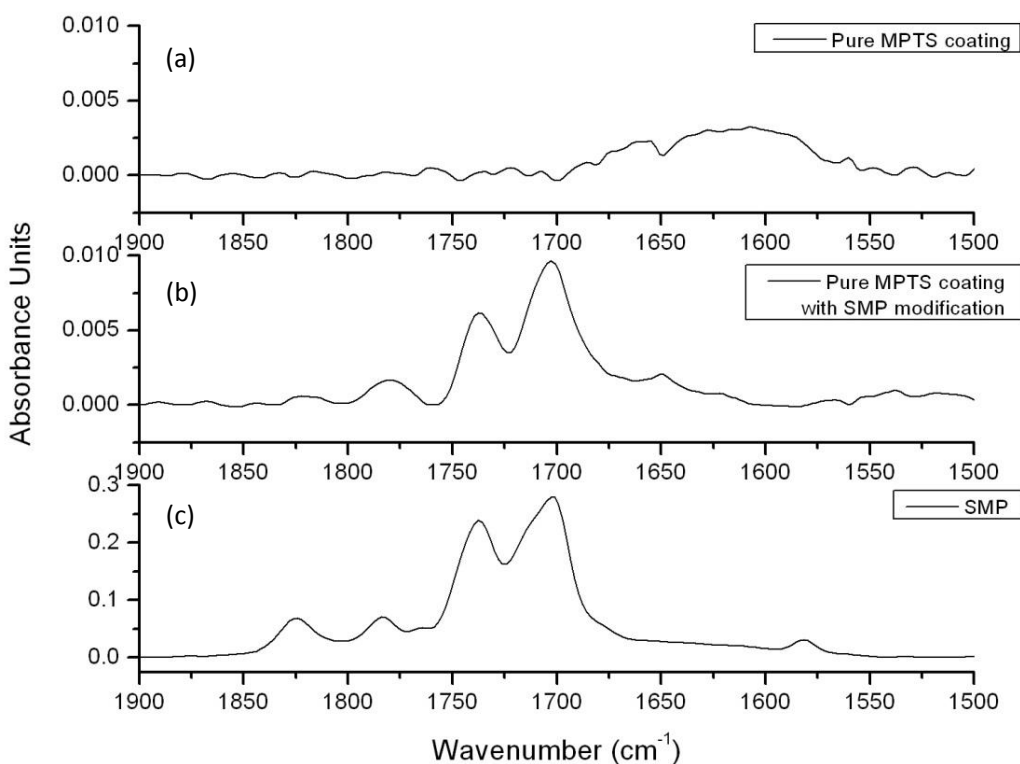**Figure 4.22 Comparison ATR-FTIR spectra of Pure MPTS organosilane modified Mg AZ31 substrates before and after SMP modification with standard SMP spectrum. (a) Pure MPTS organosilane modified Mg AZ31 substrates; (b) Pure MPTS organosilane modified Mg AZ31 substrates with SMP modification; (c) standard SMP.**

Figure 4.22 compares the ATR-FTIR results obtained for the pure MPTS coated Mg AZ31 before (panel a) and after reaction with SMP (panel b). After SMP treatment, four new peaks appeared at 1700, 1740, 1780 and 1816 cm^{-1} confirming the presence of SMP at the surface. The

intensities of these bands are high, which can again be explained by the observed increase in surface thiol density for these samples (Section 4.1.2). In addition, the spectra collected from random spots on SMP modified pure MPTS coatings did not vary from spot to spot (results not shown). This result is in accordance with the previously described AFM study (Section 4.1.2.4) in which gold nanoparticles were shown to adsorb in a uniform layer to the pure MPTS modified Mg AZ31 indicating uniform thiol distribution at the coating surface.

4.3.2 Covalent Immobilization of RGD

In this section, XPS analysis was used to evaluate the surface atomic elements to confirm the successful covalent binding of RGD on substrate surfaces.
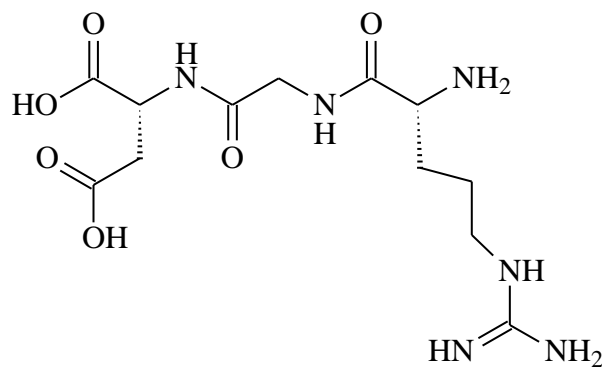
Figure 4.23 Chemical structure of RGD peptide.

The chemical structure of RGD structure is shown in Figure 4.23. It can be seen from this structure that there are 6 nitrogen atoms in each RGD molecule. Therefore, by comparing the N/Si atomic ratio for different surfaces, successful bonding of RGD to the substrate surface can be confirmed. These N/Si ratios also reflect the influence of the overall surface thiol density and subsequent SMP surface density on the RGD surface density of the final modified material.
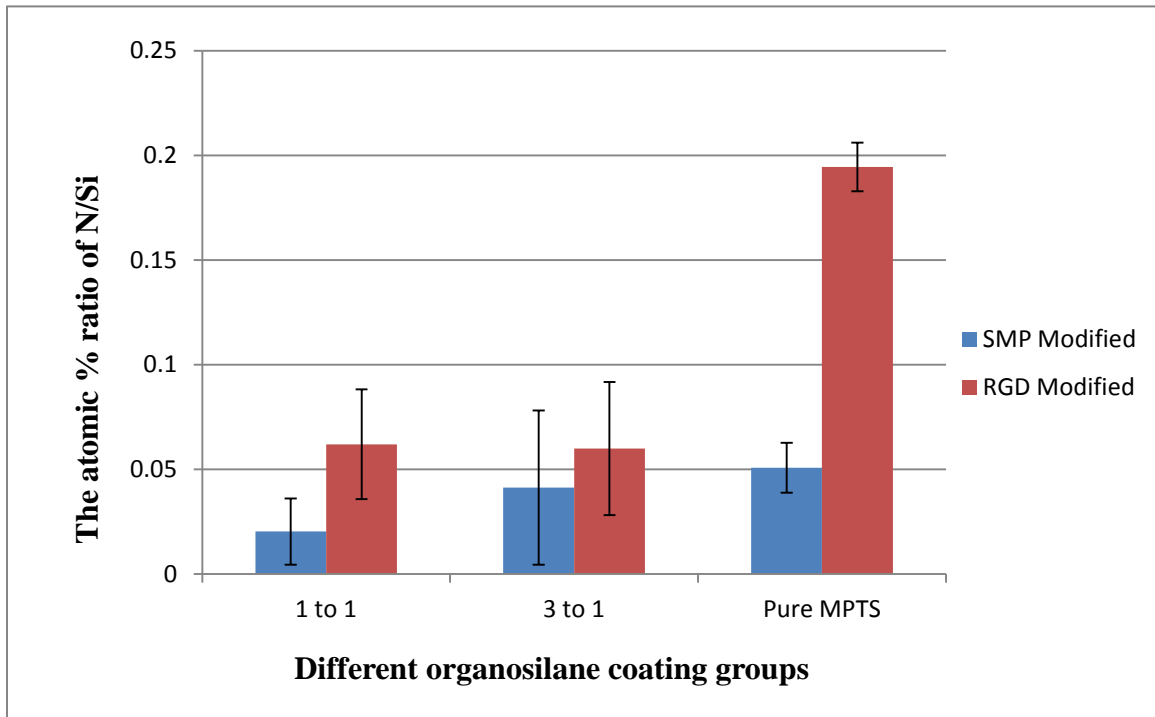
Figure 4.24 XPS analysis of mixed organosilane coatings. N/Si atomic percent ratio comparison for three different organosilane coated Mg AZ31 substrates after SMP (blue) and further after RGD peptide (red) modifications. Data are the average ± standard deviation of 3 measurements.

Figure 4.24 gives the surface atomic ratio of N/Si for the three different coating types before and after RGD modification. The SMP molecule itself has 2 nitrogen atoms per molecule therefore nitrogen was observed on all of the SMP treated samples with an average increase consistent with the previously discussed ATR-FTIR results observed for these samples. For all three coatings, the average atomic ratio of N/Si was increased after the RGD peptide treatment compared with that of the samples treated with SMP alone. However, there is no statistically significant difference in N/Si ratio between the 1:1 and 3:1 coatings.

In the case of the 1:1 coated group, the RGD modified surfaces had a slightly higher N/Si ratio demonstrating the RGD molecules were successfully attached on the substrate surface. The large error bars are likely due to the low surface density and random distribution of thiol groups for this coating.

Compared with the 1:1 coating, higher N/Si ratios were expected on RGD-modified 3:1 substrate due to the higher SMP surface density detected on these substrates. However, compared with 1:1 substrates, the difference in N/Si atomic ratio on 3:1 substrates was not statistically significant

The N/Si ratio of MPTS-silanized substrate showed a significant increasing after the RGD treatment, and the small error bars were indicative that RGD molecules were distributed evenly over the whole surface.

From the XPS results, the variations of N/Si atomic ratio before and after RGD treatment on all of three different Mg AZ31 coated substrates indicates that RGD molecules were successfully immobilized on all of three different coating substrates through the cross-linker SMP. Furthermore, the immobilized RGD surface densities were controlled by varying the ratio of the two organosilanes in the coating. However, in all cases the N/Si ratio is very low indicating that we did not achieve one RGD molecule bonded for every available thiol group; the overall low yield observed is typical for these types of surface reactions.

4.4 Saos-2 Cell Behavior on RGD-Modified Mg AZ31

Finally, the effect of Mg AZ31 surface modification on the cell adhesion and proliferation properties was evaluated. Because human primary cells are difficult to maintain in culture [89], we selected the osteosarcoma-derived Saos-2 cell line for our biocompatibility studies. This cell line is considered as a valuable model for osteoblast/implant interactions studies [89].

A commonly used assay for cell counts is the MTT assay. However, previous studies in Dr. Gray-Munro's lab showed that the MTT assay could be reduced by electrons produced during anodic dissolution of Mg ($Mg \rightarrow Mg^{2+} + 2e^-$) [33] from the substrate, and this reaction impacted the accuracy of cell quantification. Therefore, in order to better quantify cell adhesion and proliferation, the CyQUANT Cell Proliferation Assay Kit was employed. This assay is designed for cell proliferation studies and also can be utilized to detect the adherence of cells to surfaces. When using the CyQUANT kit, cells are first lysed and then nucleic acids are dyed in the same solution. The cell number can be obtained by detecting the fluorescence intensity of the DNA-bound dye in the cell lysate. In addition, because the mechanism of The CyQUANT Cell Proliferation Assay Kit does not rely on the reaction with cellular metabolic products but on the interaction of a dye with the cellular nucleic acids, it is more rapid and convenient than other assays for cell count.

4.4.1 Saos-2 Cell Adhesion Assay

Cell adhesion on biomaterial surfaces is an essential step for the complex osseointegration process on implants, and a number of factors are considered to be involved in terms of new bone formation onto implant materials. Therefore, improving cell/surface interactions on implants has been attempted by immobilizing specific cell recognizable ligands on implant materials which can further stimulate cell adhesion and osseointegration process on implants [91].

In this study, a three amino acid peptide, RGD, was chosen as a cell/surface interaction promoter immobilized on Mg AZ31 substrate surfaces. The biocompatibility of RGD-modified Mg AZ31 was evaluated in terms of the capacity of cell adhesion and subsequent proliferation on substrate surfaces.

4.4.1.1 Optimization of Cell Number for Adhesion Assay

We first determined the maximum number of Saos-2 cells which could be seeded in a 24-well cell culture plate while still giving a linear signal using the CyQUANT assay. This was evaluated by seeding different amount of cells in the wells of a 24-well cell culture plate for 16 hours. Saos-2 cell numbers were in the range of 0 to 150,000 cells per well, in triplicate. The cells were allowed to adhere for 16 h, after which time the samples were processed for cell content using the CyQUANT assay.

Figure 4.25 shows the signal intensity as a function of the number of cells seeded in the wells. In the range of 0-20,000 cells, signal intensities were proportional to the amount of seeded cells. The use of a larger amount of cell resulted in the loss of the linearity of the signal. This might due to two main reasons: 1) the Saos-2 cell capacity for well of 24-well cell culture plate, and 2) the linear detection range of CyQUANT kit.
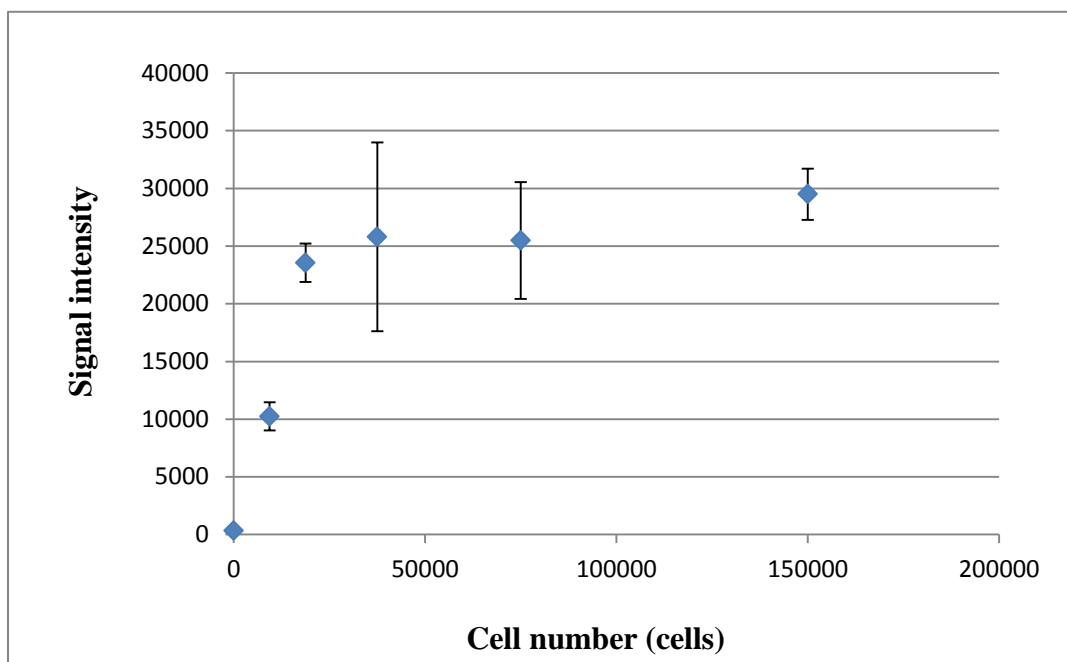
Figure 4.25 Signal intensities of serial cell numbers in range of 0-150,000 cells adhered on 24-wells cell culture plate after 16 hours incubation. Data are the average ± standard deviation of 3 replicates/3 independent experiments.

We next repeated the standard curve but this time the number of cell per well was narrowed down to the range from 0 to 50000 cells.

Figure 4.26 shows the result of this experiment. It was clear that cell number from 0 to 50,000 fell in the linear detection range of the CyQUANT kit. Therefore, 40,000 cells were chosen as the optimum cell number for the adhesion test.
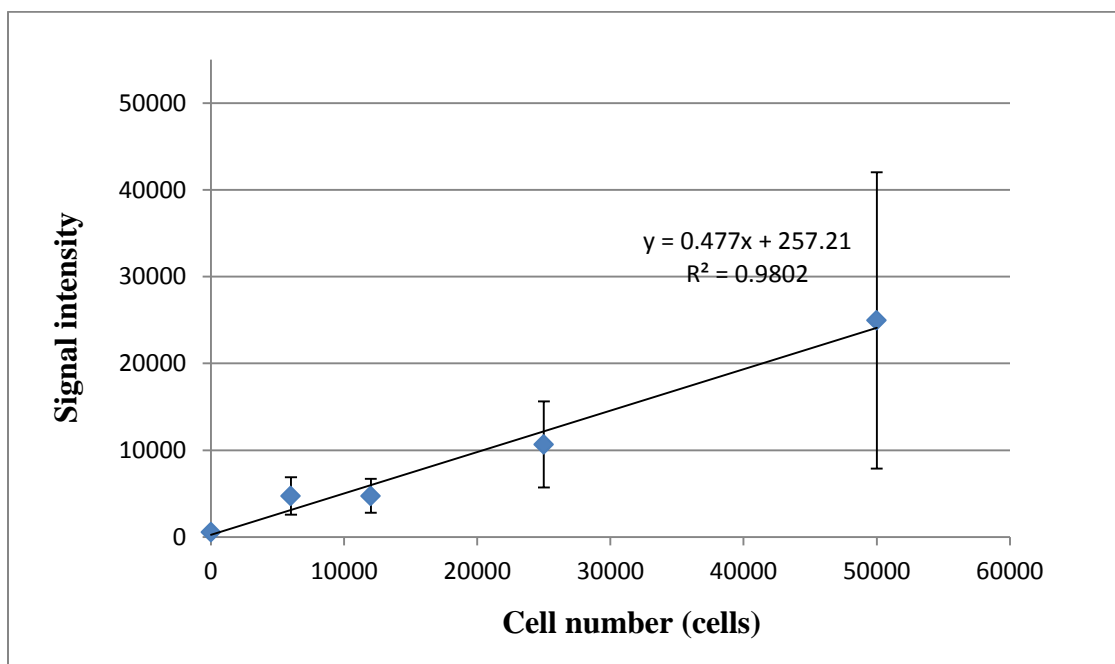
Figure 4.26 Signal intensities of serial cell numbers in range of 0-50,000 cells adhered on 24-wells cell culture plate after 16 hours incubation. Data are the average ± standard deviation of 3 replicates/2 independent experiments.

4.4.1.2 Saos-2 Cell Adhesion Time Optimization

In order to estimate the impact of RGD modified Mg AZ31 substrate on cell adherence, the optimum adhesion time should first be determined.

Forty thousand cells were seeded per well on a 24-well culture plate, and cell adherence was monitored by the CyQUANT kit 1, 2, 4, 6 and 8 hours after seeding. The data indicated that the signal intensity demonstrated a linear increasing trend during the first 6 hours (Figure 4.27). When the adhesion period was extended to 8 hours, the linearity of the signal intensity was lost. This result indicated that the majority of the seeded Saos-2 cells had adhered to the plate after 6 hours.
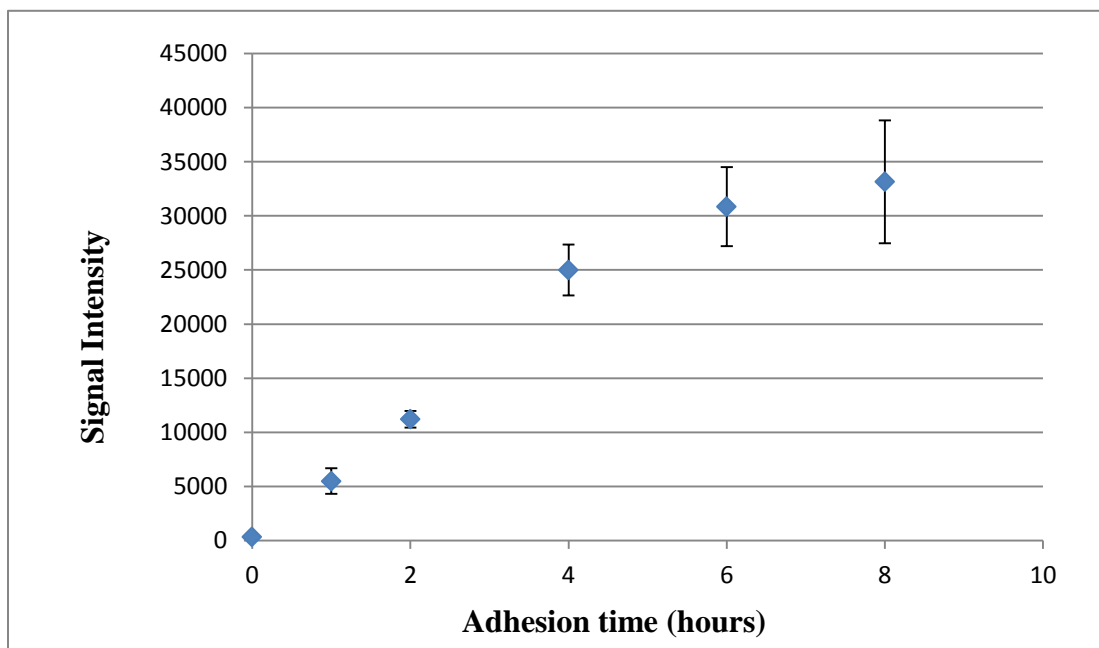
Figure 4.27 Signal intensity of Saos-2 cell adhered on 24-wells cell culture plate after different incubation periods. Data are the average ± standard deviation of 3 replicates /3 independent experiments.

Therefore, we chose an incubation time of 3 hours for testing cell adhesion on RGD-modified Mg AZ31. The 3-hour adhesion period provided enough time for initial cell adhesion and, because the signal obtained was well within the linear portion of the standard curve, enabled us to reliably detect differences in adhesion behavior among the unmodified and RGD-modified groups as well as among three substrate groups with different RGD surface densities.

4.4.1.3 Cell Adhesion Assay

Following the result of our preliminary experiments, 40,000 cells were seeded on the investigated substrates and allowed to adhere for 3 hours. Bare substrate and silanized samples were used as control groups to evaluate the capacity of RGD-modified Mg AZ31 to promote the adhesion of Saos-2 cells. After 3 hours, the number of cells adhered on the control and test (i.e. RGD-modified) surfaces were determined using the CyQUANT Kit. The number of adherent cells was determined using a standard curve which was prepared with a known number of Saos-2

cells. The comparison of adherent cell number on different pre-treated substrates is shown in Figure 4.28. After 3 hours incubation, little cell adherence was detected on polished bare Mg AZ31, which was likely caused by the low corrosion resistance of polished bare Mg AZ31 substrate. Polished bare Mg AZ31 coupons began to corrode and bubble from the edge of coupons 1 minute after being exposed to the cell suspension. Since the entire surface of the coupons became black after a mere 5 minute exposure, the corrosion process dissolves the substrate surface. The cathodic reaction of Mg substrate dissolution ($2H_2O + 2e^- \rightarrow H_2 \uparrow + 2OH^-$) caused OH^- ions releasing into cell culture medium which further led to an increase in pH [33]. In turn, this may further affect Saos-2 cell attachment and adhesion on polished bare Mg AZ31.

As shown in Figure 4.28, Saos-2 cells adhered on all silanized Mg AZ31 substrate surfaces but with varied efficiencies. Compared with polished bare Mg AZ31, a significant increase in cell adhesion was observed on all three silanized substrates. In addition, among the silanized Mg AZ31 substrates, the 1:1 coated surfaces performed the best in terms of cell adherence capacity, and a clear reduction in adhesion was noted as the ratio of MPTS in the organosilane coatings increased. Nine to 16 times more adherent cells were observed on the silanized substrate surfaces than the polished bare Mg AZ31 control group. Compared with polished bare Mg AZ31, the higher cell adhesion capacities can be attributed to the presence of organosilane coatings which provided a layer of protection on Mg AZ31 substrate from corrosion attacks caused by the cell culture medium, and allowed cells to adhere on a stable physical surface. The decrease in cell adherence observed for the different silanized substrate surfaces might relate to the density of the different chemical components and surface functional groups. In general, the hydrophilic surfaces perform better in promoting cell adhesion compared with hydrophobic surfaces [58]. In addition, Ertel et al. reported that a surface with high oxygen-containing functional groups benefited cell growth onto the substrate [3]. Moreover, Keselowsky et al. found, on –OH enriched substrate surfaces, that fibrinogen was tightly bonded showing high levels of $\alpha_5\beta_1$ levels which were able to promote cell adhesion [3]. In this regard, it is interesting to note that the decrease in Saos-2 cell adhesion correlated with the decrease in the –OH surface density from

the 1:1 MPTS-TEOS to pure MPTS surfaces.
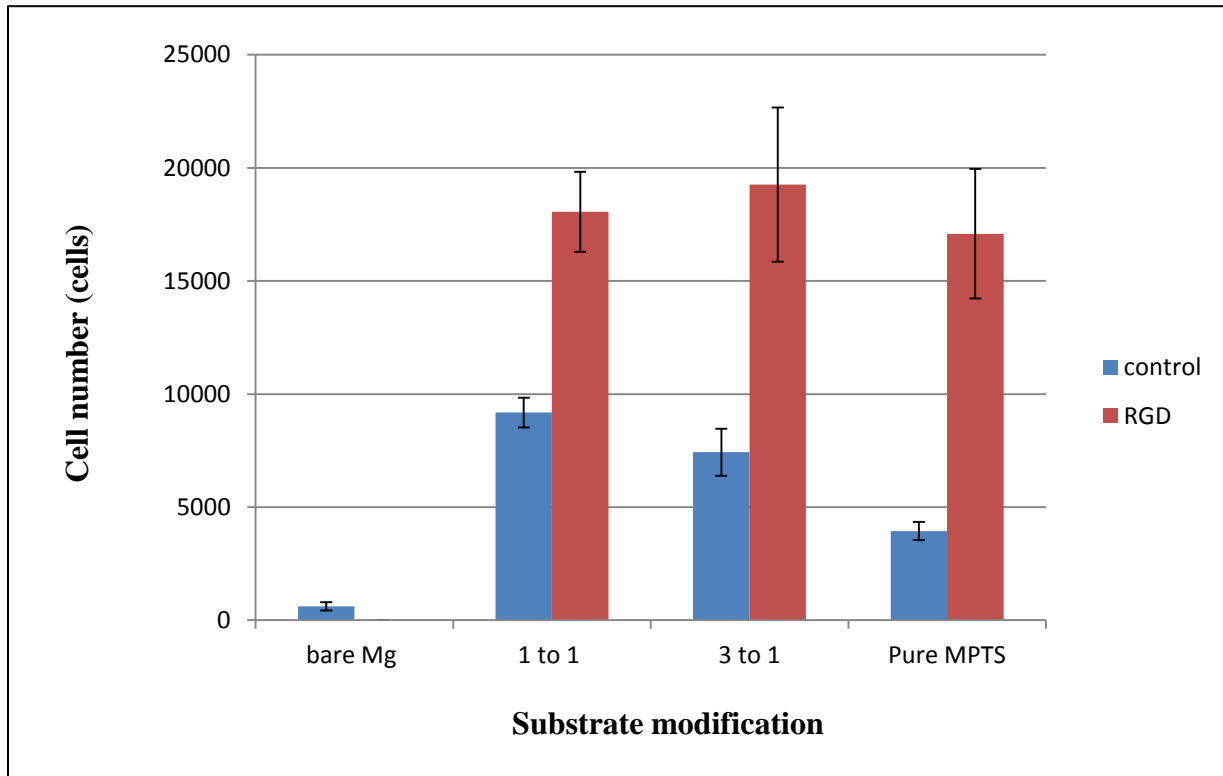
Figure 4.28 Cell numbers of Saos-2 cell adhered on Mg AZ31 substrate surfaces after 3 hours incubation period. Bare Mg AZ31 substrates, 1:1 (MPTS:TEOS) mixed organosilane coated Mg AZ31 substrate, 3:1 (MPTS:TEOS) mixed organosilane coated Mg AZ31 substrate and Pure MPTS organosilane coated MgAZ31 substrate were applied as control groups (blue, from left to right); RGD-modified 1:1 (MPTS:TEOS) mixed organosilane coated Mg AZ31 substrate, 3:1 (MPTS:TEOS) mixed organosilane coated Mg AZ31 substrate and Pure MPTS organosilane coated MgAZ31 substrate were investigated samples (red, from left to right). Data are the average ±standard deviation of 2 replicates /2 independent experiments.

Figure 4.28 also shows that all three RGD-modified substrates recruited more Saos-2 cells than control groups after a 3-hour incubation period. Moreover, the adhered cell numbers were the same regardless of the RGD surface density. These results demonstrated that chemically bonded RGD peptide acts as a bioactive ligand which could stimulate the specific interactions between RGD sequence and integrins on cell membrane and improve the adherence of Saos-2 cells onto modified substrate surfaces when compared with silanized ones. On the other hand, the same

level of cell adhesion to all densities RGD-modified substrates indicated that the difference in RGD surface density is not the main factor responsible for the cell adhesion process. In addition, the CyQUANT Kit could not estimate live and dead cells, thus the survival of adhered Saos-2 cells on the different substrate surfaces could not be evaluated, and dead cells would detach from substrate surfaces while the incubation period was extended.

4.4.2 Saos-2 Cell Proliferation Assay

4.4.2.1 Optimization of Cell Number for Proliferation Assay

Even though the expected differences in cell adherence capacity were not observed on modified substrates with different RGD surface density, the surface peptide density could affect the cell adhesion strength and also the cell focal contact formation which is essential for cell survival as well as cell spreading, migration, proliferation and differentiation [86, 87, 89].

Therefore, the impact of RGD surface density on a long term cell behavior, proliferation, was investigated. In order to keep the cell number in the linear detection range, preliminary experiments were carried out by seeding 5,000 and 15,000 cells and evaluating proliferation by determining the number of cells in the wells at different time intervals. According to another study, Saos-2 exhibit little cell proliferation in the first 3 days after seeding [101]. Therefore, the cell numbers in the wells was evaluated with the CyQUANT kit after 3, 6, 7, 9 and 10 days of culture, and the results are shown in Figure 4.29. Unsurprisingly, for the 15,000-cell group, the cell number at day 9 had increased beyond the maximum cell number range which could be measured using the CyQUANT kit. After 10 days of culture, the cell number dropped below 40,000 cells, which was probably caused by a deficiency in nutrients and/or contact inhibition. On the contrary, using 5,000 cells as initial seeded cell number led to a gradual increase in proliferation over the 10 day period. Moreover, at day 10 the cell number reached a maximum of approximately 32,000 cells, which was still in the linear detection range of the CyQUANT kit.

Therefore, we chose to use 5,000 cells per well in our investigation of the effect of RGD-modified Mg AZ31 on Saos-2 cell proliferation.
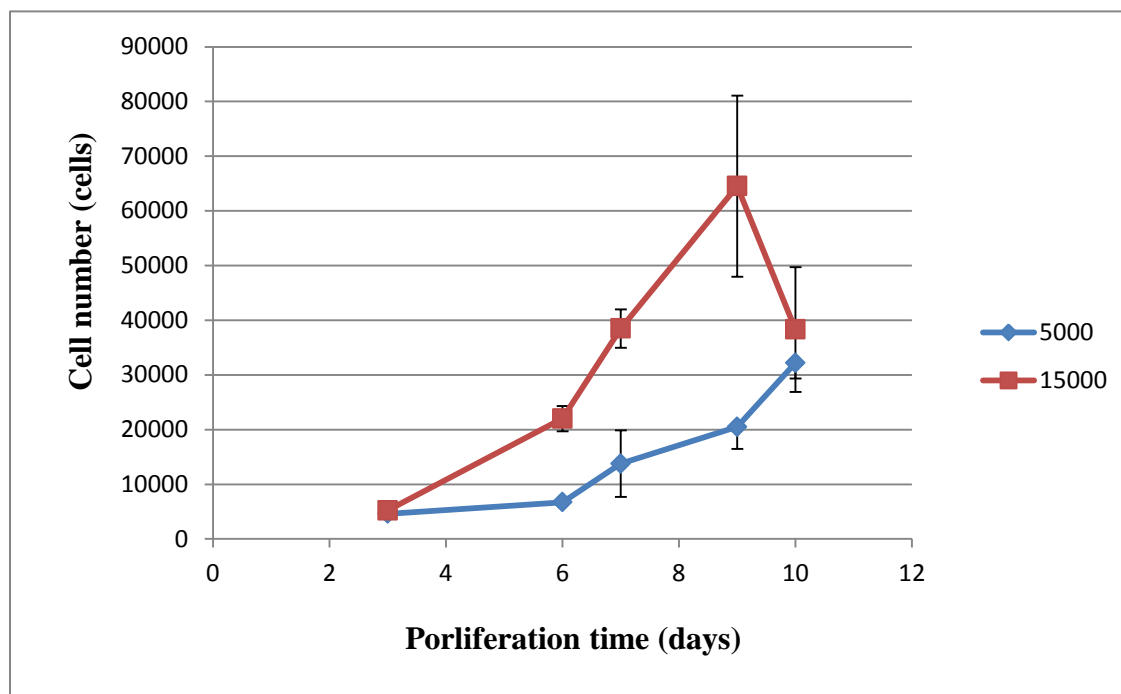
Figure 4.29 Effect of the initial seeding cell density on the growth profile of Saos-2 cell. Data are the average ±standard deviation of 2 replicates /2 independent experiments.

4.4.2.2 Cell Proliferation Assay

As mentioned above, the adherent cells on substrates proliferated only marginally in the first 3 days of culture [101]. Thus, the cell adhesion numbers by day 3 were assigned as the baseline for the evaluation of cell proliferation. Five thousand cells were seeded on RGD-modified substrates and also on the corresponding control groups. Figure 4.30 shows the cell number on investigated substrates by day 3 of the incubation period.

Figure 4.30 Saos-2 cell proliferation numbers on Mg AZ31 substrates modified with three different RGD surface densities after 3 days proliferation period. Bare Mg AZ31 substrates, 1:1 (MPTS:TEOS) mixed organosilane coated Mg AZ31 substrate, 3:1 (MPTS:TEOS) mixed organosilane coated Mg AZ31 substrate, Pure MPTS organosilane coated MgAZ31 substrate and bare wells were applied as control groups (blue, from left to right); RGD-modified 1:1 (MPTS:TEOS) mixed organosilane coated Mg AZ31 substrate, 3:1 (MPTS:TEOS) mixed organosilane coated Mg AZ31 substrate and Pure MPTS organosilane coated MgAZ31 substrate were investigated samples (red, from left to right). Data are the average ± standard deviation of 2 replicates /2 independent experiments.

The cells which adhered on the polished bare Mg AZ31 corresponded to only 3% of initial seeded cells, in agreement with the results of our cell adhesion assay (Figure 4.28). Compared with polished bare Mg AZ31 substrates, the adhered cell numbers on 1:1 (MPTS:TEOS) mixed organosilane coated and pure MPTS coated Mg AZ31 substrates were slightly increased by 2 times and 4 times respectively. And a significant enhancement in adhered cell number was observed on 3:1 (MPTS:TEOS) mixed organosilane coated Mg AZ31 substrates which was almost 17 times more than that on polished bare Mg AZ31 substrates. This result represented that the organosilane coatings efficiently protected Mg AZ31 substrates from corrosion in the cell

culture medium and provided a stable surface for cell adhesion and further proliferation. On the other hand, the adhered cell numbers showed no significant differences between RGD-modified and non-modified control substrates in each coating group.

Interestingly, Saos-2 cells proliferation was significantly increased when the 3:1 coating group was used: about 50% of initial seeded cells adhered on both RGD-modified and non-modified substrate surfaces by day 3. The adhesion test above (Figure 4.28) showed 19% and 48% cell adhesion on non-modified and RGD-modified 3:1 substrates, respectively, after a 3-hour incubation. The results presented here indicate that the presence of covalently bonded RGD peptides facilitated the initial adhesion to the substrate, but did not impact on cell adhesion when longer incubation times were studied. On the other hand, low cell numbers on the 1:1 and the pure MPTS coating groups (which were around 14% and 7% of initial seeded cell numbers on substrates, whether or not they had undergone RGD modification), suggests that these two types of organosilane coating were not compatible with long term cell viability and/or proliferation.

Figure 4.31 shows the cell adhesion number on investigated substrates by day 10 of the incubation period. On polished bare Mg AZ31, a little cell proliferation (from 138 to 519 cells) was observed from day 3 to day 10. For 1:1 and pure MPTS silanized Mg AZ31 substrates, a few of Saos-2 cells (305 and 576 cells respectively) initially adhered and survived on the surfaces (Figure 4.30); however, by day 10, cell numbers were reduced by 15% and 65%, indicating that both silanized surfaces were not sufficient for long term cell adhesion and proliferation. Interestingly, the cell proliferation capacity on 1:1 and pure MPTS silanized substrates was enhanced by RGD modification, but the cell numbers on substrates were still well below the initial seeded cell number. Thus, compared to the polished bare Mg AZ31, RGD-modified 1:1 and pure MPTS silanized could not significantly improve the biocompatibility of the Mg AZ31 substrate.
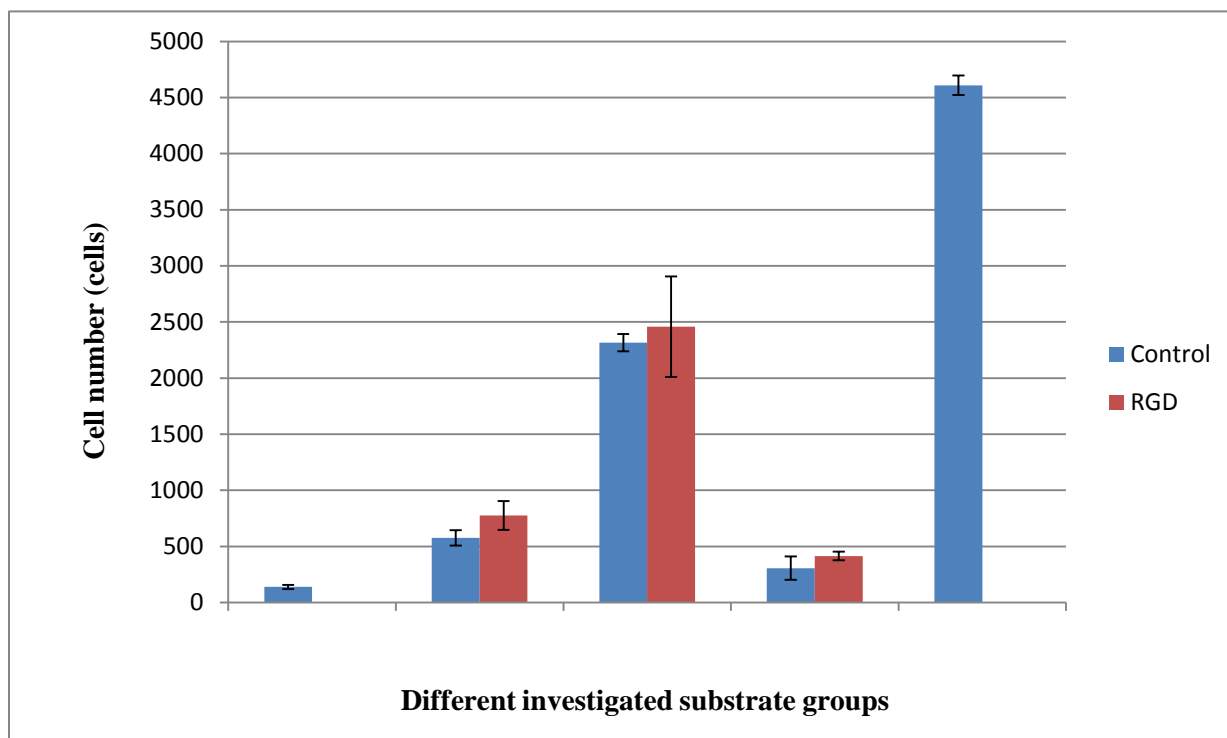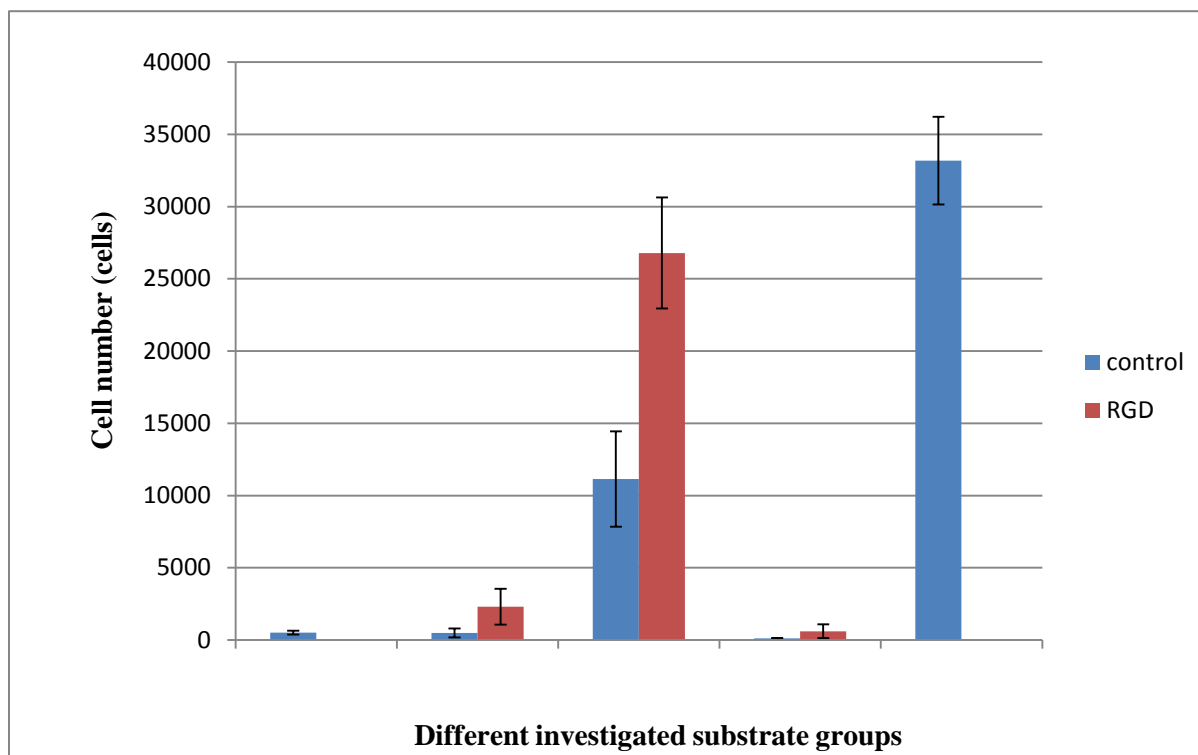
Figure 4.31 Saos-2 cell proliferation numbers on Mg AZ31 substrates modified with three different RGD surface densities after 10 days proliferation period. Bare Mg AZ31 substrates, 1:1 (MPTS:TEOS) mixed organosilane coated Mg AZ31 substrate, 3:1 (MPTS:TEOS) mixed organosilane coated Mg AZ31 substrate, Pure MPTS organosilane coated MgAZ31 substrate and bare wells were applied as control groups (blue, from left to right); RGD-modified 1:1 (MPTS:TEOS) mixed organosilane coated Mg AZ31 substrate, 3:1 (MPTS:TEOS) mixed organosilane coated Mg AZ31 substrate and Pure MPTS organosilane coated MgAZ31 substrate were investigated samples (red, from left to right). Data are the average ± standard deviation of 2 replicates /2 independent experiments.

Remarkably, the highest cell proliferation rates were observed on the RGD-modified and unmodified 3:1 coated substrates, with approximately 11-fold and 5-fold increases in cell number from day 3 to day 10, respectively (Figure 4.31). In addition, by day 10, the number of cells on RGD-modified 3:1 substrates was 2.4 times greater than that on the unmodified ones, and 52 times greater than that on the polished bare Mg AZ31 substrates. In fact, the number of cells on the RGD-3:1 substrates at day 10 was close to the bare wells positive control group. These results indicated that the protected coating deposited from 3:1 mixed organosilane solution

provided an appropriate environment for cell adhesion, survival and proliferation. In turn, this shows that the optimal RGD surface density on 3:1 (MPTS:TEOS) mixed organosilane coated Mg AZ31 substrates induced specific interactions between Saos-2 cells and substrate surfaces which enhanced cell proliferation rate.

The low proliferation capacity of Saos-2 cells on RGD-modified 1:1 substrates might be related to the low RGD surface density as well as the poor corrosion resistance of 1:1 organosilane coating. The low surface density of RGD peptides might not provide sufficient cell adhesion sites onto which Saos-2 cell could build up strong binding. Therefore, after initial cell adhesion, Saos-2 cells would detach from RGD modified 1:1 substrates, resulting in low capacity in Saos-2 cell proliferation. Moreover, as mentioned above, the 1:1 substrates demonstrated a low corrosion resistance, and they started to corrode from the edges after 5 min exposure to cell suspension by visual observation. Thus 1:1 coated substrates could not provide a stable environment for cell survival, proliferation and other complex cell behaviors.

On the other hand, the RGD-modified pure MPTS substrates showed the highest RGD surface density, however, the surfaces had the lowest cell proliferation capacity. Some studies have shown that the surface density of RGD peptides plays an important role in cell/substrate interactions which can further influence the signal pathways for cell behaviors on substrates [72, 86]. Along with RGD surface density enhancement, the cell adhesion number shows a generally increasing trend [72]. Moreover, for different cell lines, there are various optimal RGD surface densities for cell adhesion [72]. Chollet et al. [87] demonstrated that endothelial cells and osteoblastic cells had different requirements with regards to the optimal RGD surface densities for cell adhesion. Moreover, they showed that endothelial cell adhesion decreased with increasing RGD surface density on polymer substrates [87]. A similar observation was made when we tested the proliferation of Saos-2 cell on RGD-modified pure MPTS coated substrates (Figure 4.31). This result could be explained by the phenomenon of steric crowding of RGD peptides on surfaces of pure MPTS coated substrates [90]. On the pure MPTS coated Mg AZ31

substrates, RGD peptides were closely packed which might cause the RGD peptides to be sterically unavailable, impeding the access of integrins exposed on Saos-2 cells and their binding to RGD ligands [90].

The significant enhancement in the biocompatibility of Mg AZ31 by the 3:1 coating with RGD modification could be attributed to the appropriate corrosion resistance of the 3:1 coating which allowed the substrates to release an optimal Mg^{2+} amount while keeping the surface of the Mg AZ31 substrate stable for cell adhesion.

Various studies have demonstrated that the presence of bivalent cations, such as Mg^{2+}, Ca^{2+}, Mn^{2+}, could affect the function of integrins which could increase the affinity of integrin/ligand recognition and further influence cell adhesion. Also, a number of studies have reported that Mg^{2+} plays an essential role in cell proliferation and differentiation [19, 102]. Abed et al. showed that low extracellular Mg^{2+} concentrations inhibited the proliferation of different osteoblastic cell lines [103]. On the other hand, other studies demonstrated that high extracellular Mg^{2+} induced the synthesis of DNA and protein which further stimulated cell division [19]. On the basis of the well-known importance of Mg^{2+} in cell behavior, Zreiquat et al. investigated the enhancement of the biocompatibility of a Mg^{2+}-modified bioceramic substrate (Al_2O_3-Mg^{2+}) using human bone-derived cells (HBDC). The results demonstrated that Mg^{2+}-modified substrates recruited more HBDC compared to the original Al_2O_3 substrate, and that this was the result of an increase in the levels of $\alpha_5\beta_1$- and β_1- integrins on the cell surface, which was promoted by the presence of Mg^{2+} [102]. Therefore, our observation that the 3:1 coated Mg AZ31 substrates provided the best performance in terms of cell proliferation could be attributed to the fact that this coating possessed the optimal corrosion resistance for Mg AZ31 implant biomaterial. The Mg^{2+} could be released from substrates at a certain rate which would be optimal for the promotion of cell/substrate interactions, further improving the biocompatibility of Mg AZ31.

Chapter 5: Conclusions

In this study, a simple immersion method for depositing mixed organosilane coatings with variable surface thiol densities was developed. Under the optimal organosilane concentration and deposition time, three orgaosilane coatings with different MPTS to TEOS ratios were successfully and uniformly deposited on Mg AZ31.

The surface chemical components were analysed by ATR-FTIR, water contact angle and XPS. The results demonstrated that the surface density of thiol functional groups followed the percentage of MPTS in the coating bath solutions. Furthermore, the distribution of thiol functional groups was assessed through the specific interaction between thiol groups and AuNP by AFM. A pattern similar to that previously reported for block co-polymer distributions was observed on 3:1 coated substrates. This pattern seemed to have an impact on cell proliferation on the coated surfaces.

The corrosion resistance of three different coated Mg AZ31 substrates was evaluated by an immersion test carried out in 3.5% NaCl solution for up to 14 days. All three organosilane coatings exhibited a significant enhancement in Mg AZ31 substrate corrosion resistance compared with polished bare Mg AZ31. Moreover, pure MPTS coated Mg AZ31 substrates had the best corrosion resistance among the three different organosilane coatings.

Through the heterobifunctional cross-linker SMP, RGD peptides were covalently bonded onto organosilane-coated Mg AZ31 substrates. The XPS results indicated that RGD ligands were successfully immobilized on Mg AZ31 substrates. Furthermore, the RGD surface density was controlled by the surface density of thiol functional groups at the coating surface.

As a candidate for future biomaterials, one important aspect is the biocompatibility of Mg AZ31, which is determined by various factors including hydrophilicity, roughness, surface functional groups and the presence of some specific biomolecules. In this thesis, the RGD tripeptide was

considered as an active ligand which could be recognized by integrins on cell membrane. RGD was covalently immobilized onto silanized Mg AZ31 substrates to mimic the ECM environment. The presence of RGD peptide and its surface density effects on cell adhesion and proliferation were also evaluated with the Saos-2 cell line. The cell adhesion results indicated that the presence of immobilized RGD peptides increased the adhesion of Saos-2 cell on Mg AZ31 substrates compared with either bare or silanized biomaterials. However, there was no significant difference in cell adhesion when the density of the RGD peptide was increased. On the other hand, Saos-2 cell preferred to proliferate on 3:1 coated Mg AZ31 substrates, especially the ones with the RGD modification. The results from the cell assays indicated that the 3:1 coated surfaces obtained the most appropriate RGD surface density which enhanced the biocompatibility of Mg AZ31.

Chapter 6: Future Work

The 3:1 coating developed in this study was a uniform, stable and reproducible corrosion resistant surface coating which, upon RGD modification, also improved the biocompatibility of Mg AZ31. However, there are some important aspects which still need to be further studied. The first one is the accurately determine the RGD surface density on 3:1 coated substrates. Our study showed that the RGD surface density on 3:1 coated substrates gave the best result with regard to cell/biomaterials interactions. Therefore, the quantification of this optimal RGD surface density will be necessary and beneficial for further *in vitro* and *in vivo* studies, such as the extent of cell spreading. Moreover, the surface distribution of the RGD peptide is another important factor which can affect cell responses to substrates. The ligand distribution in the ECM is definitely different from the uniform distribution of ligands on artificial mimic substrates such as the RGD distribution on pure MPTS coated substrates. The AFM results exhibited an interesting pattern of functional thiol group distribution which could further influence the distribution of RGD peptides on substrate surfaces. Therefore, the effect of this interesting pattern on cell/substrate interactions should be further evaluated with advanced methods. In addition, Saos-2 cell spreading and actin distribution should be observed by confocal microscopy to evaluate cell morphology on RGD-modified substrates. In the end, the *in vivo* studies should be considered to evaluate potential acute and chronic toxicity. Moreover, the RGD-modified Mg AZ31 should be implanted into the damage bone tissue of animal models to evaluate their usefulness in *in vivo* situations.

Chapter 7: References

1. B.D. Ratner, A.S. Hoffman, F.J. Schoen, J.E. Lemons. (2004). *Biomaterials Science: An Introduction to Materials in Medicine.* 2nd edn. Academic Press. United States of America.

2. M. Vandrovcová, L. Bačáková. (2011). Adhesion, growth and differentiation of osteoblasts on surface-modified materials developed for bone implants. *Physiological Research.* 60 (3), 403-417.

3. P. Thevenot, W. Hu, L. Tang. (2008). Surface chemistry influences implant biocompatibility. *Current Topics in Medicinal Chemistry.* 8 (4), 270-280.

4. I. G. Trumpy, T. Lyberg. (1993). *In vivo* deterioration of proplast-teflon temporomandibular joint interpositional implants: a scanning electron microscopic and energy-dispersive X-ray analysis. *Journal of Oral and Maxillofacial Surgery.* 51 (6), 624-629.

5. K. Sutherland, J.R. Mahoney, A.J. Coury, J.W. Eaton. (1993). Degradation of biomaterials by phagocyte-derived oxidants. *The Journal of Clinical Investigation*. 92 (5), 2360-2367.

6. L.P. Carro, G.G. Suarez. (1999). Intercondylar notch fibrous nodule after total knee replacement. *Arthroscopy: The Journal of Arthroscopic & Related Surgery.* 15 (1), 103-105.

7. H.A. Clayton, R.F.L. James, N.J.M. London. (1993). Islet microencapsulation: a review. *Acta Diabetologica*. 30 (4), 181-189.

8. B. Kasemo. (2002). Biological surface science. *Surface Science*. 500 (1-3), 656-677.

9. W. Wang, Y. Ouyang, CK. Poh. (2011). Orthopaedic implant technology: biomaterials from past to future. *Annals of the Academy of Medicine-Singapore*. 40 (5), 237-244.

10. I. Gotman. (1997). Characteristics of metals used in implants. *Journal of Endourology*. 11 (6), 383-389.

11. A review of Corrosion Behavior of Surgical Implant Alloys (PerkinElmer instruments)

12. M.I.Z. Ridzwan, Solehuddin Shuib, A.Y. Hassan, A.A. Shokri and M.N. Mohamad Ibrahim. (2007). Problem of Stress Shielding and Improvement to the Hip Implant Designs: A Review. *Journal of Medical Sciences*. 7 (3), 460.

13. H. Weinans, D.R. Sumner, R. Igloria, R.N. Natarajan. (2000). Sensitivity of periprosthetic stress-shielding to load and the bone density-modulus relationship in subject-specific finite element models. *Journal of Biomechanics*. 33 (7), 809-817.

14. M. Niinomi, M. Nakai. (2011). Titanium-Based Biomaterials for Preventing Stress Shielding between Implant Devices and Bone. *International Journal of Biomaterials*. 2011, 10.

15. S. Shadanbaz, G.J. Dias. (2012). Calcium phosphate coatings on magnesium alloys for biomedical applications: a review. *Acta Biomaterialia*. 8 (1), 20-30.

16. M.P. Staigera, A.M. Pietaka, J. Huadmaia, G. Diasb. (2006). Magnesium and its alloys as orthopedic biomaterials: A review. *Biomaterials*. 27 (9), 1728-1734.

17. G. Song. (2007). Control of biodegradation of biocompatable magnesium alloys. *Corrosion Science*. 49 (4), 1696-1702.

18. F. Wittea, V. Kaeseb, H. Haferkampb, E. Switzerc, A. Meyer-Lindenbergc, C.J. Wirtha, H. Windhagena. (2005). In vivo corrosion of four magnesium alloys and the associated bone response. *Biomaterials*. 26 (17), 3667-3563.

19. F.I. Wolf and A. Cittadini. (1991). Magnesium in Cell Proliferation and Differentiation. *Frontiers in Bioscience*. 4, 607-617.

20. C. Fox, D. Ramsoomair, C. Carter. (2001). Magnesium: its proven and potential clinical significance. *Southern Medical Journal.* 19 (12), 1195-1201.

21. H. Rubin. (1975). Central role for magnesium in coordinate control of metabolism and growth in animal cells. *Proceeding of the National Academy of Sciences of the United States of America.* 72 (9), 3551-3555.

22. A. Hartwig. (2001). Role of magnesium in genomic stability. *Mutation Research/Fundamental and Molecular Mechanisms of Mutagenesis.* 475 (1-2), 113-121.

23. A. Pietak, P. Mahoney, G.J. Dias, M.P. Staiger. (2008). Bone-like matrix formation on magnesium and magnesium alloys. *Journal of Materials Science: Materials in Medicine.* 19 (1), 407-415.

24. T. Kraus, S.F. Fischerauer, A.C. Hänz, P.J. Uggowitzer, J.F. Löffler, A.M. Weinber. (2012). Magnesium alloys for temporary implants in osteosynthesis: in vivo studies of their degradation and interaction with bone. *Acta Biomaterialia.* 8 (3), 1230-1238.

25. H. Kuwahara, Y. Al-Abdullat, N. Mazaki, S. Tsutsumi, T. Aizawa. (2001). Precipitation of magnesium apatite on pure magnesium surface during immersing in Hank's solution. *Materials Transactions.* 42 (7), 1317-1321.

26. L. Xu, G. Yu, E. Zhang, F. Pan, K. Yang. (2007). *In vivo* corrosion behavior of Mg-Mn-Zn alloy for bone implant application. *Journal of Biomedical Materials Research Part A.* 83 (3), 703-711.

27. E. Zhang, L. Xu, G. Yu, F. Pan, K. Yang. (2009). *In vivo* evaluation of biodegradable magnesium alloy bone implant in the first 6 months implantation. *Journal of Biomedical Materials Research Part A.* 90 (3), 882-893.

28. F. Witte, V. Kaese, H. Haferkamp, E. Switzer, A. Meyer-Lindenberg, C.J. Wirth, H. Windhagen. (2005). *In vivo* corrosion of four magnesium alloys and the associated bone response. *Biomaterials*. 26 (17), 3557-63.

29. Z. Li, X. Gu, S. Lou, Y. Zheng. (2008). The development of binary Mg-Ca alloys for use as biodegradable materials within bone. *Biomaterials*. 29 (10), 1329-1344.

30. T. Mano, Y. Ueyama, K. Ishikawa, T. Matsumura, K. Suzuki. (2002). Initial tissue response to a titanium implant coated with apatite at room temperature using a blast coating method. *Biomaterials*. 23 (9), 1931-1936.

31. H. Hornberger, S. Virtanen, A.R. Boccaccini. (2012). Biomedical coatings on magnesium alloys - a review. *Acta Biomaterialia*. 8 (7), 2442-2455.

32. R. Zeng, J. Zhang, W. Dietzel, K.U. Kainer, C. Blawert, W. Ke. (2006). Review of studies on corrosion of magnesium alloys. *Transactions of Nonferrous Metals Society of China.* 16 (2), s763–s771.

33. S. Zhang, X. Zhang, C. Zhao, J. Li, Y. Song, C. Xie, H. Tao, Y. Zhang, Y. He, Y. Jiang, Y. Bian. (2010). Research on an Mg-Zn alloy as a degradable biomaterial. *Acta Biomaterialia.* 6 (2), 626-640.

34. Z. Liu, W. Gao. (2006). Electroless nickel plating on AZ91 Mg alloy substrate. *Surface and Coatings Technology*. 200 (16-17), 5087–5093.

35. D. Xue, Z. Tan, M.J. Schulz, W.J. Vanooija, J. Sankar, Y. Yuna, Z. Dong. (2012). Corrosion studies of modified organosilane coated magnesium–yttrium alloy in different environments. *Materials Science and Engineering: C*. 32 (5), 1230–1236.

36. J.P. Matinlinna, K. Laajalehto, T. Laiho, I. Kangasniemi, L.V.J. Lassila, P.K. Vallittu. (2004). Surface analysis of Co–Cr–Mo alloy and Ti substrates silanized with trialkoxysilanes and silane mixtures. *Surface and Interface Analysis*. 36 (3), 246–253.

37. C. Heitz, G. Laurent, R. Briard, E. Barthel. (2006). Cross-condensation and particle growth in aqueous silane mixtures at low concentration. *Journal of Colloid and Interface Science*. 298 (1), 192-201.

38. A. Scott, J.E. Gray-Munro. (2009). The surface chemistry of 3-mercaptopropyltrimethoxysilane films deposited on magnesium alloy AZ91. *Thin Solid Films*. 517 (24), 6809–6816.

39. A.F. Scott, J.E. Gray-Munro, J.L. Shepherd. (2010). Influence of coating bath chemistry on the deposition of 3-mercaptopropyl trimethoxysilane films deposited on magnesium alloy. *Journal of Colloid and Interface Science*. 343 (2), 474–483.

40. A. Najari, P. Lang, P.C. Lacaze, D. Mauer. (2012). Adsorption of γ-mercaptopropyltrimethoxysilane on zinc: A study of the competition between thiol and silanol functions related to the age of the siloxane solution, its pH and the oxidation state of the surface. *Surface Science*. 606 (3-4), 137–145.

41. I. Lee, R.P. Wool. (2000). Controlling amine receptor group density on aluminum oxide surfaces by mixed silane self-assembly. *Thin Solid Films*. 379 (1-2), 94–100.

42. V. Palanivel, Y. Huang, W.J. van Ooij. (2005). Effects of addition of corrosion inhibitors to silane films on the performance of AA2024-T3 in a 0.5 M NaCl solution. *Progress in Organic Coatings*. 53 (2), 153–168.

43. P.H. Suegama, H.G. de Melo, A.A.C. Recco, A.P. Tschiptschin, I.V. Aoki. (2008). Corrosion behavior of carbon steel protected with single and bi-layer of silane films filled with silica nanoparticles. *Surface and Coatings Technology*. 202 (13), 2850–2858.

44. W. Trabelsi, P. Cec Íio, M.G.S. Ferreira, K. Yasakau, M.L. Zheludkevich, M.F. Montemor. (2007). Surface evaluation and electrochemical behaviour of doped silane pre-treatments on galvanised steel substrates. *Progress in Organic Coatings*. 59 (3), 214–223.

45. D.A. Ramrus, J.C. Berg. (2004). Characterization and adhesion testing of mixed silane-treated surfaces. *Journal of Adhesion Science and Technology*. 18 (12), 1395-1414.

46. D. Zhu, W.J. van Ooij. (2004). Enhanced corrosion resistance of AA 2024-T3 and hot-dip galvanized steel using a mixture of bis-[triethoxysilylpropyl]tetrasulfide and bis-[trimethoxysilylpropyl]amine. *Electrochimica Acta*. 49 (7), 1113–1125.

47. G. Pan, D.W. Schaefer, W.J. van Ooij, M.S. Kent, J. Majewski, H. Yim. (2006). Morphology and water resistance of mixed silane films of bis[3-(triethoxysilyl) propyl]tetrasulfide and bis-[trimethoxysilylpropyl]amine. *Thin Solid Films*. 515 (4), 2771–2780.

48. J.P. Matinlinna, M. Özcan, L.V. Lassila, P.K. Vallittu. (2004). The effect of a 3-methacryloxypropyltrimethoxysilane and vinyltriisopropoxysilane blend and tris(3-trimethoxysilylpropyl)isocyanurate on the shear bond strength of composite resin to titanium metal. *Dental Materials*. 20 (9), 804–813.

49. M. Dettin, A. Bagno, R. Gambaretto, G. Iucci, M.T. Conconi, N. Tuccitto, A.M. Menti, C. Grandi, C. Di Bello, A. Licciardello, G. Polzonetti. (2008). Covalent surface modification of titanium oxide with different adhesive peptides: Surface characterization and osteoblast-like cell adhesion. *Journal of Biomedical Materials Research Part A*. 90A (1), 35–45.

50. Y. Hu, S.R. Winn, I. Krajbich, J.O. Hollinger. (2003). Porous polymer scaffolds surface-modified with arginine-glycine-aspartic acid enhance bone cell attachment and differentiation in vitro. *Journal of Biomedical Materials Research Part A*. 46A (3), 583–590.

51. S.W. Park, Y.I. Kim, K.H. Chung, S.W. Kim. (2001). Quantitative analysis of the degree of silanization by the ninhydrin method and its application to the immobilization of GL-7-ACA acylase and cellulolytic enzyme. *Journal of Microbiology and Biotechnology*. 11 (2), 199-203.

52. R.A. Shircliff, I.T. Martin, J.W. Pankow, J. Fennell, P. Stradins, M.L. Ghirardi, S.W. Cowley, H.M. Branz. (2011). High-Resolution X-ray Photoelectron Spectroscopy of Mixed Silane Monolayers for DNA Attachment. *ACS Applied Materials & Interfaces*. 3 (9), 3285–3292.

53. W.E.G. Hansal, S. Hansal, M. Pölzler, A. Kornherr, G. Zifferer, G.E. Nauer. (2006). Investigation of polysiloxane coatings as corrosion inhibitors of zinc surfaces. *Surface and Coatings Technology*. 200 (9), 3056–3063.

54. P. R. Underhill and D. L. Duquesnay. (2000). Corrosion resistance imparted to aluminum by silane coupling agents. *Silanes and Other Coupling Agents*. 2, 149-158.

55. A.M. Cabral, R.G. Duarte, M.F. Montemor, M.G.S. Ferreira. (2005). A comparative study on the corrosion resistance of AA2024-T3 substrates pre-treated with different silane solutions: Composition of the films formed. *Progress in Organic Coatings*. 54 (4), 322–331.

56. S.K. Bhatia, L.C. Shriver-Lake, K.J. Prior, J.H. Georger, J.M. Calvert, R. Bredehorst, F.S. Ligler. (1989). Use of thiol-terminal silanes and heterobifunctional crosslinkers for immobilization of antibodies on silica surfaces. *Analytical Biochemistry*. 178 (2), 408-13.

57. B.D. Ratner, S.J. Bryant. (2004). Biomaterials: where we have been and where we are going. *Annual Review of Biomedical Engineering*. 6, 41-75.

58. K. Anselme. (2000). Osteoblast adhesion on biomaterials. *Biomaterials*. 21 (7), 667-681.

59. J.M. Lackner, W. Waldhauserb. (2010). Inorganic PVD and CVD Coatings in Medicine — A Review of Protein and Cell Adhesion on Coated Surfaces. *Journal of Adhesion Science and Technology*. 24 (5), 925-961.

60. C.J. Wilson, R.E. Clegg, D.I. Leavesley, M.J. Pearcy. (2005). Mediation of biomaterial-cell interactions by adsorbed proteins: a review. *Tissue Engineering*. 11 (1-2), 1-18.

61. T. Albrektsson, C. Johansson. (2001). Osteoinduction, osteoconduction and osseointegration. *European Spine Journal.* 10 (2), 96-101.

62. S. Gronthos, P.J. Simmons, S.E. Graves, P.G. Robey. (2001). Integrin-mediated interactions between human bone marrow stromal precursor cells and the extracellular matrix. *Bone*. 28 (2), 174-81.

63. S. Gronthos, K. Stewart, S.E. Graves, S. Hay, P.J. Simmons. (1997). Integrin Expression and Function on Human Osteoblast-like Cells. *Journal of Bone and Mineral Research*. 12 (8), 1189-1197.

64. R.O. Hynes. (1993). Integrins: versatility, modulation, and signaling in cell adhesion. *Cell*. 69 (1), 11-25.

65. N.J. Boudreau, P.L. Jones. (1999). Extracellular matrix and integrin signalling: the shape of things to come. *Biochemical Journal*. 339 (Pt: 3), 481-8.

66. M.B. Rahmany, M. Van Dyke. (2013). Biomimetic approaches to modulate cellular adhesion in biomaterials: A review. *Acta Biomaterialia*. 9 (3), 5431-5437.

67. R.L. Juliano and S. Haskill. (1993). Signal transduction from the extracellular matrix. *Journal of Cell Biology*. 120 (3), 577–585.

68. R.G. LeBaron, K.A. Athanasiou. (2000). Extracellular matrix cell adhesion peptides: functional applications in orthopedic materials. *Tissue Engineering*. 6 (2), 85-103.

69. G. Schneider, K. Burridge. (1994). Formation of focal adhesions by osteoblasts adhering to different substrata. *Experimental Cell Research*. 214 (1), 264-9.

70. K.L. Kilpadi, P. Chang, S.L. Bellis. (2001). Hydroxylapatite binds more serum proteins, purified integrins, and osteoblast precursor cells than titanium or steel. *Journal of Biomedical Materials Research*. 57 (2), 258–267.

71. C.R. Howlett, M.D. Evans, W.R. Walsh, G. Johnson, J.G. Steele. (1994). Mechanism of initial attachment of cells derived from human bone to commonly used prosthetic materials during cell culture. *Biomaterials.* 15 (3), 213-22.

72. U. Hersel, C. Dahmen, H. Kessler. (2003). RGD modified polymers: biomaterials for stimulated cell adhesion and beyond. *Biomaterials*. 24 (24), 4385-415.

73. T.A. Horbett, K.R. Lew. (1995). Residence time effects on monoclonal antibody binding to adsorbed fibrinogen. *Journal of Biomaterials Science, Polymer Edition*. 6 (1), 15-33.

74. A. Hautanen, J. Gailit, D.M. Mann, E. Ruoslahti. (1989). Effects of modifications of the RGD sequence and its context on recognition by the fibronectin receptor. *The Journal of Biological Chemistry*. 264 (3), 1437-1442.

75. D.A. Puleo, R. Bizios. (1991). RGDS tetrapeptide binds to osteoblasts and inhibits fibronectin-mediated adhesion. *Bone*. 12 (4), 271–276.

76. A.J. García, P. Ducheyne, D. Boettiger. (1998). Effect of surface reaction stage on fibronectin-mediated adhesion of osteoblast-like cells to bioactive glass. *Journal of Biomedical Materials Research*. 40 (1), 48-56.

77. S.J. Xiao, M. Textor, N.D. Spencer. (1998). Covalent Attachment of Cell-Adhesive, (Arg-Gly-Asp)-Containing Peptides to Titanium Surfaces. *Langmuir*. 14 (19), 5507–5516.

78. G. Forget, L. Latxague, V. Héroguez, C. Labrugère, M.C. Durrieu. (2007). RGD nanodomains grafting onto titanium surface. *Annual International Conference of the IEEE Engineering in Medicine and Biology Society.* 2007, 5107-5110.

79. D.R. Jackson, S. Omanovic, S.G. Roscoe. (2000). Electrochemical Studies of the Adsorption Behavior of Serum Proteins on Titanium. *Langmuir*. 16 (12), 5449–5457.

80. C. Yang, K. Cheng, W. Weng, C. Yang. (2009). Immobilization of RGD peptide on HA coating through a chemical bonding approach. *Journal of Materials Science: Materials in Medicine*. 20 (11), 2349-2352.

81. H. Weng, C. Wu, C. Chen, C. Ho, S. Ding. (2010). Preparation and properties of gold nanoparticle-electrodeposited titanium substrates with Arg-Gly-Asp-Cys peptides. *Journal of Materials Science: Materials in Medicine*. 12 (5), 1511-1519.

82. G. Zorn, I. Gotman, E. Y. Gutmanas, R. Adadi, C. N. Sukenik. (2007). Surface modification of Ti45Nb alloy by immobilization of RGD peptide via self-assembled monolayer. *Journal of Materials Science: Materials in Medicine*. 18 (7), 1309-1315.

83. C. Feng, Z. Zhang, R. Förch, W. Knoll, G.J. Vancso, and H. Schönherr. (2005). Reactive Thin Polymer Films as Platforms for the Immobilization of Biomolecules. *Biomacromolecules*. 6 (6), 3243–3251.

84. Y. Hu, S.R. Winn, I. Krajbich, J.O. Hollinger. (2003). Porous polymer scaffolds surface-modified with arginine-glycine-aspartic acid enhance bone cell attachment and differentiation in vitro. *Journal of Biomedical Materials Research Part A*. 64A (3), 583–590.

85. E.J. Tocce, A.H. Broderick, K.C. Murphy, S.J. Liliensiek, C.J. Murphy, D.M. Lynn, P.F. Nealey. (2012). Functionalization of reactive polymer multilayers with RGD and an antifouling motif: RGD density provides control over human corneal epithelial cell–substrate interactions. *Journal of Biomedical Materials Research Part A*. 100A (1), 84–93

86. S. Inouea, Y. Iida, Y. Otani, Y. Hirano, Y. Tabata. (2009). Adhesion Behavior of Human Adipo-Stromal Cells on Self-Assembled Monolayers with Different Surface Densities or Gradients of RGD Peptide. *Journal of Biomaterials Science, Polymer Edition*. 20 (4), 495-510.

87. C. Chollet, C. Chanseau, M. Remy, A. Guignandon, R. Bareille, C. Labruge`re, L. Bordenave, M.C. Durrieu. (2009). The effect of RGD density on osteoblast and endothelial cell behavior on RGD-grafted polyethylene terephthalate surfaces. *Biomaterials*. 30 (5), 711–720.

88. L.C. Shriver-Lake, B. Donner, R. Edelstein, K. Breslin, S.K. Bhatia, F.S. Ligler. (1997). Antibody immobilization using heterobifunctional crosslinkers. *Biosensors and Bioelectronics*. 12 (11), 1101–1106.

89. K.L. Kilpadi, A.A. Sawyer, C.W. Prince, P. Chang, S.L. Bellis. (2004). Primary human marrow stromal cells and Saos-2 osteosarcoma cells use different mechanisms to adhere to hydroxylapatite. *Journal of Biomedical Materials Research Part A*. 68A (2), 273–285.

90. G. Le Saux, A. Magenau, T. Böcking, K. Gaus, J.J. Gooding. (2011). The Relative Importance of Topography and RGD Ligand Density for Endothelial Cell Adhesion. *PLoS One*.

91. A. Bagno, A. Piovan, M. Dettin, A. Chiarion, P. Brun, R. Gambaretto, G. Fontana, C. Di Bello, G. Palù, I. Castagliuolo. (2007). Human osteoblast-like cell adhesion on titanium substrates covalently functionalized with synthetic peptides. *Bone*. 40 (3), 693–699.

92. E.S. Gawalt, M.J. Avaltroni, M.P. Danahy, B.M. Silverman, E.L. Hanson, K.S. Midwood, J.E. Schwarzbauer, J. Schwartz. (2003). Bonding Organics to Ti Alloys: Facilitating Human Osteoblast Attachment and Spreading on Surgical Implant Materials. *Langmuir*. 19, 200-204.

93. M.C. Daniel, D. Astruc. (2004). Gold nanoparticles: assembly, supramolecular chemistry, quantum-size-related properties, and applications toward biology, catalysis, and nanotechnology. *Chemical Reviews*. 104 (1), 293-346.

94. I. Byun, A.W. Coleman, B. Kim. (2013). Transfer of thin Au films to polydimethylsiloxane (PDMS) with reliable bonding using (3-mercaptopropyl)trimethoxysilane (MPTMS) as a molecular adhesive. *Journal of Micromechanics and Microengineering*. 23 (8).

95. F. Rubio, J. Rubioa, J. L. Oteo. (1998). A FT-IR Study of the Hydrolysis of Tetraethylorthosilicate. *Spectroscopy Letters: An International Journal for Rapid Communication*. 31 (1), 199-219.

96. F. Zucchi, V. Grassi, A. Frignani, C. Monticelli, G. Trabanelli. (2006). Influence of a silane treatment on the corrosion resistance of a WE43 magnesium alloy. *Surface and Coatings Technology*. 200 (12-13), 4136–4143.

97. R.M. Silverstein, F.X. Webster, D.J. Kimle. (2005). *Spectrometric Identification of Organic Compounds.*7th edn, John Wiley & Sons, Inc. United States of America.

98. F.S. Bates, G.H. Fredrickson. (1990). Block copolymer thermodynamics: theory and experiment. *Annual Review of Physical Chemistry*. 41, 525-557.

99. E.S.M. Sherif, A.A. Almajid. (2011). Corrosion of Magnesium/Manganese Alloy in Chloride Solutions and its Inhibition by 5-(3-Aminophenyl)-tetrazole. *International Journal of Electrochemical Science.* 6, 2131-2148.

100. A. Pardo, M.C. Merino, A.E. Coy, R. Arrabal, F. Viejo, E. Matykina. (2008). Corrosion behaviour of magnesium/aluminium alloys in 3.5 wt.% NaCl. *Corrosion Science*. 50 (3), 823–834.

101. C. Pautke, M. Schieker, T. Tischer, A. Kolk, P. Neth, W. Mutschler, S. Milz. (2004). Characterization of osteosarcoma cell lines MG-63, Saos-2 and U-2 OS in comparison to human osteoblasts. *Anticancer Research.* 24 (6), 3743-3748.

102. H. Zreiqat1, C.R. Howlett, A. Zannettino, P. Evans, G. Schulze-Tanzil, C. Knabe, M. Shakibaei. (2002). Mechanisms of magnesium-stimulated adhesion of osteoblastic cells to commonly used orthopaedic implants. *Journal of Biomedical Materials Research.* 62 (2), 175–184.

103.   E. Abed, R. Moreau. (2007). Importance of melastatin-like transient receptor potential 7 and cations (magnesium, calcium) in human osteoblast-like cell proliferation. *Cell Proliferation.* 40 (6), 849–865.